GENETIC EVENTS UNDERLYING RADIATION-INDUCED

GLIOMAGENESIS

APPROVED BY SUPERVISORY COMMITTEE

Sandeep Burma, Ph.D. (Mentor)
Associate Professor, Radiation Oncology

Robert M. Bachoo, M.D., Ph.D.
Assistant Professor, Neurology

David A. Boothman, Ph.D.
Professor, Pharmacology, Radiation Oncology

Chaitanya S. Nirodi, Ph.D. (Chairman)
Assistant Professor, Radiation Oncology

DEDICATION

Dedicated to my amazing parents, Salvador and Nidia Camacho, who sacrificed so much to give me more than they ever had. You have been my most constant source of love and support in everything I have set my heart on doing. Everything that I am, all that I have accomplished is owed to you.

GENETIC EVENTS UNDERLYING RADIATION-INDUCED GLIOMAGENESIS

by

CRISTEL VANESSA CAMACHO

DISSERTATION

Presented to the Faculty of the Graduate School of Biomedical Sciences

The University of Texas Southwestern Medical Center at Dallas

In Partial Fulfillment of the Requirements

For the Degree of

DOCTOR OF PHILOSOPHY

The University of Texas Southwestern Medical Center at Dallas

Dallas, Texas

April, 2012

ACKNOWLEDGEMENTS

I would like to acknowledge, first and foremost, my PhD mentor Dr Sandeep Burma. My most sincere thank you for believing in me and my potential when I lacked all confidence. I came to your lab a complete blank slate, and I will be leaving with valuable lessons learned that have molded me into the scientist I am today. Thank you for fostering the kind of laboratory environment where not only great science is done, but also great friendships are forged.

I would like to acknowledge my thesis committee, Drs David A Boothman, Robert M Bachoo, and Chaitanya S Nirodi, who were instrumental in shaping this project. Thank you for your mentorship, support and words of encouragement throughout the years. Also, I am thankful for all the help I received along the way from Drs Debabrata Saha, Michael D Story and members of their labs. Thank you to the awesome support team at Brookhaven National Laboratory, headed by Drs Peter Guida and Adam Rusek.

I am grateful for members of the Burma lab, past and present, who have shared with me this journey: A special thank you to Brian McEllin, for all your help carrying out experiments at BNL. Thank you also to Dr Bipasha Mukherjee, from whom I learned so much about writing.

I would like to acknowledge my undergraduate professor Dr Taylor Rankin, who truly inspired me early on and made a biologist out of me. Your enthusiasm for biology was simply contagious, I could not resist!

To my husband, Evan Villarreal: Thank you for your unconditional love and for standing so firmly beside me, every single step of the way.

I am thankful for family and friends who have shared with me this PhD experience. Your love and encouragement were a great source of nourishment: My parents, Salvador and Nidia Camacho, and Patty and Jorge Villarreal; my lovely sisters and truest of friends, Jeannine and Stephanie Camacho; and my dear friend and colleague Nozomi Tomimatsu, you are a great scientist, an even greater friend and I admire you so much.

GENETIC EVENTS UNDERLYING RADIATION-INDUCED GLIOMAGENESIS

CRISTEL VANESSA CAMACHO

The University of Texas Southwestern Medical Center, 2012

SANDEEP BURMA, Ph.D.

ABSTRACT

Glioblastoma multiforme (GBM) are highly lethal brain tumors for which exposure to ionizing radiation is the only known risk factor. GBM is characterized by alterations in three core signaling pathways: 1) RTK-PI3K-Akt, 2) ARF-MDM2-p53, and 3) Ink4a-RB1. We have developed *in vitro* and *in vivo* models in order to objectively evaluate the risk of developing malignant gliomas from exposure to ionizing radiation (IR). DNA double-strand breaks (DSBs) are the most deleterious lesion inflicted by IR. We hypothesize that DSBs cooperate with pre-existing tumor suppressor loss to trigger IR-induced transformation. We demonstrate that complex DSBs induced by high linear-energy transfer (LET) Fe

ions are repaired slowly and incompletely, while those induced by low-LET gamma rays are repaired efficiently by mammalian cells. The incomplete repair of Fe-induced damage results in persistent DNA damage signaling and culminates in high levels of senescence and increased cell killing.

To examine long-term carcinogenic consequences, we used 'sensitized' Ink4a/Arf-knockout astrocytes, which are immortal but not tumorigenic. We find that Fe ions are potently tumorigenic when directed to these astrocytes, generating tumors with much higher frequency and shorter latency compared to tumors generated by gamma-rays. Tumor formation by Fe-irradiated cells is accompanied by rampant genomic instability and multiple genomic changes, the most interesting of which is loss of the p15/Ink4b tumor suppressor due to deletion of the chromosomal region harboring the *CDKN2A* and *CDKN2B* loci (the former codes for the p16/Ink4a and p19/Arf tumor suppressors and the latter for p15/Ink4b). The additional loss of p15/Ink4b in tumors derived from cells that are inherently deficient in p16/Ink4a bolsters the hypothesis that p15 plays an important role in tumor suppression, especially in the absence of p16. Indeed, we find that re-expression of p15/Ink4b in tumor-derived cells significantly attenuates the tumorigenic potential of these cells and results in delayed tumor formation and progression.

Based on our *in vitro* results, we then used transgenic mouse models with brain-specific deletions of these three key tumor suppressors (Ink4a/Ink4b/Arf)

to evaluate radiation-induced gliomagenesis *in vivo*. We find that loss of these three tumor suppressors efficiently cooperates with DNA DSBs to induce high grade gliomas, irrespective of whether the initial damage was simple or complex. Genomic analysis revealed that recurrent amplifications of the receptor tyrosine kinase MET is a frequent event in radiation-induced gliomagenesis. We found that MET expression correlated with high levels of Sox2 and associated with a stem cell-like phenotype. As MET is found to be amplified in approximately 4% of human GBM, it is likely that its activation, through amplification or mutation, is an important event in tumorigenesis triggered by DNA DSBs in this mouse model.

TABLE OF CONTENTS

PUBLICATIONS

Camacho CV, *et al.* DNA double-strand breaks cooperate with Ink4a/Ink4b/Arf loss to generate high-grade gliomas in transgenic mouse models. [In Preparation] (Chapter IV)

Mukherjee B, Tomimatsu N, Amancherla K, **Camacho CV**, Pichamoorthy N, Burma S. The Dual PI3K/mTOR Inhibitor NVP-BEZ235 Is a Potent Inhibitor of ATM- and DNA-PKCs-Mediated DNA Damage Responses. *Neoplasia* (2012) **14:** 34-43.

Camacho CV, Mukherjee B, McEllin B, Ding LH, Hu B, Habib AA *et al.* Loss of p15/Ink4b accompanies tumorigenesis triggered by complex DNA double-strand breaks. *Carcinogenesis* (2010) **31:** 1889-96. (Chapter III)

McEllin B, **Camacho CV**, Mukherjee B, Hahm B, Tomimatsu N, Bachoo RM *et al.* PTEN loss compromises homologous recombination repair in astrocytes: implications for glioblastoma therapy with temozolomide or poly(ADP-ribose) polymerase inhibitors. *Cancer Res* (2010) **70:** 5457-64.

Mukherjee B, McEllin B, **Camacho CV**, Tomimatsu N, Sirasanagandala S, Nannepaga S *et al*. EGFRvIII and DNA double-strand break repair: a molecular mechanism for radioresistance in glioblastoma. *Cancer Res* (2009) **69:** 4252-9.

Mukherjee B, **Camacho CV**, Tomimatsu N, Miller J, Burma S. Modulation of the DNA-damage response to HZE particles by shielding. *DNA Repair (Amst)* (2008)**7:** 1717-30. (Chapter II)

LIST OF FIGURES

LIST OF APPENDICES

LIST OF ABBREVIATIONS

3D	3-dimensional
53BP1	p53 Binding Protein 1
aCGH	Array Comparative Genome Hybridization
AGS	Alternating gradient synchrotron
AKT	Thymoma viral oncogene homolog 1
ARF	Alternate reading frame; p14(human)/ p19(mouse)
AT	Ataxia telangiectasia
ATM	Ataxia telangiectasia mutated
ATR	ATM and Rad3-related protein
BAX	BCL2-associated X protein
Bcl-2	B-cell lymphoma 2
Bcl-XL	B-cell lymphoma-extra large
CDK	Cyclin-dependent kinase
CDKN2A	Cyclin-dependent kinase inhibitor 2A; Ink4a/Arf; p16/p14/p19
CDKN2B	Cyclin-dependent kinase inhibitor 2B; Ink4b; p15
CNV	Copy number variation
CO_2	Carbon dioxide
CRE	Causes recombination
DAPI	4',6-diamidino-2-phenylindole
DDR	DNA-damage response

DM	Double minute
DMEM	Dulbecco's Modified Eagle Medium
DMSO	Dimethyl sulfoxide
DNA	Deoxyribonucleic acid
DNA DSB	DNA double-strand break
DNA-PKcs	DNA-dependent protein kinase catalytic subunit
EGF	Epidermal growth factor
EGFR	Epidermal growth factor receptor
EGFRvIII	Epidermal growth factor receptor version III
E	Energy
ER	Estrogen receptor
Fe	Iron
FISH	Fluorescence *in situ* hybridization
FITC	Fluorescein isothiocyanate
Frag	Fragment
GBM	Glioblastoma Multiforme
GCR	Galactic cosmic rays
GeV	Gigaelectron volt
GFAP	Glial fibrillary acidic protein
Gy	Gray
H2AX	Histone 2A variant X

H&E	Hemotoxylin and eosin
HGF	Hepatocyte growth factor
HRR	Homologous recombination repair
HSF	Human skin fibroblast
HZE	High charge (Z) and Energy (E)
INK4	Inhibitor of CDK4 kinase
IF	Immunofluorescence
IP	Immunoprecipitation
iPS	Induced pluripotent stem cell
IR	Ionizing radiation
keV	Kiloelectron volt
LET	Linear energy transfer
LOH	Loss of heterzygosity
LoxP	Locus of crossover P1
LSS	Life Span Study
MDM2	Murine double minute 2
MEM	Modified Eagle Media
MET	Hepatocyte growth factor
MeV	Megaelectron volt
M-FISH	Multi-color fluorescence *in situ* hybridization
MOI	Multiplicity of infection

MRN	Mre11/Rad50/Nbs1 complex
mRNA	Messenger RNA
mTOR	Mammalian target of rapamycin
NASA	National Aeronautics and Space Adminitration
NF1	Neurofibromatosis 1
NHEJ	Non-homologous end joining
NSC	Neural stem cell
NSCLC	Non-small cell lung cancer
NSRL	NASA Space Radiation Laboratory
PBS	Phosphate buffered saline
PCR	Polymerase chain reaction
PDGFRα	Platelet derived growth factor receptor-alpha
PDGFRβ	Platelet derived growth factor receptor-beta
PFA	Paraformaldehyde
PI3K	phosphoinositide-3-kinase
PIP2	Phosphatidylinositol-4,5-bisphosphate
PIP3	Phosphatidylinositol-3,4,5-trisphosphate
PNA	Peptide nucleic acid
PTEN	Phosphatase and tensin homolog
qPCR	Quantitative PCR
qRT-PCR	Quantitative reverse transcriptase PCR

RB	Retinoblastoma
RBE	Relative biological effectiveness
RET	Rearranged during transfection proto-oncogene
RNA	Ribonucleic acid
RTK	Receptor tyrosine kinase
RCAS	Replication-competent avian sarcoma –leukosis virus
RF	Robertsonian fusion
SA β-Gal	Senescence-associated β-Galactosidase
SGZ	Subgranular zone
shRNA	Short hairpin RNA
SMC1	Structural maintenance of chromosomes 1
SNP	Single nucleotide polymorphism
SSB	Single-strand break
SVZ	Subventricular zone
TCGA	The Cancer Genome Atlas
T-FISH	Telomere fluorescence *in situ* hybridization
TGF-α	Transforming growth factor-alpha
TRP	Translocated promoter region
TUNEL	Terminal deoxyribonucleotidyl transferase-mediated dUTP-digoxigenin nick and labeling
Tv-a	Tumor virus A

μm	Micrometer
WHO	World Health Organization
WT	Wild-type
Z	Atomic number

CHAPTER I

General Introduction

Glioblastoma Multiforme

Glioblastoma Multiforme (GBM) is the most common and malignant type of primary brain tumor in adults. Even though GBM is a relatively rare type of tumor, occuring with highest incidence in the older population and with only 2-3 cases per 100,000 people in North America, it is invariably fatal (Wechsler-Reya and Scott, 2001; Wee et al., 2011, Ohgaki and Kleihues, 2007). Despite significant advancements made in the treatment of many cancers, GBM patients still face extremely poor prognosis. Multimodal aggressive treatment comprising of maximal surgical resection, radiotherapy and chemotherapy, has only been able to extend the median survival time after diagnosis to approximately 15 months (Wee et al., 2011; Krex et al., 2007). Although radiation offers only moderate benefits in the treatment of this inherently radioresistant tumor type, it remains the mainstay of therapy. With an overall 5-year survival rate of only 3% (Sutter et al., 2007, Behin et al., 2003; Gilbert, 2010), GBM remains as one of the most devastating and deadly of all cancers.

GBM is classified as a grade IV diffuse astrocytic tumor by the World Health Organization (WHO grade IV astrocytoma). Traditionally, the classification of brain tumors has been based on the histological resemblance of tumor cells to normal cells present in the adult brain, but although GBM is classified as astrocytic, these tumors are characteristically highly complex and heterogeneous, as indicated by the term ‘multiforme’ (Holland, 2000; Sutter et al.,

2007; Wechsler-Reya and Scott, 2001; Westphal and Lamszus, 2011). Heterogeneity is observed at many levels: macroscopically, GBM shows regions of necrosis and hemorrhage, while microscopically they exhibit pseudopalisading necrosis, cellular pleomorphism, microvascular proliferation, high mitotic activity, and diffuse infiltration of tumor cells into normal tissue. Most importantly, there is heterogeneity observed at the genetic level, with various mutations (discussed below) contributing not only to specific subtypes of GBM, but also to intratumor genetic heterogeneity (Holland, 2000; Maher et al., 2001)

Glioblastomas are divided into two subtypes, primary or secondary glioblastomas. Primary GBM arises *de novo*, without any clinical or histopathological evidence of a pre-existing, less-malignant precursor lesion. On the other hand, secondary GBM is first diagnosed as lower-grade astrocytomas (grade II or III) that over time, through the step-wise acquisition of multiple genetic mutations, manifest as glioblastoma **(Fig 1.1)**. At a population level, more than 90% of cases are primary GBM, arising in patients with a mean age of 62 years, whereas secondary GBM is rarer and tends to develop in younger patients, approximately 45 years mean age. These two subtypes also develop through different genetic pathways, where primary GBM is characterized by epidermal growth factor receptor (EGFR) amplifications/mutations, while p53 mutations are dominant in secondary GBM (details outlined below). Despite this conceptual

distinction, it is important to point out that these subtypes are histopathologically indistinguishable (Rankin et al., 2011, Ohgaki and Kleihues, 2007).

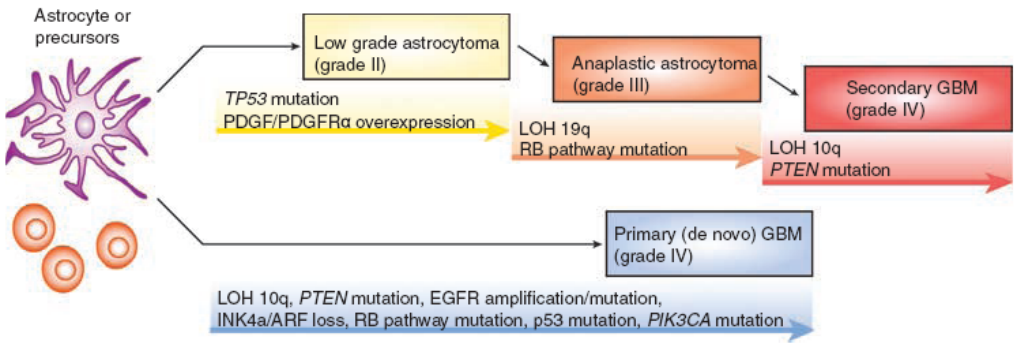

Figure 1.1 Genetic pathways involved in GBM development. Several pathways are frequently disrupted in the initiation and progression of GBM. Disruption of p53 occurs through mutations, MDM2 amplification, or ARF deletion. Disruption of the RB pathway by loss of CDKN2A/B or RB loss are frequently observed. Activation of growth factor signaling through receptor tyrosine kinase mutation or amplfication (EGFR and/or PDGFR) or PTEN loss is also common (Image by Endersby and Baker, 2008).

Key signaling Pathways Disrupted in GBM

Over the last two decades, significant insights into the molecular mechanisms underlying gliomagenesis and pathogenesis have been gained. Due to the high lethality associated with GBM, it is not surprising that it was the first cancer type to undergo comprehensive genomic characterization by The Cancer Genome Atlas (TCGA) Research Network. This large-scale integrated genomic analysis of hundreds of GBM specimens confirmed the importance of key genetic events occurring in three distinct signaling pathways commonly disrupted in human GBM: the receptor tyrosine kinase (RTK)/ phosphoinositide-3-kinase (PI3K) pathway, the p53 pathway and the retinoblastoma (RB) pathway (TCGA, 2008; Cerami et al., 2010).

1) **Receptor tyrosine kinase (RTK)/ phosphoinositide-3-kinase (PI3K) pathway:** Dysregulation of growth factor signaling is commonly achieved through amplification or mutational activation of various RTKs, most prominent being the epidermal growth factor receptor (EGFR). EGFR is membrane-bound and becomes activated upon binding of growth factors (epidermal growth factor [EGF], transforming growth factor-α [TGF-α], heparin-binding EGF, amphiregulin, epiregulin, betacellulin or decorin) to its extracellular domain. Ligand binding drives dimerization of receptor monomers, leading to reciprocal tyrosine phosphorylations which serve as docking sites for an array of signaling molecules, such as PI3K. PI3K

phosphorylates phosphatidylinositol-4,5-bisphosphate (PIP2) to phosphatidylinositol-3,4,5-trisphosphate (PIP3), activating downstream effector molecules such as AKT (thymoma viral oncogene homolog 1) and mTOR (mammalian target of rapamycin). Signaling through this pathway results in pro-proliferative and pro-survival cues, which are the driving forces of malignant cellular transformation (Lorimer, 2002; Maher et al., 2001; Ohgaki and Kleihues, 2007, Halatsch et al., 2006). Counteracting this signaling is the tumor suppressor PTEN (phosphatase and tensin homolog). PTEN functions primarily as a lipid phosphatase that dephosphorylates PIP3 to PIP2, leading to signal attenuation **(Fig 1.2)**. Deletion of PTEN through loss of heterzygosity (LOH) of chromosome 10q and mutations in its phosphatase domain are common mechanisms of inactivation in GBM, found in up to 80% of cases (Cully et al., 2006; Salmena et al., 2008; Endersby and Baker, 2008). EGFR is often overexpressed in a variety of cancers due to amplification, and plays an important role in primary GBM. Approximately 50% of glioblastomas exhibit EGFR alterations (amplification or mutation), and half of those concurrently express a mutant variant form called EGFRvIII, a mutation specific to glioblastomas (TCGA, 2008; Maher et al, 2001; Zhang et al., 2007; Bublil and Yarden, 2007; Ohgaki and Kleihues, 2007). EGFRvIII harbors a large deletion of exons 2 through 7. This truncated form of EGFR

lacks the extracellular binding domain, but is however constitutively activated; it has been shown to dramatically enhance

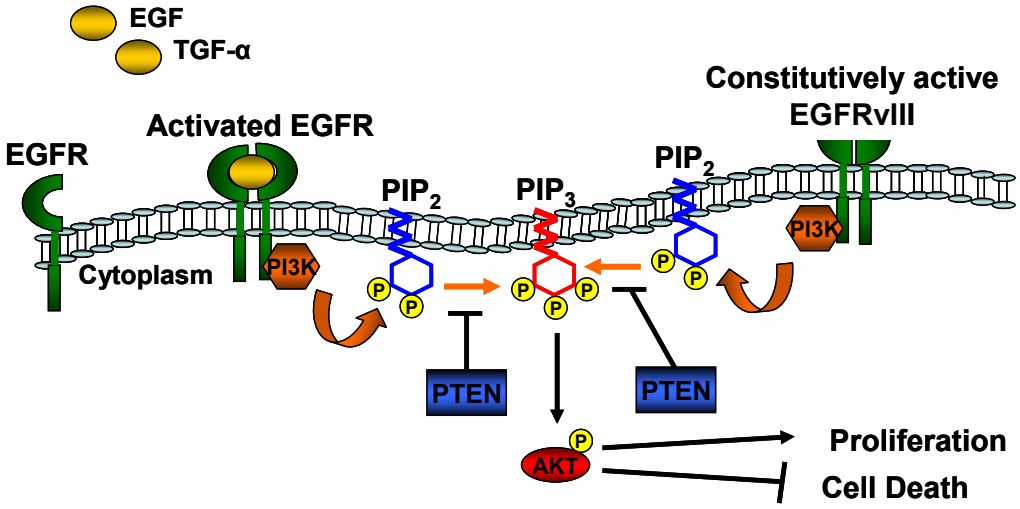

Figure 1.2. Receptor tyrosine kinase (RTK)/ phosphoinositide-3-kinase (PI3K) pathway. A simplified shematic depicting RTK/PI3K signaling. Membrane-bound EGFR binds its ligands (such as EGF and TGF-α), dimerizes and is activated by reciprocal tyrosine phosphorylations. PI3K is recruited to membrane, phosphorylating PIP2 to PIP3, activating downstream effectors such as AKT. PTEN dephosphorylated PIP3 to PIP2, attenuating the signal.

tumorigenesis *in vivo* when expressed in glioma cells by increasing proliferation and reducing apoptosis (Ekstrand et al., 1994; Nagane et al., 1996). EGFRvIII expression has been associated with worse prognosis and shorter life expectancy (Shinojima et al., 2003; Brandes et al., 2008). Studies have shown that EGFR translocates into the nucleus in response to radiation, where it directly interacts with and enhances the activity of the DNA-repair enzyme DNA-PKcs (Dittmann et al., 2005). In the context of GBM, it has also been shown that EGFRvIII can hyperactive DNA-PKcs, providing a molecular basis for the inherent radioresistance of this tumor type. (Mukherjee et al., 2009; Mukherjee et al., 2011; Golding et al., 2009; Raizer 2005; Milas et al., 2004; Weppler et al., 2007). The high frequency of EGFR associated alterations has made it an important target of inhibition in the treatment of GBM. Unfortunately, single-agent targeted therapies have not had significant improvements in the overall survival of patients, primarily due to concomitant activation of multiple RTKs. Other important RTKs also found to be altered in GBM, although at a much lower frequency, are the platelet derived growth factor receptors α and β (PDGFRα and PDGFRβ), and the hepatocyte growth factor receptor (MET) amplified in 13% and 4% of glioblastomas respectively. Interestingly, recent studies have shown that MET gene amplification is a mechanism by which tumors acquire resistance EGFR inhibitors (Engelman et al., 2007). Amplification of MET, with consequent

protein overexpression, can be a feature required to maintain the primary transformed phenotype or a secondary occurrence that serves to aggravate the malignant phenotype, by promoting metastasis for example (Trusolino et al., 2010; Comoglio et al., 2008). Targeted therapies against MET could therefore be effective as a means of treating MET-addicted tumors, or blocking tumor progression and metastatic spread; multiple drugs are currently in early phase clinical trials (Comoglio et al., 2008).

2) **p53 pathway:** In order to abrogate p53 signaling, multiple components of this pathway are also found to be altered. The tumor suppressor p53 is a transcription factor which positively or negatively regulates the expression of a large set of target genes involved in various cellular processes. Activation of p53 in response to DNA damage, oncogenic signaling, and metabolic stress to name a few, results in a number of distinct responses, including cell cycle arrest, senescence, cell death, and DNA repair (Fuster et al., 2007; Horn and Vousden, 2007; Maher et al., 2001; Lozano, 2007). One important transcriptional target of p53 is the cyclin-dependent kinase (CDK) inhibitor p21 Waf/Cip1. As CDKs drive the progression of the cell through the cell cycle, activation of p53 and consequent upregulation of p21 results in cell cycle arrest. For example, in response to DNA damage, this transient cell cycle arrest allows the cell time to repair the DNA damage and prevents expansion of damaged or mutated cells. If the initial damage cannot be

repaired, p53 can promote permanent cell cycle arrest (senescence) or trigger programmed cell death (apoptosis) by transcriptional upregulation of Puma, Noxa, BAX (BCL2-associated X protein) or induce apoptosis by directly binding to anti-apoptotic proteins like Bcl-2 (B-cell lymphoma 2) and Bcl-XL (B-cell lymphoma-extra large) (Bode and Dong, 2004). A key regulator of p53 function is the murine double minute 2 (MDM2) oncoprotein. MDM2 inhibits p53 activity by two mechanisms: it can directly bind to the transcriptional activation domain of p53 and thereby block its ability to interact with the basic transcriptional machinery, or it can act as a p53-specific E3 ubiquitin ligase, targeting p53 for nuclear export and degradation by the proteasome (Toledo and Wahl, 2006; Kim and Sharpless, 2006; Wawrzynow et al., 2007). Another component of this pathway is the tumor suppressor p14/ARF (alternate reading frame of *CDKN2A*; p19/ARF in mouse). In response to oncogenic signaling, ARF can bind to MDM2 and block its E3 ubiquitin ligase activity, thereby allowing stabilization of p53 and hence activation of its targets **(Fig 1.3A)** (Kim and Sharpless, 2006; Fuster et al., 2007). Mutations in p53 are the most frequent (>60%) and earliest detectable genetic alterations in secondary GBM. On the other hand, amplification of MDM2 is present in 14% of GBM, and is found almost exclusively in glioblastomas that lack p53 mutations. Finally, abrogation of ARF expression in both GBM subtypes (approximately 52%) is attained

through homozygous deletion of the *CDKN2A/CDKN2B* locus (discussed in detail below) or promoter methylation (Brennan, 2011; TCGA, 2008; Ohgaki and Kleihues, 2007; Kim and Sharpless, 2006).

3) **Retinoblastoma (RB) pathway:** The retinoblastoma protein (pRB) is also a major regulator of cell cycle progression. In a quiescent, non-dividing cell, pRB remains in its hypophosphorylated state, bound to the transcription factor E2F. Binding of pRB to E2F prevents progression through the G1/S checkpoint, promoting a G1 cell cycle arrest. In response to proliferative signals, complexes of cyclin D1 and CDKs 4 and 6 initiate phosphorylation of pRB, releasing E2F and allowing for transcription and activation of genes involved in the G1 to S transition. The INK4 class of cell cycle inhibitors p16/Ink4a, p15/Ink4b, p18/Ink4c and p19/Ink4d bind to and inhibit CDKs by abrogating binding to the D-type cyclins, in turn preventing CDK-mediated phosphorylation of pRB, culminating in G1 arrest. Interestingly, the three tumor suppressors p15/Ink4b, p16/Ink4a and p19/ARF (discussed above) all reside in a small 35 kilobase stretch within the genome. Whereas p15/Ink4b has its own open reading frame, p16/Ink4b and p19/ARF have different first exons that are spliced to a common second and third exon (Sharpless, 2004) **(Fig 1.3B)**. Homozygous deletion of this entire locus (Ink4a/ARF/Ink4b, also known as *CDKN2A* and *CDKN2B*) is a common event in GBM and thus forms the basis of the models used in this body of work. Coupled with

mutations and methylation, this component of the RB pathway is altered in 52% of cases. CDK4 is found amplified in nearly 18%, while pRB is inactivated by homozygous deletion, mutation, or methylation in 11% of GBMs (Brennan, 2011; TCGA, 2008; Ohgaki and Kleihues, 2007; Maher et al., 2001; Kim and Sharpless, 2006).

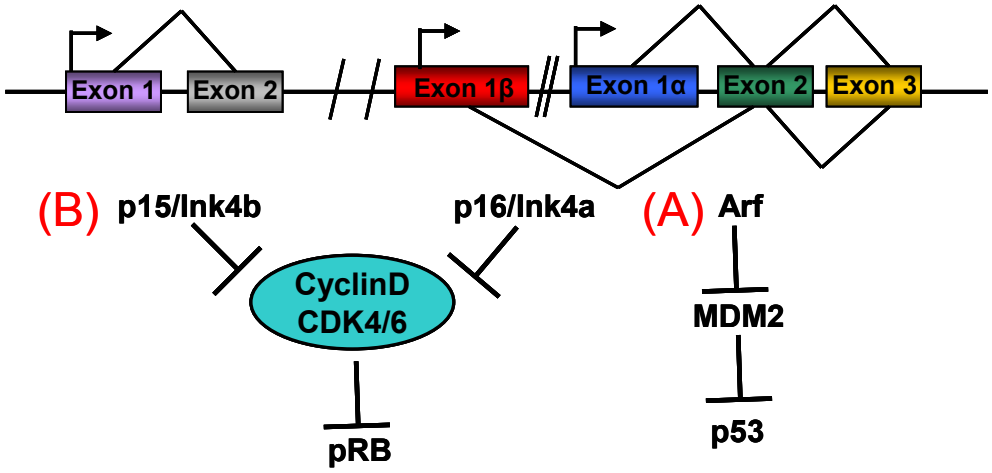

Figure 1.3. Regulation of RB and p53 pathways. The Ink4a/ARF/Ink4b locus encodes three genes with 35 kilobases: p16/Ink4a, ARF and p15/Ink4b. **(A)** ARF inhibits MDM2, resulting in p53 stabilization. **(B)** Members of the INK4 family of CDK inhibitors bind to and inactivate CDK4/6, maintaining Rb-family proteins in a hypophosphorylated state, resulting in G1 arrest.

Mouse Models of Gliomagenesis

The development of mouse models has allowed for systematic evaluation of the contribution of each specific pathway known to be disrupted in human GBM (as discussed above) to the initiation, promotion, progression and maintenance of gliomas. Various strategies have been employed in an effort to generate a mouse model that closely resembles the human disease.

Transplantation models using human glioma cell lines injected subcutaneously or orthotopically into immunocompromised mice are advantageous because they are highly reproducible, with high tumor growth rates and incidence. However, they lack in one very important aspect, and that is that these tumors grow in an inaccurate microenvironment and do not mimic the invasive nature of the disease (Hambardzumyan et al., 2011; Rankin et al., 2011; Maher et al., 2001; Wee et al., 2011). Other drawbacks include the use of glioma cell lines cultured *in vitro* that have been shown to poorly represent the genomic changes and gene expression profiles of primary human gliomas (Li et al., 2008). Also, given the importance of immune surveillance in recognizing and eliminating incipient cancer cells, the normal course of tumor progression cannot be fully recapitulated in an immunocompromised model system (Hanahan and Weinberg, 2011).

Over the years, more sophisticated techniques have resulted in multiple genetically engineered mouse models, in which glioma-relevant alterations have

been conditionally targeted to the brain, or specific cell-types of the brain, through the use of the Cre-Lox system. In this system, Cre (Causes recombination) expression is driven by a tissue-specific promoter, mediating deletion of target genes that are flanked by LoxP (locus of crossover P1) sequences (Hambardzumyan et al., 2011; Cheon and Orsulic, 2010; Wee et al., 2011). The most popular drivers of Cre recombinase used in glioma modeling are the nestin promoter, directing expression in neural progenitor cells, or GFAP (glial fibrillary acidic protein) promoter, targeting mature astrocytes and a subpopulation of progenitor cells in the subventricular zone (SVZ) (Gaveriaux-Ruff and Kieffer, 2007). Spatial activation of cre recombinase has been further refined by use of an inducible Cre system which allows for temporal regulation of Cre activity, hence gene deletion or oncogene activation. This has been achieved through the fusion of Cre to a mutated estrogen receptor ligand binding domain (Cre-ER). Upon tamoxifen administration, the Cre-ER fusion protein is able to translocate to the nucleus and mediate recombination (Rankin et al., 2011; Cheon and Orsulic, 2010, Wee et al., 2011; Holland, 2001). Examples include GFAP-Cre/K-rasG^{12D} mice, which develop bilateral, multifocal, infiltrating glioma with 100% penetrance in and Ink4a/ARF-deficient background (Abel et al., 2009; deVries et al., 2010), hGFAP-Cre; $NF1^{f/f}/p53^{-/-}$ and Nestin-Cre-ER^{T2}; $NF1^{f/+};p53^{f/f};PTEN^{f/+}$ mice, which develop high-grade, diffusely infiltrating astrocytomas or GBM (Zhu et al., 2005; Kwon et al., 2008; Alcantara-Llaguno et

al., 2009), and hGFAP-Cre/ $p53^{f/f}$;$PTEN^{f/+}$ mice which develop high-grade astrocytomas or GBM (Zheng et al., 2008).

In order to mimic tumor initiation which presumably takes place in a single cell through step-wise accrual of various mutations resulting in a growth advantage and clonal expansion, somatic gene transfer strategies have also been widely used. Strategies involving viral delivery of oncogenes use primarily the RCAS/tv-a system. First, the retrovirus RCAS (replication-competent avian sarcoma –leukosis virus) in engineered to encode powerful oncogenes, such as EGFR, Akt, K-ras, etc. Infection of cells by the retrovirus is accomplished by engineering mice that express the viral receptor tv-a (tumor virus A) under tissue-specific promoters, such as Nestin (Ntv-a) and GFAP (Gtv-a). Other non-targeted approaches involve the use of lentiviruses or adenoviruses for delivery of the desired oncogene (Hambardzumyan et al., 2011; Hambardzumyan et al., 2009; Wee et al., 2011; Cheon and Orsulic, 2010; Holland, 2001). Examples include the RCAS-EGFR*/Gtv-a or Ntv-a system, which induces glioma-like lesions in Ink4a/ARF deficient mice (Holland et al., 1998), RCAS-K-ras+Akt/Gtv-a or Ntv-a, which results in the formation of gliomas with variable astrocytic character in Ink4a/ARF deficient mice (Uhrbom et al., 2002; Uhrbom et al., 2005), and the RCAS-$BRAF^{V600E}$ or RCAS-MEK/Ntv-a system, which induces highly invasive and necrotic gliomas also in the context of Ink4a/ARF deficiency (Robinson et al., 2010a; Robinson et al., 2010b), and combined delivery of pTomo-Flag H-

RasV12 and Akt lentiviral vectors in GFAP-Cre; $p53^{+/-}$ mice resulting in the formation of high-grade gliomas (Marumoto et al., 2008).

Radiation and Gliomagenesis

Even though a substantial amount of progress has been made in understanding and modeling the critical genetic alterations underlying gliomagenesis, very little is known about the etiology of GBM and other central nervous system tumors in general. With few exceptions, most glioblastomas appear to be sporadic, without any known genetic predispositions (Krex et al., 2007). Multiple studies have tried to evaluate and link specific risk factors to glioblastoma, such as smoking (Zheng et al., 2001), diet (Lee et al., 1997), ionizing radiation (Neglia et al., 1991), electromagnetic fields (Theriault et al., 1994), medical risk factors such as allergies (Weimels et al., 2002) and viral infections (Vilchez et al., 2003) to name a few. To date, the only established risk factor clearly and unequivocally linked to glioblastoma is ionizing radiation (IR). Extensive epidemiological evidence exists, primarily from pediatric and adolescent populations that have been exposed to IR, showing elevated risk and incidence of brain tumors (Salvati et al., 2003; Cavin et al., 1990; Shapiro et al., 1989). Examples include children given therapeutic irradiation to the scalp for the treatment of tinea capitis (Sadetzki et al., 2005; Ron et al., 1988), and pediatric patients receiving prophylactic cranial irradiation for treatment of leukemia or

lymphoma (Neglia et al., 1991; Brustle et al., 1992). Importantly, a study carried out at the Ames Research Center showed that 3 out of 10 monkeys exposed to high-energy protons and surviving 3-5 years post-IR developed glioblastomas (Haymaker et al., 1972). A report also exists of a single monkey developing glioblastoma 2.8 years after receiving irradiation to the spinal cord (Price et al., 1996). With substantial epidemiological evidence, radiation is accepted as the only known risk factor for developing GBM.

Radiation Carcinogenesis

The association between radiation and carcinogenesis was recognized soon after the discovery of X-Rays in 1985. Within a few years, the first radiation-induced cancer was identified arising in an ulcerated area of the skin, followed by multiple cases of skin cancers and leukemias occurring in radiation workers (Samet, 2011; Williams, 2008; Little, 2000; Wakeford, 2004). To date, evidence supporting the carcinogenic potential of IR stems from various epidemiological studies on human populations that have been exposed to radiation from occupational, medical and accidental sources. The largest body of supporting evidence comes from the ongoing Life Span Study (LSS), a cohort of 120,000 atomic bomb survivors from the Hiroshima and Nagasaki nuclear blasts (Samet, 2011; Little, 2000).

Ionizing radiation refers to radiation that has sufficient energy to eject one or more orbital electrons from the atoms of exposed materials. Radiation is classified as electromagnetic or particulate. Electromagnetic radiation (X- or gamma-rays) is composed of photons, which deposit their energy in a uniform and sparse fashion (low linear-energy transfer [LET]) **(Fig 1.4A)**. Particulate radiation on the other hand, refers to physical particles such as electrons, protons, α-particles, neutrons, and heavy charged particles. Particulate radiation differs significantly from photons in the manner in which it spatially ionizes its target. Heavy particles cause dense tracks of ionization along their trajectories (high-LET) (Hall, 2006) **(Fig 1.4B)**. In either case, radiation can interact directly or indirectly with the target material, that is the DNA of mammalian cells. Direct action means that the atoms of the target itself may be ionized or excited, resulting in a chain of events that leads to a biological effect. This is the dominant form of interaction for high-LET radiations. Indirect action, on the other hand, means that radiation interacts with other atoms or molecules, such as water in the cell, to produce free radicals that are then able to cause damage to the target material. This process is most dominant with sparsely ionizing radiation (Hall, 2006).

A unique feature of high-LET particles is the ability to efficiently induce complex or clustered DNA lesions. These lesions consist of multiple closely spaced damages, such as single-strand breaks (SSBs), double-strand breaks

(DSBs), oxidized bases and apurinic-apyrimidinic (AP) sites, within a short segment of DNA (Hada and Georgakilas, 2008). This feature of heavy particles enhances the biological effect per unit dose absorbed when compared to X- or gamma-rays (Hall, 2006). Carcinogenesis is a complex process, requiring multiple steps to initiate, promote, progress and maintain tumorigenesis. In the case of radiation-induced carcinogenesis, very little is known about the underlying mechanisms. The damaging effects of ionizing radiation are based on its ability to directly or indirectly break chemical bonds in a target material, such as a cell. Within a cell, the critical target which results in a biological effect (cell killing, mutation, and carcinogenesis), is DNA. One way in which DNA can be damaged by radiation is through the induction of strand breaks; single-strand breaks (SSBs) are readily repaired, and hence have negligent biological consequences. However, if the single-strand breaks occur in close proximity and on opposing strands, they result in double-strand breaks (DSBs), the most toxic of all DNA lesions (Hall, 2006). DSBs are extremely effective at promoting cell death, but breaks that are illegitimately repaired allowing cell survival, are responsible for chromosomal abnormalities and gene mutations, important events in the initiation of cancer (Wakeford, 2004; Little, 2000).

Radiation is an indispensable tool for effective cell-killing during treatment of many cancers. However, it is the nonlethal DNA modifications that are the root of an emerging problem in radiotherapy. Over the years, advances

made in screening, early detection and treatment modalities have allowed for cancer patients to live much longer. Unfortunately, coupled with longer survival is the increased risk of developing secondary cancers as a late consequence of radiation exposure for the treatment of the initial primary tumor (Morton and Chanok, 2011; Newhauser and Durante, 2011). The more recent clinical use of protons and heavier ions in the treatment of non-small cell lung cancer (NSCLC), prostate, head and neck cancers to name a few, raises concerns about safety of these particles. With the increased use of particle therapy, it is speculated that the risks, as well as the benefits, will greatly increase (Newhauser and Durante, 2011; Schulz-Ertner and Tsujii, 2007). Outside the clinic, space radiation, composed of high-energy protons and HZE (high charge [Z] and energy [E]) particles, poses a significant cancer risk to astronauts during prolonged missions (Durante and Cucinotta, 2008). Currently though, significant uncertainties exist in estimates of cancer risks from exposure to heavy ion particles given that there is no epidemiological data from human populations that have been exposed to such radiation quality (Newhauser and Durante, 2011; Maalouf et al., 2011; Durante and Cucinotta, 2008).

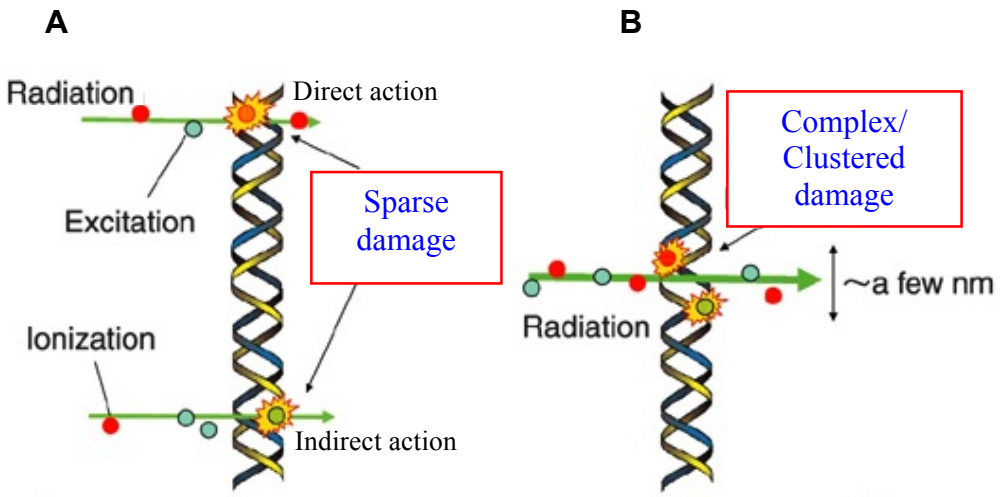

Figure 1.4. Induction of DNA damage by ionizing radiation. Radiation can be directly or indirectly ionizing **(A)**. Electromagnetic radiation causing ionization at low density (low LET radiation) creates randomly isolated damage **(A)**, whereas particulate radiation, ionizing in high density (high LET radiation) induces clustered DNA damage, which is defined as multiple lesions (SSBs, DSBs, and/or AP site) within a few nanometers in a DNA molecule **(B)** (Image modified from Urushibara et al., 2008).

Modeling Radiation-Induced Gliomagenesis

The work presented here sets out to gain a better understanding of the molecular mechanisms of radiation-induced gliomagenesis by testing the hypothesis that DSBs cooperate with tumor suppressor loss to initiate gliomagenesis in a sensitized model system. Importantly, the question of whether complex lesions induced by particle irradiation are more tumorigenic when compared to gamma-rays, which induce breaks that are more easily repaired is carefully addressed. Finally, a critical analysis of the genomic and gene expression changes underlying radiation-induced transformation in our model systems has been carried out. This work can thus be summarized as follows:

1) Short-term biological responses to two very different qualities of radiation, gamma- and particle- irradiation (representing transient vs persistent DNA lesions) were examined *in vitro* using normal human skin fibroblasts (Chapter II).
2) A simple yet sensitive *in vitro* model system, *CDKN2A*- knockout astrocytes, was used to evaluate long-term biological responses to ionizing radiation, namely transformation and tumorigenesis. This mutation (*CDKN2A*-loss) and cell type (astrocytes) are both relevant to GBM given that loss of *CDKN2A* is thought to be one of the earliest events in gliomagenesis, and provide a useful system to quickly examine transformation *in vitro* (Chapter III).

3) Based on *in vitro* results, a mouse model with targeted *CDKN2A/B* deletions to the brain was used to evaluate gliomagenesis and underlying genomic changes in a fully *in vivo* system (Chapter IV).

CHAPTER II

DNA damage responses to gamma- versus particle irradiation

INTRODUCTION

High atomic number and high energy (HZE) particles are the most damaging component of galactic cosmic rays (GCR) and a serious health risk for humans in space, especially outside the protective effects of the Earth's magnetic field (NAS, 2006; Setlow, 2003). Originating in cataclysmic astronomical events such as supernova explosions, the GCR is composed of protons (85%), alpha particles (14%) and HZE particles (about 1%) (Simpson et al., 1983). HZE particles, while relatively small in number, are highly ionizing and penetrating. It is accepted that they have a higher relative biological effectiveness (RBE) compared to gamma-rays and must pose a significant cancer risk to humans in space (ICRP, 1991). Heavy ions are also being increasingly used in targeted cancer therapy because of their higher RBE and because particle beams can be focused so as to deliver a much greater dose to the tumor while sparing normal tissue (Halperin, 2006).

From a biological standpoint, large uncertainties exist in estimates of cancer risks from HZE particles because of limited data on their biological effects (Cucinotta et al., 2001; Esposito et al., 2005). Previous attempts to directly evaluate the biological effects of these particles at the cellular level involved relatively late end points such as chromosome aberrations and cell survival and transformation (Brooks et al., 2001; George et al., 2001; Durante et al., 2005; Alpen et al., 1993; Yang et al., 1985; Yang et al., 1997). The major

damage inflicted by ionizing radiation, whether gamma-rays or high-Z ions, is DSBs; an inadequate or improper response to these breaks will promote carcinogenesis (Bartkova et al., 2006; Burma et al., 2006; Di Micco et al., 2006; Gorgoulis et al., 2005; Halazonetis, 2004; Khanna and Jackson, 2001). The mammalian DNA damage response (DDR) involves orchestration of multiple events including recruitment of kinases/adaptors/substrates to DNA breaks, phosphorylation of chromosomal/recruited proteins at these breaks and implementation of DNA repair/cell cycle arrest/apoptosis (Shiloh, 2006). The goal of the work presented here is to evaluate the long-term carcinogenic and transforming potential of heavy particles when compared to gamma-rays, both *in vitro* (Chapter III) and *in vivo* (Chapter IV). However, understanding short-term biological responses to these breaks is a necessary foundation for examining long-term consequences. For this initial stage of my project, I worked closely with Dr Bipasha Mukherjee, a senior member of the laboratory, to examine pertinent DDR events in order to understand the short-term biological consequences of heavy ion irradiation, whether in space or in the clinic.

MATERIALS AND METHODS

Irradiation, dosimetry, and LET spectrum calculation. Particle beams were provided by the NASA Space Radiation Laboratory (NSRL) at Brookhaven National Laboratory. After acceleration in the AGS Booster

synchrotron, particles are extracted and transported to an irradiation station on which dose monitoring and beam characterization devices and experimental samples are mounted. The dose is measured by ionization chambers—which have very low mass and affect the beam energy and composition only slightly—and monitored by a computer-controlled dosimetry system that automatically cuts off the beam when the specified dose is reached. For these experiments, the linear-energy transfer (LET) spectrum of radiation incident on the targets was measured by silicon solid-state detectors with areas similar to that of the biological samples. Energy lost by a charged particle in the silicon is converted into a voltage signal that is digitized and converted to an energy loss or LET spectrum. This system is similar to the beam characterization method described in (Zeitlin et al., 1998). For gamma-ray irradiation, a ^{137}Cs source (JL Shepherd and Associates, CA) was used.

Cell culture, immunostaining, and microscopy. Low passage (4 to 6 population doublings), primary human skin fibroblasts (HSFs) (Ding et al., 2005) and primary ATM-deficient fibroblasts (AT2052)(Sasai et al., 1994) were maintained in alpha-MEM media supplemented with 10% fetal bovine serum in a humidified 37°C incubator in the presence of 5% CO_2. Cells were seeded in glass chamber slides 48 hours before irradiation such that they were approximately 70% confluent at the time of irradiation. Cells were irradiated with a total dose of 1 Gy, fixed at the indicated time points, and co-immunostained with anti-γH2AX

(clone JBW301; Upstate) and anti-53BP1 (Cell Signaling) primary antibodies and Rhodamine Red-conjugated goat anti-mouse and FITC-conjugated goat anti-rabbit secondary antibodies (Molecular Probes) as described in (Mukherjee et al., 2006). For imaging particle-generated damage tracks, cells were irradiated parallel to the particle beams, fixed at 0.5 h post-irradiation, and immunostained. A stack of images along the Z-axis (ten image slices at intervals of 0.38 μm) was obtained with a Zeiss LSM 510 META laser scanning confocal microscope. Z-stacks obtained were used to generate 3D reconstructions of nuclear regions with DNA damage using Imaris software. To obtain DNA repair kinetics, cells were irradiated vertical to the particle beams, fixed at time points ranging from 0.5 to 24 h post irradiation, and immunostained. The number of γH2AX or 53BP1 foci was determined for each time point (average of 100 nuclei) and, after subtracting background (number of foci in unirradiated nuclei), the percentage foci remaining was plotted against repair time to obtain DNA repair kinetics.

Treatment with ATM or DNA-PKcs inhibitors. Where indicated, cells were pre-treated for 1h with the DNA-PKcs inhibitor NU7026 (Veuger et al., 2006) or with the ATM inhibitor KU55933 (Hickson et al., 2004), both at 10 μM, prior to irradiation.

Western blotting. HSFs were mock-irradiated or irradiated with a total dose of 4 Gy and protein extraction and Western blotting were carried out as described before (Mukherjee et al., 2006). The antibodies used were anti-DNA-

PKcs (phospho-serine2056) (Abcam), anti-DNA-PKcs (clone25-4) (Neomarkers), anti-Ku80 (kind gift from David Chen), anti-ATM (phospho-serine1981) (GenScript Corporation), anti-ATM (clone 2C1) (Santa Cruz Biotechnology), anti-SMC1 (phospho-serine966) (Bethyl Laboratories), anti-SMC1 (Bethyl Laboratories), anti-p53(phospho-serine15) (Cell Signaling Technology), anti-p53(clone DO-1) (Santa Cruz Biotechnology), anti-p21 (Santa Cruz Biotechnology), anti-p16 (Calbiochem), and anti-actin (Sigma).

Senescence-associated β-galactosidase activity assay. HSFs were mock-irradiated or irradiated (4 Gy), fixed after 10 days and stained with an X-gal-containing reaction mixture using a Senescent Cell Staining Kit (Sigma). The proportion of senescence-associated β-galactosidase (SA β-Gal)-positive cells was quantified using an Olympus microscope with 20X objective. Flasks were stained in triplicate with about 1000 cells scored per flask.

Radiation survival assay. To determine radiation survival, cells were plated in T25 flasks and irradiated with radiation doses ranging from 0-4 Gy. After 10-14 days, surviving colonies were stained with crystal violet, colonies with more than 50 cells scored and mean values for triplicate counts determined as described in (Kurimasa et al., 1999). Cell survival was normalized to plating efficiency of untreated controls.

RESULTS

Human cells are incapable of completely repairing DNA damage inflicted by Fe ions. Iron ions are the most densely ionizing particles that are present in significant numbers in the GCR (Miller et al., 2005). Therefore, in this study, we used ^{56}Fe ions with a kinetic energy of approximately 1 GeV/nucleon at the NASA Space Radiation Laboratory (NSRL) at Brookhaven National Laboratory. 1 GeV/nucleon is near the peak of the GCR energy spectrum (Simpson et al., 1983). The ionization energy loss per unit path length of charged particles is conventionally expressed as linear energy transfer (LET) in water. For 1 GeV/nucleon Fe ions, the LET in water is approximately 150 keV/μm (Zeitlin et al., 1998). Gamma rays from a ^{137}Cs source, which have an LET of about 0.8 keV/μm, were used for comparison. Very early passage (4 to 6 population doublings) human skin fibroblasts (HSFs) (Ding et al., 2005) were used in this study as they, unlike established cell lines, exhibit very low levels of background DNA damage **(Fig 2.1A)**. Two end points were used to visualize DSBs and to quantify repair: 1) the extensive phosphorylation of histone H2AX at the sites of DSBs resulting in discrete γ-H2AX "foci" that constitute the "gold standard" for measuring rates of DSB repair (Burma et al., 2001; Fernandez-Capetillo et al., 2004) and 2) the rapid recruitment of 53BP1 to DSBs that occurs in a γ-H2AX-dependent manner (Mochan et al., 2004). HSFs growing on glass

slides were irradiated with Fe ions at the NSRL as described in materials and methods.

Gamma rays result in diffuse DNA damage as is evident from the 3D reconstructions derived from Z-stack images **(Fig 2.1B)**. In striking contrast, a single Fe ion leaves in its wake a well-defined track of DNA damage consisting of voluminous areas of H2AX phosphorylation and 53BP1 accumulation. Such γH2AX tracks have been reported before (Desai et al., 2005; Jakob et al., 2003; Asaithamby et al., 2008) and are entirely consistent with the unique pattern of energy deposition associated with heavy ions (Magee and Chatterjee, 1980). Cells irradiated with 1 Gy of gamma-rays are mostly able to complete DSB repair by 12 h as has been demonstrated before (Kuhne et al., 2004) **(Fig 2.1C, D and E)**. In contrast, cells irradiated with 1 Gy of Fe ions are unable to repair approximately 30 percent of the initial DNA damage incurred by 12 h; no evidence of further repair is seen after 12 h. Similar results obtained with both γH2AX and 53BP1 (which co-localize at the sites of DSBs as is evident from the merged images) attest to the accuracy of these findings. These results corroborate the impaired repair of HZE-inflicted DNA damage reported previously (Desai et al., 2005; Asaithamby et al., 2008; Karlsson and Stenerlow et al., 2004).

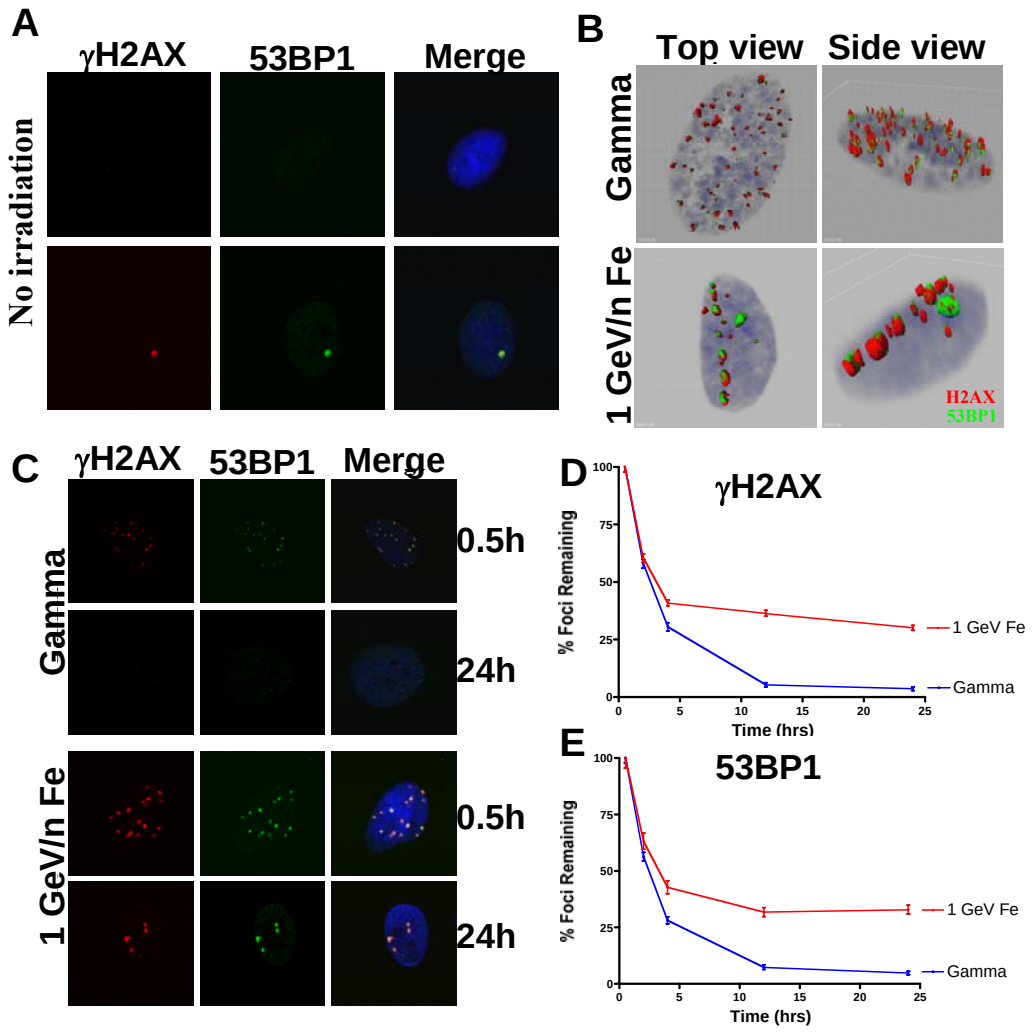

Figure 2.1. DNA damage responses to high Z particles. (A) Early passage, primary HSFs were co-immunostained with anti-γH2AX (red) and anti-53BP1 (green) antibodies. Nuclei were stained with 4,6-diamidino-2-phenylindole (DAPI) (blue). The majority of nuclei (approximately 90%) display no background DNA damage as evidenced by the absence of γH2AX or 53BP1 foci (top panel). The remaining nuclei display an average of one focus per nucleus (bottom panel). **(B)** For imaging particle-generated damage tracks, cells were irradiated parallel to the particle beam, fixed at 0.5 h post irradiation, and immunostained. A stack of images along the Z-axis (ten image slices at intervals of 0.38 µm) was obtained and used to generate 3D reconstructions using Imaris software. Please note a discrete track of DNA damage in the nucleus traversed by

a Fe particle in sharp contrast to the diffuse areas of DNA damage induced by gamma-rays. **(C)** HSFs were irradiated with 1 Gy of γ-rays or with 1 Gy of 1 GeV/nucleon Fe and co-immunostained at time points ranging from 0.5 to 24 h post irradiation. The pictures depict the initial DNA damage (0.5 h) and the residual DNA damage (24 h). **(D, E)** γH2AX or 53BP1 foci were scored at 0.5, 2, 4, 12 and 24 h post-irradiation. The number of γH2AX or 53BP1 foci was determined for each time point (average of 100 nuclei) and, after subtracting background (number of foci in unirradiated nuclei), the percentage foci remaining was plotted against repair time to obtain DNA repair kinetics. Error bars represent standard error of the mean. Please note nearly complete repair in cells irradiated with γ-rays and incomplete repair in cells irradiated with Fe particles. The difference in percent foci remaining at 24 h post-irradiation was determined to be statistically significant by a two-tailed t test (P value < 0.0001).

Both DNA-PKcs and ATM are required for the repair of Fe ion-induced DNA damage. Non-homologous end-joining (NHEJ) is the predominant repair pathway in mammalian cells that responds to gamma ray-induced DSBs (Burma et al., 2006). NHEJ occurs in two phases: 1) an initial rapid phase (dependent on DNA-PKcs and core NHEJ components) when simple lesions are repaired and 2) a slower phase (dependent on ATM and the MRN complex) when more complex breaks are resolved (Nussenzweig and Nussenzweig, 2007). In order to assess the relative contributions of DNA-PKcs and ATM to the repair of Fe ion-induced DNA damage, HSFs were pre-treated with NU7026 or KU55933, specific and potent inhibitors of DNA-PKcs or ATM, respectively (Veuger et al., 2003; Hickson et al., 2004) or with the solvent (DMSO) as control. Activation of DNA-PKcs and ATM upon irradiation with 1 GeV/nucleon Fe ions was assayed by Western blotting with antibodies recognizing autophosphorylated sites on these kinases, serine2056 on DNA-PKcs (Mukherjee et al., 2006) and serine1981 on ATM (Bakkenist and Kastan, 2003) **(Fig 2.2A)**. DNA-PKcs autophosphorylation was abrogated in cells treated with NU7026 while ATM autophosphorylation was abrogated in cells treated with KU55933 confirming the efficacy of the small-molecule inhibitors. Cells treated with NU7026 carried out DNA repair with significantly slower kinetics, indicating that DNA-PKcs is the major enzyme involved in the repair of DSBs after Fe-irradiation **(Fig 2.1E)**. Cells treated with KU55933 were also impaired

in repair, though to a lesser extent. The requirement of ATM for repair is presumably due to the complexity of Fe-induced DNA damage as ATM is involved in the repair of complex breaks (Kuhne et al., 2004; Jeggo and Lobrich, 2005; Lobrich and Jeggo 2005; Riballo et al., 2004). Interestingly, NU7026-treated cells were able to carry out DNA repair to the same extent as untreated cells, albeit with much slower kinetics. The slow repair upon DNA-PKcs inhibition could possibly be attributed to backup-NHEJ, a slow and error prone pathway that operates in the absence of DNA-PKcs (Rosidi et al., 2008) or to homologous recombination repair (HRR) (Weinstock et al., 2006). Both pathways have been recently reported to be functional in HZE-irradiated cells (Wang et al., 2008).

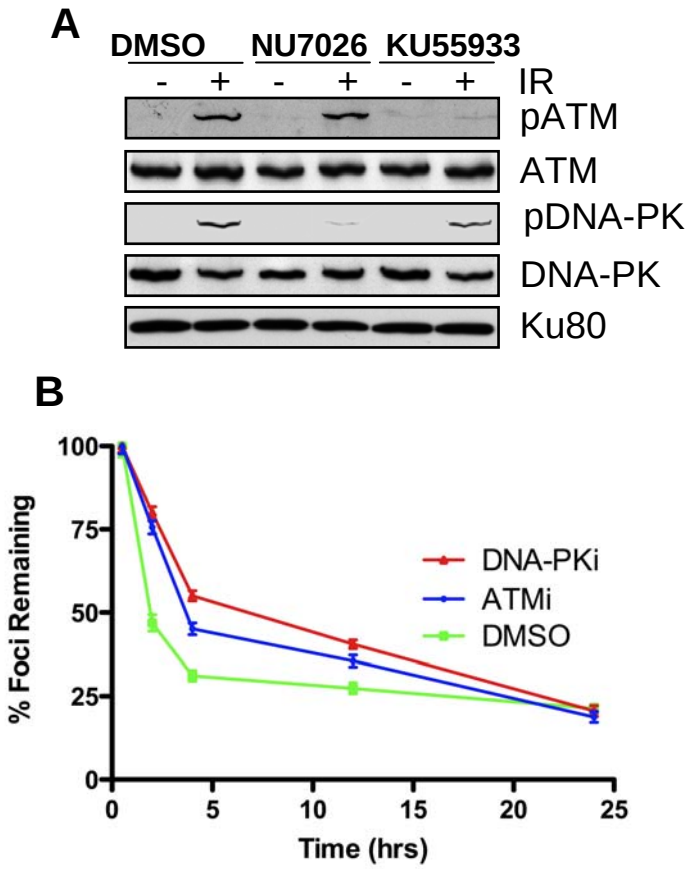

Figure 2.2. Requirement of DNA-PKcs and ATM for repair of Fe-induced DNA damage. (**A**) HSFs were pre-treated with a DNA-PK inhibitor (NU7026) or with an ATM inhibitor (KU55933) or with the solvent (DMSO) and irradiated with 4 Gy of 1 GeV/nucleon Fe. Activation of DNA-PKcs and ATM was assayed at 1 h post-irradiation by Western blotting with phospho-specific antibodies as indicated. **(B)** HSFs were pre-treated with inhibitors as indicated and irradiated with 1 Gy of 1 GeV/nucleon Fe. DSB repair kinetics were obtained by scoring γH2AX foci. Please note further impairment of repair in cells pre-treated with inhibitors. The differences in percent foci remaining at 4 h post-irradiation were determined to be statistically significant by a two-tailed t test (P value < 0.0001).

Cells irradiated with Fe ions display biphasic p53 and p21 induction and high levels of senescence. Unrepaired DNA lesions, such as those observed in response to Fe ions, would presumably result in persistent DNA-damage signaling culminating in senescence or apoptosis, both processes constituting *bona fide* barriers to carcinogenesis (Bartkova et al., 2006; Burma et al., 2006; Di Micco et al., 2006; Gorgoulis et al., 2005; Halazonetis, 2004; Khanna and Jackson, 2001. In response to DSBs, the tumor suppressor p53 is phosphorylated at serine 15 by ATM (Banin et al., 1998; Canman et al., 1998) and enforces either cell cycle arrest or apoptosis depending upon the cell type (Bargonetti and Manfredi, 2002; Shiloh, 2003). We examined the activation of p53 as a first step towards understanding the long-term consequences of the failure to repair Fe-induced DNA damage. HSFs irradiated with gamma-rays display rapid and transient p53 accumulation and phosphorylation at serine 15 **(Fig 2.3A)**. The reduction in p53 signals at 4 h post-irradiation correlates with the rapid repair of DSBs observed in these cells. The transient p53 activation correlates with transient induction of the cyclin-dependent kinase (CDK) inhibitor p21 (Waf1/Cip1), a downstream target of p53 (Fei and El-Deiry, 2003). Phosphorylation of SMC1 (at serine 966), an ATM substrate that is involved in both checkpoint activation (Kim et al., 2002; Yazdi et al., 2002) and DSB repair (Lehmann, 2005; Strom et al., 2004), also follows a similar transient pattern. In contrast, cells irradiated with Fe ions display a biphasic response with an initial

transient response similar to that seen with gamma-rays and a second sustained response starting at about 3 days post-irradiation and lasting for at least 10 days. The second response results in the induction of high levels of p21. A high level of the CDK inhibitor p16 (INK4a), that independently arrests cell proliferation in response to stress (Campisi, 2007), is also induced during this stage. The sustained induction of p21 and p16 in fibroblasts would be expected to result in damage-induced premature senescence (Campisi, 2007). We, therefore, quantified the proportion of senescent (β-gal-positive) (Dimri et al., 1995) HSFs in irradiated cultures at 10 d post-irradiation. Mock-irradiated cells display very low levels of SA β-Gal-positive cells (~3%) while gamma ray-irradiated cells display increased levels of senescence (~24%) **(Fig 2.3B)**. In sharp contrast, Fe-irradiated cells display a very high percentage of intensely-staining SA β -Gal-positive cells at 10 d post-irradiation (~84%). This is clearly a consequence of the sustained p53 activation and p21/p16 induction observed in these cells.

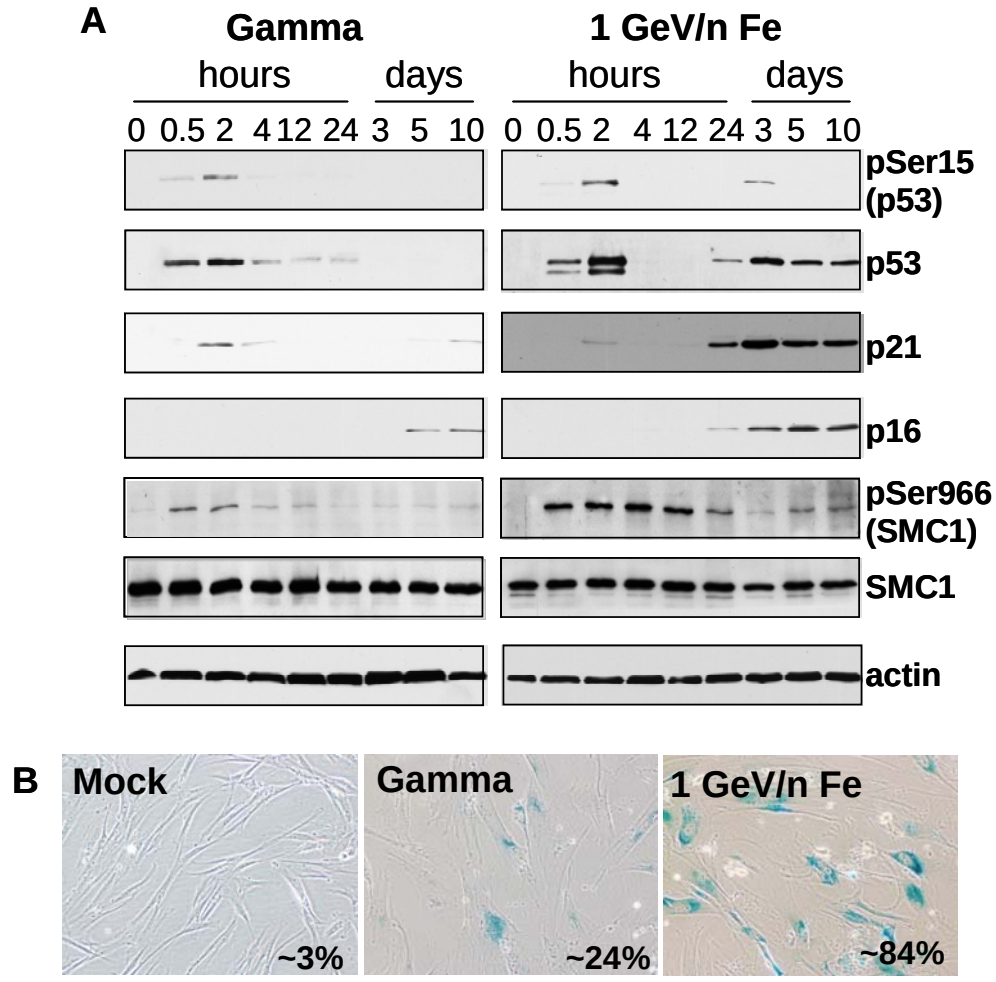

Figure 2.3. Activation of p53 and induction of senescence in response to Fe ions. (A) Human skin fibroblasts were irradiated with 4 Gy of γ-rays or 1 GeV/nucleon Fe. Cells were harvested at the indicated time points and analyzed by Western blotting. Note the biphasic phosphorylation p53/SMC1 and accumulation of p53/p21/p16 in Fe-irradiated cultures. **(B)** HSFs were mock-irradiated or irradiated with 4 Gy as indicated and stained after 10 days for senescene-associated β-galactosidase activity (blue). The approximate percentages of senescent cells are given: Mock-irradiation (3%); gamma rays (24%); Fe ions (84%).

ATM is dispensable for the accumulation of p53 and induction of senescence in response to Fe ions. ATM is the primary kinase responding to radiation-induced DSBs (Shiloh, 2006; Lavin, 2007) while ATR responds to single-stranded DNA regions generated by resection of DSBs or stalling of replication forks (Cuadrado et al., 2006; Jazayeri et al., 2006; Paulsen and Cimprich, 2007). In order to examine if ATM is essential for the biphasic p53 response seen in Fe-irradiated cells, we irradiated primary ATM-deficient fibroblasts (AT2052) (Sasai et al., 1994) with gamma-rays or Fe ions and assayed for p53 induction and downstream events by Western blotting. As has been reported previously (Banin et al., 1998; Canman et al., 1998), phosphorylation of p53 at serine 15 was completely abrogated in these cells **(Fig 2.4A)**. The accumulation of p53 and p21 in response to gamma-rays was attenuated in AT cells compared to HSFs but followed a transient pattern. Interestingly, despite the absence of ATM, p53/p21 accumulation in response to Fe ions was quite robust and followed a biphasic pattern similar to that seen in wild type fibroblasts **(Fig 2.4A)**. The induction of p21 and p16 in these cells was clearly responsible for the high levels of Fe-induced senescence (81%) observed by SA β-Gal staining **(Fig 2.4B)**. Taken together, these results imply that the sustained p53/p21 induction and high levels of senescence triggered by Fe ions do not necessarily require ATM and could, therefore, possibly be mediated by ATR (Cuadrado et al., 2006; Jazayeri et al., 2006; Paulsen and Cimprich, 2007).

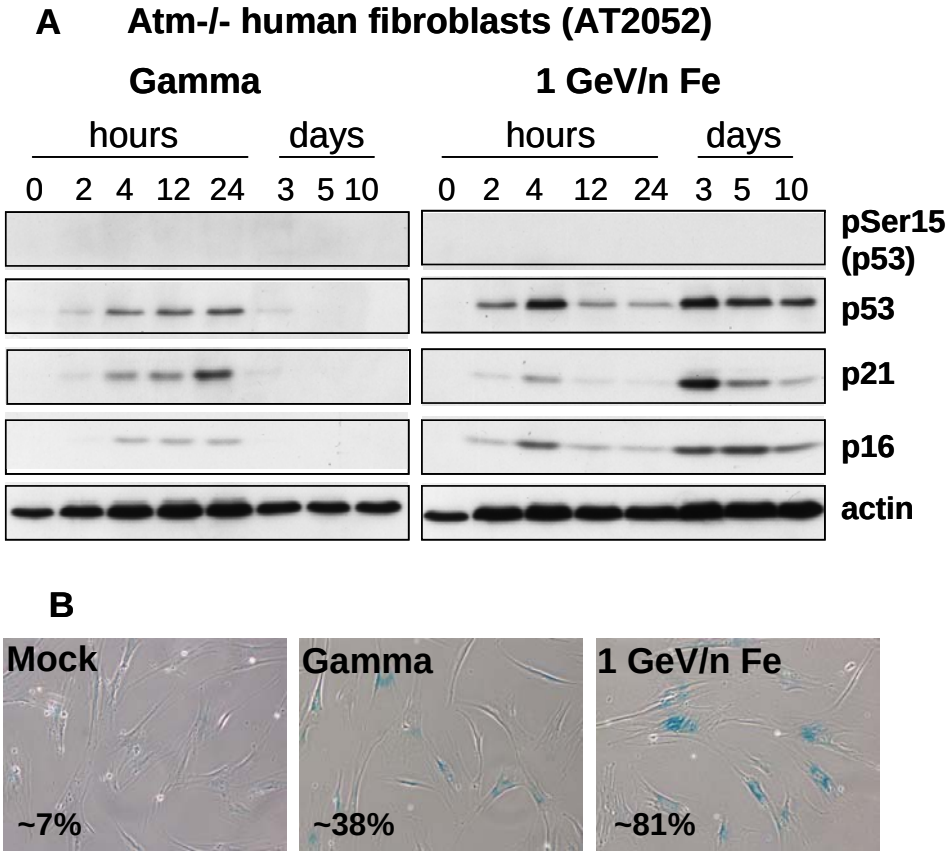

Figure 2.4. Activation of p53 and induction of senescence in ATM-deficient fibroblasts. (A) ATM-deficient human fibroblasts (AT2052) (Sasai et al., 1994) were irradiated with 4 Gy of γ-rays or 1 GeV/nucleon Fe. Cells were harvested at the indicated time points and analyzed by Western blotting. Please note the late induction of p53, p21, and p16 in Fe-irradiated AT cultures. **(B)** AT cells were mock-irradiated or irradiated with 4 Gy as indicated and stained after 10 days for senescence-associated β-galactosidase activity (blue). The approximate percentages of senescent cells are given in parentheses: Mock-irradiation (7%); gamma rays (38%); Fe ions (81%).

Enhanced cell killing in response to Fe ions. Finally, we wanted to comprehensively evaluate the effect of radiation on the survival of HSFs by a colony forming assay. HSFs are extremely sensitive to Fe ions as compared to gamma-rays **(Fig 2.5)**, as would be expected as a consequence of the incomplete repair, enhanced DDR and increased senescence observed in cells after Fe ion irradiation. These results provide a biological basis for the efficacy of cell killing by Fe ions. They also underscore the need for understanding the effects of particle irradiation in human tissue during radiotherapy with heavy ions. The survival of a small percentage of cells after Fe- or gamma- irradiation increases the potential of cells eventually acquiring cancer promoting mutations. Therefore, it is important as a next step to evaluate and better understand the tumorigenic potential of heavy ions (Chapters III and IV).

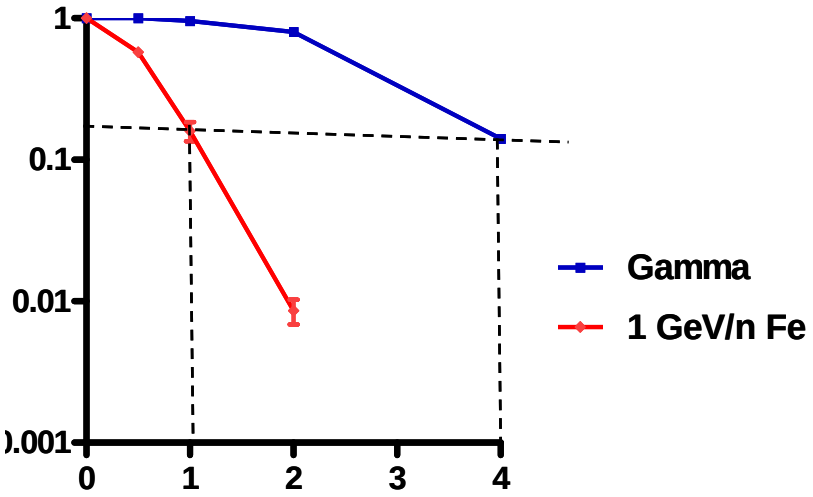

Figure 2.5. Cell survival in response to Fe ions or γ-rays. Radiation survival of HSFs was quantified by the colony formation assay. The fraction of surviving colonies (Y-axis) was plotted against the corresponding radiation dose. Error bars represent standard error of the mean. Please note the reduced survival with Fe-ions, with an RBE of 4 at approximately 15% survival.

DISCUSSION

An understanding of the DNA damage response (DDR) to HZE particles is very important not only because of cancer risks to astronauts but also because of increasing use of protons and carbon ions for targeted cancer therapy Schulz-Ertner et al., 2006). Clearly, the capacity of a human cell to repair DSBs is severely limited when the damage is inflicted by a high-Z particle possibly because of multiple ionization sites in close proximity (Antonelli et al., 2004). It is apparent that the total absorbed energy or dose is not as important a determinant of repair as the LET of the charged particle imparting that dose. While DSBs induced by 1 Gy of gamma-rays or protons are almost completely repaired, the cell is unable to repair a significant fraction of the evidently more complex damage inflicted by 1 Gy of 1 GeV/nucleon Fe. The observed inability to repair DSBs to completion clearly plays a major role in the increased chromosome aberrations, cell killing and tumor induction reported earlier for high Z particles (Brooks et al., 2001; George et al., 2001; Durante et al., 2005; Alpen et al., 1993; Yang et al., 1985). We find that DNA-PKcs, the key kinase involved in NHEJ (Burma et al., 2004), is required for the repair, albeit incomplete, of Fe-induced DNA damage. In addition, we find that HSFs treated with an ATM inhibitor also display a pronounced defect in the repair of Fe-induced DNA damage. As ATM is required for the repair of a subset of complex lesions (Kuhne et al., 2004; Jeggo and Lobrich, 2005; Lobrich and Jeggo, 2005;

Riballo et al., 2004), our observations indicate that Fe ions inflict more complex DNA damage compared to gamma-rays. Blocking DNA-PK or ATM with small-molecule inhibitors does not abrogate repair but merely slows it down. Presumably, therefore, other pathways of repair such as backup-NHEJ (Rosidi et al., 2008) or HRR (Weinstock et al., 2006) can partly compensate for the inactivation of DNA-PKcs or ATM.

As expected from the DSB repair kinetics, we find that the induction of p53 and p21 is transient in gamma-irradiated HSFs. In contrast, a sustained, second-phase induction of p53, p21 and p16 is observed in response to Fe ions. This is clearly a consequence of unrepaired DNA lesions in these cells though it is not yet understood why a biphasic response is seen. The high levels of p21 and p16 in Fe-irradiated cells are evidently responsible for the high levels of senescence observed in these cells. Senescence or permanent cell cycle arrest serves as a barrier to tumorigenesis by preventing the propagation of cells with unrepaired DNA lesions (Campisi, 2007). Interestingly, though ATM is the primary kinase responding to gamma-radiation induced DSBs (Shiloh, 2006; Lavin, 2007), it appears to be dispensable for the late accumulation of p53 and p21 and induction of senescence in response to Fe ions. ATM is backed up by the related kinase ATR that responds to single-stranded regions generated by resection of DSBs or stalling of replication forks (Cuadrado et al., 2006; Jazayeri et al., 2006; Paulsen and Cimprich, 2007). Ectopic activation of ATR, even in the

absence of DNA breaks, can drive cells into senescence (Toledo et al., 2008). Conversely, a small molecule inhibitor of ATR can reverse senescence in fibroblasts (Won et al., 2006). It is quite plausible then that ATR may be activated by the more complex DNA damage inflicted by Fe ions and could drive these cells into senescence even in the absence of ATM.

Since a direct link exists between persistent DNA damage and cancer (Bartkova et al., 2006; Burma et al., 2006; Di Micco et al., 2006; Gorgoulis et al., 2005; Halazonetis, 2004; Khanna and Jackson, 2001), the cancer risk to astronauts could, possibly, be much greater than that estimated from extrapolation of the human database for low LET exposures (Cucinotta et al., 2001). The risk of cancer could be even more significant for crewmembers of long-duration missions outside the geomagnetosphere, such as planned Mars missions. The ability or inability of a cell to repair DSBs and the resulting damage responses are excellent end points for examining the short-term biological effects of heavy ions. The persistence of DNA breaks and damage signaling influence subsequent outcomes, whether it be chromosome aberrations, cell death or cancer (Chapter III and IV).

CHAPTER III

Loss of p15/Ink4b accompanies tumorigenesis triggered by complex DNA double-strand breaks

INTRODUCTION

IR has long been recognized as a carcinogen, although the exact mechanisms underlying radiation-induced carcinogenesis remain largely unknown (Little, 2000; Wakeford, 2004). The carcinogenic effects of radiation are attributed to its clastogenic and mutagenic effects, although unique radiation-induced genetic alterations have yet to be identified in humans except in the case of thyroid cancers (Volpato et al., 2008; Hamatani et al., 2008). The most deleterious lesion inflicted by IR is the DNA double-strand break (DSB). A causal relationship between DSBs and cancer is clear from the cancer-predisposition of humans (and knock-out mice) with deficiencies in proteins responding to DSBs (O'Driscoll et al., 2006). While DNA breaks can be potentially carcinogenic, it is not clear whether complex DSBs that are refractory to repair are more potently tumorigenic than simple breaks that can be rapidly repaired, correctly or incorrectly, by mammalian cells.

Although DSBs induced by gamma rays (i.e., low-linear energy transfer [LET] radiation) are amenable to repair, the same does not necessarily hold true for damage induced by high atomic number and energy (HZE) particles (i.e., high-LET radiation) that inflict complex DNA lesions (Hada and Sutherland et al., 2006)**.** HZE particles are an important component of galactic cosmic rays and are of serious concern to astronauts on long-duration space missions due to their proposed higher carcinogenic potential; however, considerable uncertainties exist

regarding the estimation of cancer risks from these particles (Durante et al., 2008). Importantly, heavy ion beams are being increasingly and effectively used for targeted cancer therapy; therefore, it is critical to understand the potential for induction of secondary cancers from these ions (Cucinotta et al., 2006; Schulz-Ertner and Tsujii, 2007). We previously demonstrated that DSBs induced by 1 GeV/nucleon Fe ions are slowly and incompletely repaired, triggering persistent DNA damage signaling events and senescence in primary human skin fibroblasts while DSBs induced by gamma rays are rapidly and completely repaired by these cells (Mukherjee et al., 2008).

To investigate whether complex DNA breaks that are slowly and incompletely repaired are more potently tumorigenic compared to breaks that are efficiently repaired, we used a very simple and sensitive paradigm of cellular transformation. We previously demonstrated that primary Ink4a/Arf-/- astrocytes are immortal but not tumorigenic (Bachoo et al., 2002). However, these "sensitized" cells can be potently transformed by a single oncogenic event, such as expression of kRas, myrAkt, or EGFRvIII. By assessing the tumor-forming abilities of irradiated Ink4a/Arf-/- astrocytes, we directly investigated the transforming potential of Fe ions compared to gamma rays with the goal of identifying Fe-induced genomic changes responsible for triggering tumorigenesis in this model system. We show here that Fe ions are potently tumorigenic when directed to these sensitized astrocytes, generating tumors with significantly

higher frequency and shorter latency compared to tumors generated by gamma rays. Tumor formation by Fe-irradiated cells is accompanied by rampant genomic instability and multiple genomic changes, the most significant of which is loss of the p15/Ink4b tumor suppressor due to deletion of the chromosomal region harboring the *CDKN2A* and *CDKN2B* loci. The additional loss of p15/Ink4b in tumors derived from p16/Ink4a-null astrocytes is interesting and bolsters the hypothesis that p15 has a critical 'back-up' function in p16-mediated tumor suppression (Krimpenfort et al., 2007). Indeed, we find that re-expression of p15/Ink4b in tumor-derived cells delays tumor progression thereby confirming the importance of p15 loss in particle-induced cellular transformation. In sum, this work reports detailed analyses of genomic changes occurring after HZE-particle irradiation that possibly underlie cellular transformation and tumorigenesis. Our data provide a greater understanding of the link between complex DNA damage induced by charged particles and the resultant genomic changes triggering radiation-induced carcinogenesis.

MATERIALS AND METHODS

Cell culture. Primary murine astrocytes were isolated from Ink4a/Arf-/- five day old pups as described (Bachoo et al., 2002). Primary mouse astrocytes and *ex vivo* tumor cultures were all maintained in α-MEM media containing 10%

FBS in a humidified 37°C incubator in the presence of 5% CO_2. All cells were mycoplasma free.

Irradiations. Fe-ions with a kinetic energy of 1 GeV/nucleon were provided by the NASA Space Radiation Laboratory (NSRL) at Brookhaven National Laboratory as described (Mukherjee et al., 2008). For gamma-irradiation, a ^{137}Cs source (JL Shepherd and Associates, CA) was used.

Colony formation assays. For colony formation assays, 300 cells were plated in triplicate 60 mm dishes, irradiated with graded doses of radiation (high or low LET, as indicated) and surviving colonies stained with crystal violet 6-8 days post-irradiation as described (Mukherjee et al., 2008).

Immunofluorescence staining, immunoprecipitations, and Western blotting. Immunofluorescence staining of cells and tissue sections and Western blotting of whole-cell extracts were performed as described (Mukherjee et al., 2009). Antibodies used were anti-actin (Sigma, St Louis, MO), anti-Ki67 (Novocastra, Wetzlar, Germany), anti-p53BP1, anti-phospho-Akt(Ser473), anti-phospho-Erk1/2(Thr202/Tyr204), anti-CDK4, anti-CDK6 (Cell Signaling, Beverly, MA), anti-p15 (Santa Cruz, Santa Cruz, CA), anti-V5, anti-V5-fluorescein isothiocyanate (FITC) (Invitrogen, Carlsbad, CA), and rhodamine red-conjugated goat anti-mouse and FITC-conjugated goat anti-rabbit (Molecular Probes, Eugene, OR). Anti-V5 antibody (Invitrogen) and Dynabeads® sheep anti-mouse IgG (Invitrogen) were used for immunoprecipitations.

DSB repair assay. DSB repair rates were assessed by quantifying the time-dependent dissolution of γH2AX and 53BP1 foci as described (Mukherjee et al., 2008).

Metaphase spreads, Multicolor fluorescence *in situ* hybridization (M-FISH), and Telomere fluorescence *in situ* hybridization (T-FISH). Metaphase chromosome spreads were prepared after treatment with 1μg/ml colcemid (Sigma) using standard procedures. M-FISH was performed using the 21XMouse M-FISH probe kit according to manufacturer's specifications (MetaSystems, Altlussheim, Germany). For T-FISH, a Cy3-labeled peptide nucleic acid (PNA) probe was used and hybridization was performed as described (Zijlmans et al., 1997).

Subcutaneous injections. Cells (as indicated) were suspended in Hank's Buffered Salt Solution and 10^6 cells were subcutaneously injected into the flanks of six weeks old Nu/Nu nude mice (Charles River Laboratories International, Wilmington, MA). Mice were monitored daily for tumor formation and growth over a span of 8 weeks. All animal studies were performed under protocols approved by the Institutional Animal Care and Use Committee (IACUC) of UT Southwestern Medical Center.

Polymerase chain reaction (PCR), quantitative PCR, and quantitative reverse transcriptase-PCR. DNA was isolated using the DNeasy Blood & Tissue Kit (Qiagen, Germantown, MD). RNA was extracted using

RNeasy Mini Kit (Qiagen) and complementary DNA synthesized using SuperScriptIII First Strand Synthesis System (Invitrogen). qPCR and qRT- PCR was carried out using the LightCycler-FastStart DNA Master SYBR-Green I kit (Applied Biosystems, Foster City, CA). Standard curves were established following serial sample dilutions and data normalized to the housekeeping gene glyceraldehyde 3-phosphate dehydrogenase (GAPDH).

Array comparative genomic hybridization (aCGH). Genomic DNA from two mock-irradiated parental cells and two *ex vivo* tumor cultures were extracted using the DNeasy Blood & Tissue Kit (Qiagen) and, after quality check, 2.5μg of DNA for each sample was sent to the NimbleGen Inc. (Madison, WI) mouse aCGH hybridization service. The NimbleGen MM8 WG CGH array, which spans the entire non-repetitive regions of the mouse genome in a single array, was used. Normalization and segmentation of raw signals were processed by NimbleGen and subsequently loaded into Nexus Copy Number Analysis software (Biodiscovery, El Segundo, CA) for rank segmentation analysis and generation of ratios of DNA copy number changes.

Generation of tumor cells re-expressing p15/Ink4b. Human *p15/Ink4b/CDKN2B* cDNA was obtained from Addgene, Cambridge, MA (pCRII-p15; 16454) and sequentially cloned into pLenti6.3/V5-DEST by BP and LR clonase reactions (Invitrogen). Final vector was confirmed by sequencing. pLenti6.3/p15-V5/DEST vector was transfected into Fe-derived tumor cells

using Lipofectamine 2000 (Invitrogen) as per manufacturer's protocol. To establish stable clones expressing p15/Ink4b, transfected cells were selected with 5μg/ml Blasticidin (Invitrogen), and screened for expression of p15-V5 by Western blotting.

Statistical analyses. Frequencies of tumor formation by Fe- and gamma-irradiated cells were compared using Fisher's exact test. Tumor growth curves for these two irradiation conditions were compared using the Generalized Estimating Equations (GEE) method with AR(1) correlation structure used. All the statistical analyses were performed with SAS 9.1.3 Service Pack 3.

RESULTS

DSBs induced by Fe ions are refractory to repair. For these studies, we used a very simple and sensitive paradigm of cellular transformation – 'sensitized' Ink4a/Arf-/- astrocytes that can be potently transformed by a single oncogenic event (Bachoo et al., 2002). We previously reported that DSBs induced in human fibroblasts by 1 GeV/nucleon Fe ions are repaired slowly and incompletely compared to those induced by gamma rays (Mukherjee et al,. 2008). We first confirmed that this difference in DSB repair is also manifested in the primary murine Ink4a/Arf-/- astrocytes used in this study. Fe-irradiated cells exhibited slower DSB repair kinetics, as well as persistent DNA lesions at 24 h. In contrast, gamma-irradiated cells completely repaired their DNA by 8 h **(Fig**

3.1A). The higher relative biological effectiveness (RBE) of Fe ions compared to gamma rays (Durante et al., 2008) was confirmed by colony formation assays **(Fig 3.1B)**. On the basis of these results, cells were either mock-irradiated or irradiated with 1 Gy of Fe ions or with 1 Gy (equal dose) or 4 Gy ('equal-survival' dose) of gamma rays. After approximately 14 days of recovery, surviving cells were assayed *in vitro* as well as subcutaneously injected into nude mice. Metaphase chromosome spreads revealed that cells irradiated with Fe ions (but not those irradiated with gamma rays) exhibited a significant increase in Robertsonian fusions (50% of metaphase spreads, with an average of 8 fusions per metaphase) **(Fig 3.1C** and **D)**. These fusions, resulting from centromeric breakage by IR followed by fusion of two chromosomes at breakage points, are a reliable indicator for the assessment of radiation-induced genomic instability (Boei et al., 1996). These data strongly suggest that inefficiently repaired DNA damage induced by Fe ions caused significantly more genomic instability compared to damage induced by gamma rays.

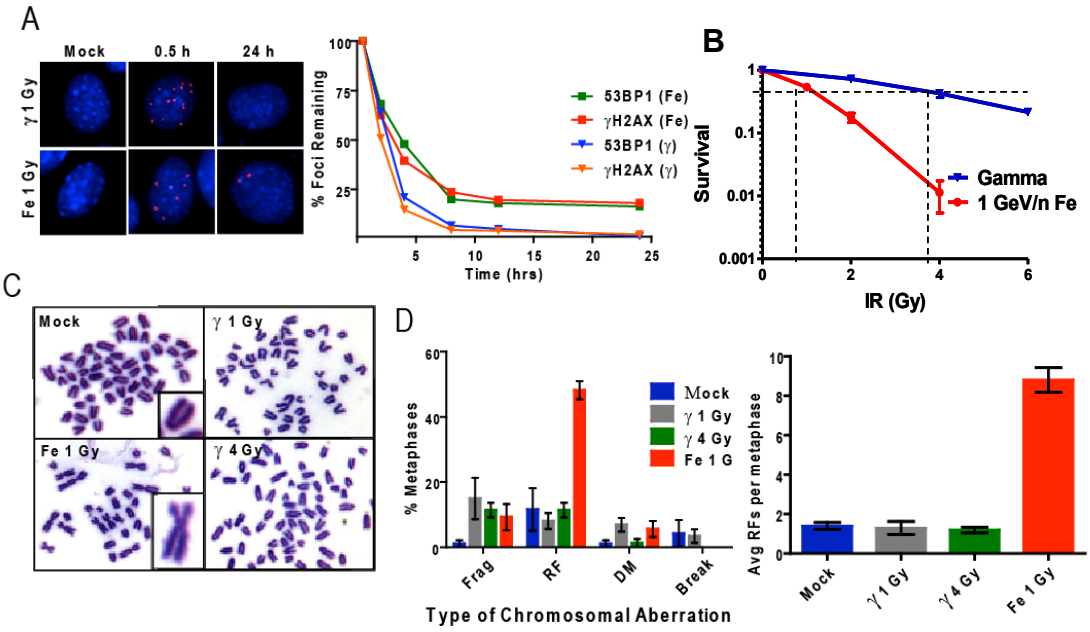

Figure 3.1. DSBs induced by Fe ions are refractory to repair. (A) Primary Ink4a/Arf-/- astrocytes were irradiated with 1 Gy of γ-rays or with 1 Gy of 1 GeV/nucleon Fe ions and co-immunostained with anti-γH2AX and anti-53BP1 antibodies. Initial damage (0.5 h) and residual damage (24 h) is depicted as γH2AX foci (red); nuclei are stained with 4',6-diamidino-2-phenylindole (DAPI; blue). γH2AX or 53BP1 foci were scored at different times post-irradiation to obtain DSB repair kinetics. Percentage of foci remaining (*y*-axis) was plotted against repair time (*x*-axis). **(B)** Radiation survival was measured by colony formation assays. Fraction of surviving colonies (*y*-axis) was plotted against the corresponding radiation dose (*x*-axis). Dotted lines mark equal survival doses. **(C)** Metaphase chromosome spreads were prepared from mock or Fe-irradiated cells. Note increased frequency of Robertsonian fusions upon Fe irradiation **(D)** Frequency of chromosome aberrations (Frag, Fragments; RF, Robertsonian fusions; DM, double minutes; representative images in Figure 3.3) were scored from metaphase spreads of mock- or γ- or Fe-irradiated cells (average of 50 metaphases). Note significant increase in frequency of Robertsonian fusions in Fe-irradiated cells with an average of 8 fusions per metaphase. Error bars represent standard error of the mean for all plots.

Ink4a/Arf-/- astrocytes irradiated with Fe ions are potently tumorigenic. We wanted to determine if some of the genomic changes wrought by Fe-irradiation might have significant tumorigenic consequences, and whether the degree of cellular transformation might be greater in magnitude after Fe exposure compared to gamma irradiation. Upon subcutaneous injection of surviving irradiated cells into nude mice, we found that mock-irradiated Ink4a/Arf-/- astrocytes consistently failed to generate tumors, confirming their lack of tumorigenic potential (0/8 for mock-gamma irradiation and 0/8 for mock-Fe irradiation). Significantly, cells irradiated with Fe ions rapidly and consistently generated tumors 100% of the time (12/12) (**Fig 3.2A)**. Cells irradiated with 1 Gy of gamma rays failed to form tumors (0/8) while those irradiated with a higher dose of 4 Gy formed tumors but only with a low frequency (2/8). The difference in frequency of tumor formation between Fe- and gamma-irradiated cells was determined to be statistically significant using Fisher's exact test (P value= 0.0007). A striking difference was also observed in the latency of tumor formation between Fe- and gamma-irradiated cells. On average, Fe-derived tumors first became palpable after 10.67 ± 2.7 days (mean ± s.d.) while the two gamma-derived tumors first became palpable only after 46.5 ± 0.7 days. The difference in tumor growth curves for these two irradiation conditions was determined to be statistically significant using the Generalized Estimating Equations method (P value = 0.001). Tumors derived from the Fe-

irradiated cells stained positive for Ki67, pAkt, and pErk, clearly indicating the activation of pro-proliferative pathways commonly upregulated in most cancers (Altomare et al., 2005; Roberts et al., 2007) **(Fig 3.2B)**.

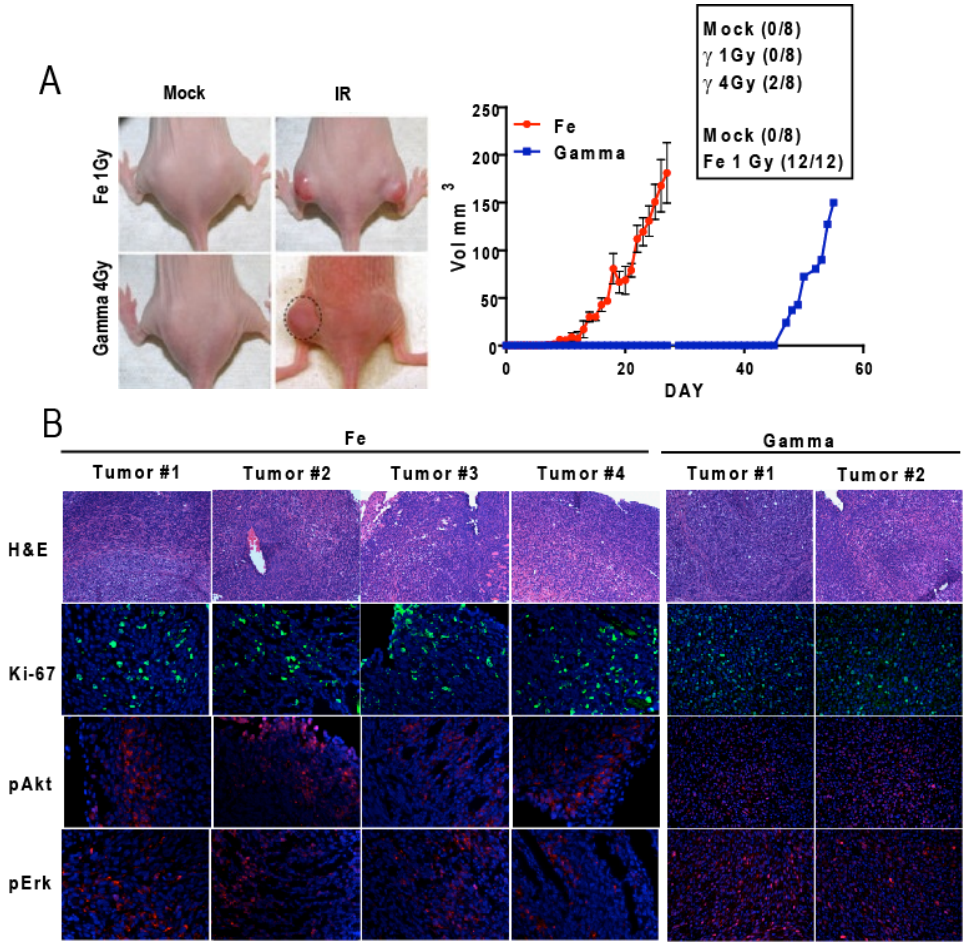

Figure 3.2. Fe-irradiated Ink4a/Arf-/- astrocytes are potently tumorigenic. (A) Tumor development was monitored after subcutaneous injection ($1x10^6$ cells) of mock- or γ- or Fe-irradiated astrocytes into nude mice. Representative pictures of tumor-bearing mice are shown (please note that only the left flank of Gamma 4 Gy mouse shows tumor development; dashed circle). Tumor volume (*y*-axis) was plotted against days post-inoculation (*x*-axis). Tumor development frequencies are indicated as "total tumors/total injections" (*box*). Differences in tumor frequency and growth were determined to be statistically significant using Fisher's exact test (P value= 0.0007) and Generalized Estimating Equations method (P value= 0.001), respectively. Note rapid tumor development with Fe-irradiated astrocytes and slow and infrequent tumor formation with γ-irradiated astrocytes. Error bars represent standard error of the mean. **(B)** Excised Fe-derived tumors were sectioned and stained with hematoxylin and eosin (H&E) or with the indicated antibodies. Nuclei are stained with DAPI (blue).

***Ex-vivo* cultures of Fe-derived tumors exhibit rampant genomic instability.** *Ex vivo* cultures of Fe-derived tumors displayed evidence of rampant genomic instability with high levels of Robertsonian fusions (100% of metaphase spreads and with an average of 8 fusions per metaphase) and other gross chromosomal aberrations (such as double minutes and dicentric chromosomes) **(Fig 3.3A)**. In order to identify the chromosomes participating in the Robertsonian fusions, we employed M-FISH staining, which allows simultaneous labeling of each mouse chromosome with a different color (Bayani et al., 2004) **(Fig 3.3B).** M-FISH revealed that the Robertsonian fusions observed in Fe-derived tumor cells were random, inolving almost all chromosomes **(Fig 3.3C)**. These fusions were not seen at such high frequencies in the gamma-derived tumor cells, though very low frequencies of simple and reciprocal translocations were observed in these cells. In order to investigate telomere integrity, both at the chromosome ends as well as at the fusion points, we employed T-FISH staining, which specifically labels the telomeric sequences (Scherthan et al., 2002). T-FISH revealed the loss of telomeric signals, as expected (Boei et al., 1996), at the Robertsonian fusion points confirming that these fusions arose from centromeric breakage resulting in loss of telomeres at the short arms of acrocentric chromosomes **(Fig 3.3B)**. Loss of telomeric signals was also observed at the ends of some chromosomes, only in Fe-derived tumors,

which would presumably perpetuate genomic instability through chromosome end-to-end fusions and repeated breakage-fusion-bridge cycles (Murnane, 2006).

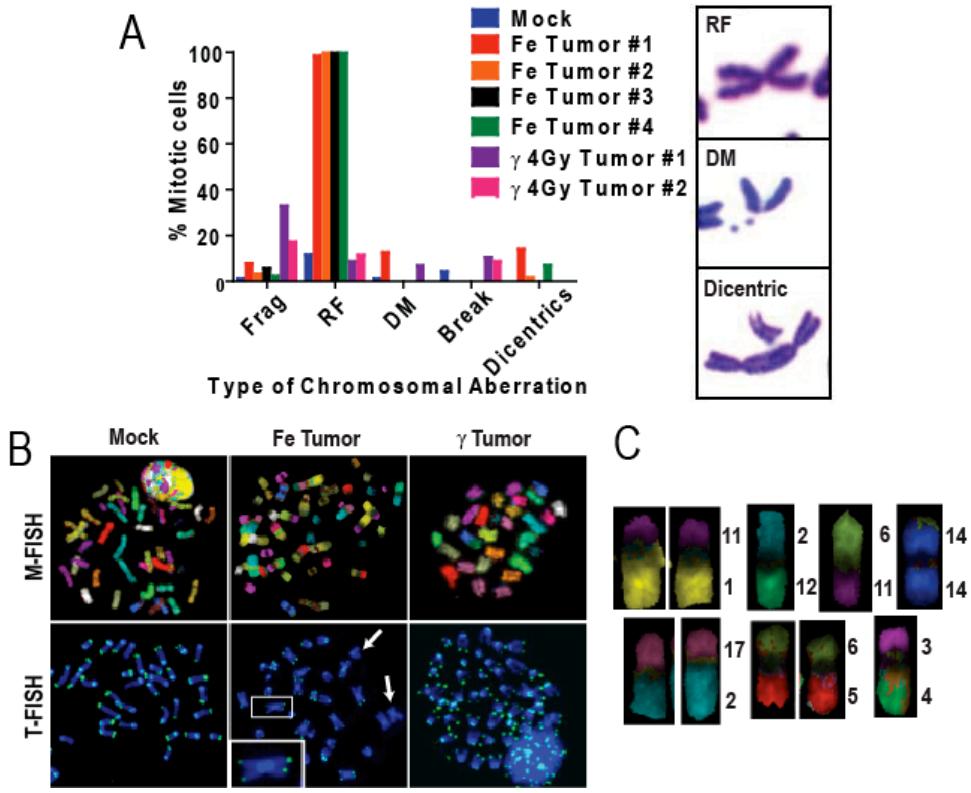

Figure 3.3. Chromosomal aberrations showing rampant genomic instability. (A) Frequency of chromosome aberrations (Frag, Fragments; RF, Robertsonian fusions; DM, double minutes) observed in metaphase spreads from mock-irradiated or tumor-derived cells (average of 50 metaphases). Representative aberrations are shown. **(B)** For M-FISH, metaphase spreads from Fe-derived tumor cultures were hybridized with M-FISH probes comprising of a cocktail of DNA labeling all mouse chromosomes. Representative metaphase shows Robertsonian fusions occurring randomly between multiple chromosomes. For T-FISH, metaphase spreads from mock-irradiated or Fe-derived tumor cells were hybridized to a Cy3-PNA probe and counterstained with DAPI. Representative metaphase from tumor cells shows chromosomes with loss of telomeric signal at fusion points or at chromosome ends highlighted by *arrows*. Inset shows magnified image of Robertsonian chromosome with loss of telomeric signal at the fusion point. **(C)** Representative M-FISH staining shows Robertsonian fusions occurring randomly between multiple chromosomes in Fe-derived tumors.

Fe-derived tumors exhibit common patterns of chromosomal copy number variation. Clearly, the tumor-derived cells were significantly altered compared to mock-irradiated cells due to stochastic genomic changes induced by Fe ions, some of which, logically, were conducive to rapid tumor growth. Cells with such transforming genomic changes should have been selected for upon subcutaneous injection. We analyzed tumor-derived *ex vivo* cultures by array comparative genomic hybridization (aCGH) with the goal of identifying the common regions of deletion or amplification that would presumably harbor changes critical for tumorigenesis. Chromosomal copy number variation (CNV) within the tumor isolates is shown, with green bars representing amplifications and red bars representing deletions (**Fig 3.4)**. Although both tumors had unique regions of deletion/amplification, there were also regions of CNV that were shared between the tumor samples and that might harbor genes important for particle-induced transformation: (i) a 13.9 megabase amplification of chromosome 2 (2qH1-qH3) harboring 160 genes, of which at least 17 are potential oncogenes; (ii) a 17.3 megabase amplification of chromosome 4 (4qD3-qE2) harboring 268 genes, of which 8 are potential oncogenes; (iii) a 190 kilobase deletion on chromosome 5 (5qA3) harboring a single gene with no reported role in tumor suppression; (iv) a 250 kilobase amplification of chromosome 8 (8qA2) harboring 4 genes, with no known oncogenes; (v) a 1.8 megabase amplification of chromosome 9 (9qA5.1) harboring 10 genes, with one

potential oncogene; (vi) a 489 kilobase amplification of chromosome 17 (17qA1) harboring 6 genes, with no known oncogenes; and (vii) a 276 kilobase deletion on chromosome 4 (4qC4-qC5) harboring 2 genes, both with critical tumor-suppressor functions **(**see **Appendix A** for potential oncogenes in the amplified regions**)**.

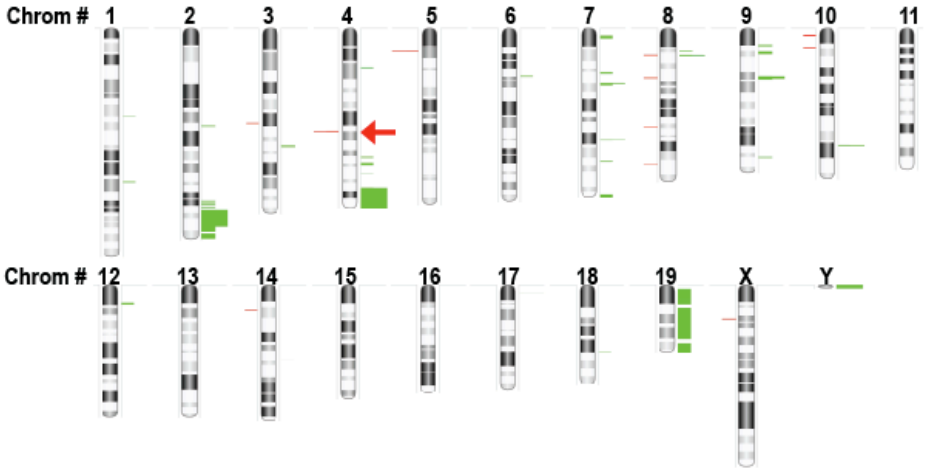

Figure 3.4. Common patterns of chromosomal copy number variation. Chromosomal map of regions of copy number variation (CNV) in tumor samples *vs* mock-irradiated cells derived by array comparative genomic hybridization (aCGH) and analyzed for DNA copy number changes using Nexus Copy Number Analysis software. The colored bands represent regions of amplification (green) or deletion (red) along each chromosome. The width of the band represents changes in either one or both samples. *Red arrow* marks the *CDKN2A/CDKN2B* locus.

Loss of p15/Ink4b is seen in tumors derived from Fe-irradiated Ink4a/Arf-/- astrocytes. Of these genomic alterations, we were particularly intrigued by the deleted region of chromosome 4 (4qC4-qC5) as there are only 2 genes mapping to this region, *CDKN2A* and *CDKN2B* **(Fig 3.5A**) and our experiments involved irradiation of astrocytes derived from *CDKN2A* knockout mice (Serrano et al., 1996). Clearly, deletion of the entire region must have provided the cells with an additional tumorigenic advantage over and above that conferred by the loss of *CDKN2A* alone. The only other gene in the deleted region, *CDKN2B*, codes for the p15/Ink4b tumor suppressor protein that has been reported to assume a greater role in tumor suppression in the absence of p16/Ink4a (Krimpenfort et al., 2007). We obtained evidence for loss of the *p15/Ink4b* locus in all 12 *ex vivo* tumor cultures by PCR and this was confirmed by qPCR analyses of four tumor-derived cultures **(Fig 3.5B)**. Loss of p15/Ink4b transcript and protein was confirmed by qRT-PCR **(Fig 3.5B)** and western analyses **(Fig 3.5C)**, respectively, of four tumor-derived cultures. Immunofluorescent staining of four Fe-derived tumors showed major areas that were negative for p15/Ink4b staining **(Fig 3.5C)**. Interestingly, the two gamma-derived tumors were positive for p15/Ink4b and exhibited intense nuclear staining for this protein **(Fig 3.5C)**. Retention of p15/Ink4b in the gamma-derived tumors was confirmed by PCR and Western analyses **(Fig 3.5B** and **C)**. These results independently confirm the importance of p15/Ink4b in tumor

suppression, especially in the absence of p16/Ink4a, and help explain why the entire *CDKN2A/CDKN2B* region is lost in many cancers (Cannon-Albright et al., 1992; Lukas et al., 1995; Nobori et al., 1994). Given the striking differences in latency and frequency between high LET Fe- and low LET gamma-derived tumors, it is tempting to speculate that loss of p15/Ink4b might contribute to the reduced latency and increased frequency of Fe-derived tumors.

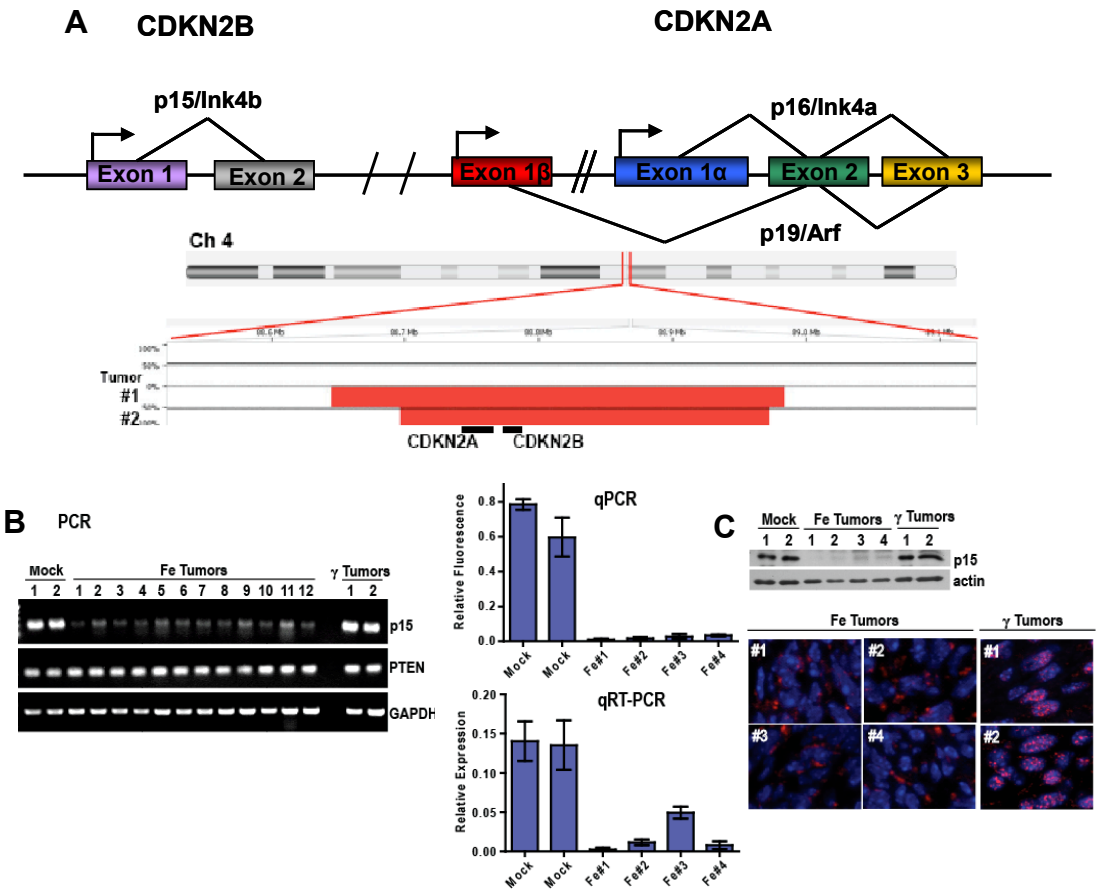

Figure 3.5. Loss of p15/Ink4b in tumors derived from Fe-irradiated cells. **(A)** Schematic of the *CDKN2A/CDKN2B* genomic region which encodes three tumor suppressors: p16/Ink4a, p19/Arf, and p15/Ink4b. Map represents the deleted region of chromosome 4 for two tumor samples (derived by aCGH and analyzed using Nexus software) showing the locations of *CDKN2A* and *CDKN2B* loci. **(B)** Loss of *p15/CDKN2B* locus was analyzed by PCR in 12 different *ex-vivo* Fe-derived tumor cultures and the two γ-derived tumor cultures; PCR analysis of the *PTEN* tumor suppressor locus was carried out for comparison. Loss of *p15/CDKN2B* locus was confirmed by qPCR using genomic DNA from 4 different *ex-vivo* tumor cultures. Loss of p15/Ink4b transcript was quantified by qRT-PCR. Data was normalized to GAPDH levels. Error bars represent standard error of the mean. **(C)** Loss of p15/Ink4b protein was analyzed by western blotting of whole cells extracts from *ex-vivo* tumor cultures and by staining tumor sections with anti-p15/Ink4b antibody. Note intense nuclear staining of p15/Ink4b in γ-derived tumors and lack thereof in Fe-derived tumors.

Re-expression of p15/Ink4b results in inhibition of tumor growth. In order to investigate the possible effects of p15/Ink4b on tumor growth, we re-expressed V5-tagged human p15 in *ex vivo* cultures of Fe-derived, p15-null tumors **(Fig 3.6A)**. Tumor cells were transfected with pLenti6.3/p15-V5/DEST or with pLenti6.3/V5-GW/*lacZ* as a control. The Ink4 cell-cycle inhibitors exert their functions by binding to the cyclin-dependent kinases, CDK4 and CDK6 (Kim et al., 2006). We first confirmed that the ectopically expressed p15 was functional and capable of binding both CDK4 and CDK6 by co-immunoprecipitation **(Fig 3.6B)**. Tumor cells (parental or p15-expressing) were then injected subcutaneously into nude mice and monitored for tumor formation. Although we did not observe a difference in tumor frequency, we observed a significant delay in the onset of tumor formation upon p15 re-expression **(Fig 3.6C)**. On average, tumors generated from the parental cells first became palpable after 6.58 ± 1.5 days (mean ± s.d.) whereas tumors from p15-expressing cells became palpable only after 19.17 ± 1.12 days. The difference in tumor growth curves was determined to be statistically significant using the Generalized Estimating Equations method (P value = 0.0039). Expression of p15 in tumors derived from p15-expressing cells was confirmed by immunofluorescence staining **(Fig 3.6D)**. In sum, these results indicate that p15 loss may be a critical event in particle-induced tumorigenesis.

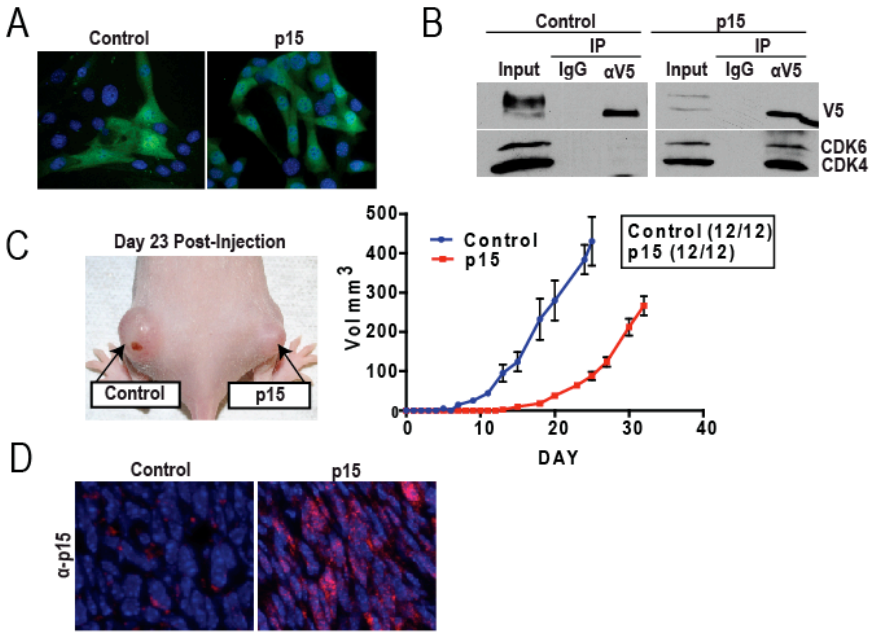

Figure 3.6. Inhibition of tumor growth upon re-expression of p15/Ink4b. **(A)** *Ex-vivo* cultures from Fe-derived, p15-null tumors were transfected with a lentiviral vector expressing V5-tagged human p15. Immunofluorescent images of parental and p15 re-expressing cells show negative and positive staining, respectively, using anti-V5-FITC conjugated antibody (green). Nuclei are stained with DAPI (blue). P15-null tumor cells are designated "parental" and tumor cells re-expressing p15 are designated "p15". **(B)** Binding of ectopically-expressed p15 to CDK4/6 was demonstrated by immunoprecipitating p15 with an anti-V5 antibody and Western blotting the immunoprecipitates with anti-CDK4 and anti-CDK6 antibodies. Note co-IP of CDK4/6 from tumor cells re-expressing p15 but not from parental tumor cells. **(C)** Tumor development was monitored after subcutaneous injection of parental or p15-expressing tumor cells into nude mice. Representative picture of tumor-bearing mouse is shown. Note significant difference in tumor volume between "parental" and "p15" tumors at 23 days post-injection. Tumor volume (*y*-axis) was plotted against days post-inoculation (*x*-axis). Differences in tumor growth were determined to be statistically significant using the Generalized Estimating Equations method (P value= 0.001). Tumor development frequencies show no difference and are indicated as "total tumors/total injections" (*box*). **(D)** Excised tumors were sectioned and stained with anti-p15 antibody. Note positive p15 staining in tumors derived from p15-expressing cells and lack thereof in tumors derived from parental cells.

DISCUSSION

In this study, we evaluated whether complex DSBs that are repaired slowly and incompletely (those induced by high LET Fe ions) are more potently tumorigenic than simple breaks that can be repaired rapidly and completely (those induced by low LET gamma rays). We hypothesized that Fe ions might generate a greater repertoire of genomic alterations compared to gamma rays that, in turn, might increase the likelihood of transforming genetic changes in the surviving cells. As wild type cells usually harbor a number of fail-safe mechanisms to prevent tumorigenesis, we used "sensitized" Ink4a/Arf-/- astrocytes (Serrano et al., 1996) that might be rapidly transformed by IR thus providing a simple yet sensitive paradigm for direct comparison of Fe ions with gamma rays. HZE particles are known to be more clastogenic than gamma rays (Durante et al., 2008), and a number of *in vitro* studies are testament to the transforming potential of these ions (Borek et al., 1978; Hei et al., 2001; Li et al., 2007; Yang et al., 1997; Zhao et al., 2004). Yet, very few studies have directly assessed the tumorigenic potential of these ions except for the mouse Harderian gland studies carried out at the Lawrence Berkeley and Oak Ridge National Laboratories (Alpen et al., 1993; Fry et al., 1985); however, these studies did not analyze the genomic changes underlying tumor formation. In fact, genomic changes underlying IR-induced tumors are, in general, not well understood, except for radiation-induced thyroid cancers, where very specific gene

rearrangements involving the RET (rearranged during transfection) proto-oncogene have been identified in humans (Volpato et al., 2008), and for IR-induced medulloblastomas in *Ptch*+/- mice caused by loss of heterozygosity at the *Ptch* locus (Pazzaglia et al., 2006).

Our study is a careful analysis of genetic events that might play a causal role in particle-induced tumorigenesis. Using our model system, we show that Fe ions are potently tumorigenic compared to gamma rays, and that the tumor-derived cells are significantly genetically altered compared to the parental mock-irradiated cells. Copy number variation analyses of the Fe-derived tumor samples by aCGH revealed common areas of amplifications and deletions. The amplified regions harbored a number of potential oncogenes (**Appendix A**), some of which could have contributed to cellular transformation in our model system, and these will be analyzed in future studies. In this study, we focused on a small deletion in chromosome 4 resulting in loss of p15/Ink4b. Corresponding deletions in humans (in chromosome 9p21) are very common in many cancers including glioblastomas, which are tumors originating from astrocytes (Cannon-Albright et al., 1992; Lukas et al., 1995; Nobori et al., 1994). The deleted region harbors the *CDKN2A* gene that codes for two very important tumor suppressors via alternate reading frames, Ink4a and Arf, which regulate the Rb and p53 tumor suppressor pathways, respectively **(Fig 3.5A)** (Kim et al., 2006). Deletion of this region in our model system was particularly intriguing as this occurred in cells that were

CDKN2A-/- to begin with, thereby indicating the importance of a second tumor suppressor gene in the deleted region, *CDKN2B*. In fact, it was first proposed by Bert Vogelstein that deletions in the 9p21 region are significantly more common than intragenic mutations in *CDKN2A* because of the presence of the neighboring gene *CDKN2B,* whose product (p15/Ink4b) might also play an important role in tumor suppression (Jen et al., 1994). Although the role of p16 as a *bona fide* tumor suppressor is well documented, the importance of p15 in tumor suppression remains less well understood. Indeed, it was only recently demonstrated that p15 performs a critical backup function for p16 and that cells compensate for loss of p16 by increasing the levels of p15 protein under conditions of stress (Krimpenfort et al., 2007). Our results provide independent verification of the important tumor suppressor function of p15/Ink4b, especially in the context of p16/Ink4a loss, by demonstrating that (i) additional loss of p15/Ink4b upon Fe irradiation provides a tumorigenic advantage to cells already deficient in p16/Ink4a, and (ii) re-expression of p15/Ink4b in tumor cells significantly delays tumor progression. The overall importance of the *CDKN2A/2B* locus is underscored by the following: (i) this region is deleted in many cancers including gliomas (Cannon-Albright et al., 1992; Lukas et al., 1995; Nobori et al., 1994), (ii) common variations (single nucleotide polymorphisms; SNPs) in the *CDKN2A/2B* genes contribute to glioma susceptibility (Shete et al., 2009), and (iii) this locus is completely silenced in

induced pluripotent stem cells and embryonic stem cells (Li et al., 2009). Our results indicate that the *CDKN2A/2B* locus may be susceptible to deletion during particle-induced tumorigenesis thereby bolstering the role of this locus as an important barrier to carcinogenesis.

CHAPTER IV

DNA double-strand breaks cooperate with Ink4a/Ink4b/Arf loss to generate high grade gliomas in transgenic mouse models

INTRODUCTION

Glioblastoma multiforme (GBM; WHO grade IV astrocytoma) is a highly aggressive tumor, with extremely poor prognosis. Over the last two decades, significant insights into the molecular events underlying gliomagenesis have been gained. Most recently, large-scale integrated genomic analyses of GBM specimens by The Cancer Genome Atlas (TCGA) Research Network confirmed the importance of key genetic events occurring in three distinct signaling pathways commonly disrupted in human GBM: 1) receptor tyrosine kinase (RTK)/ phosphoinositide-3-kinase (PI3K) pathway, 2) p53 pathway, and 3) retinoblastoma (RB) pathway (TCGA, 2008; Cerami et al., 2010).

More than 90% of human glioblastomas appear to be sporadic, without any known genetic predispositions (Krex et al., 2007, Louis et al., 2007). To date, the only established risk factor clearly and unequivocally linked to glioblastoma is ionizing radiation (IR). Extensive epidemiological evidence exists, primarily from pediatric and adolescent populations that have been exposed to therapeutic IR, showing elevated risk and incidence of brain tumors (Salvati et al., 2003; Cavin et al., 1990; Shapiro et al., 1989). Examples include children given irradiation to the scalp for the treatment of *tinea capitis* (Sadetzki et al., 2005; Ron et al., 1988), and pediatric patients receiving prophylactic cranial irradiation for treatment of leukemia or lymphoma (Neglia et al., 1991; Brustle et al., 1991). Importantly, a study carried out at the Ames Research Center showed that 3 out

of 10 monkeys exposed to high-energy protons and surviving 3-5 years post-IR developed glioblastomas (Haymaker et al., 1971). A report also exists of a single monkey developing glioblastoma 2.8 years after receiving irradiation to the spinal cord (Price et al., 1996). Based on substantial epidemiological evidence, radiation is accepted as the only known risk factor for developing GBM.

The genetic changes underlying radiation-induced transformation are not well understood in general. An exception is the case of radiation-induced thyroid cancers, where specific gene rearrangements involving the RET (rearranged during transfection) proto-oncogene have been identified (Volpato et al., 2008), and for radiation-induced medulloblastomas, modeled in *Ptch*+/- mice, where loss of the remaining allele is sufficient for tumorigenesis (Pazzaglia et al., 2006).

Using Ink4a/Arf-null astrocytes *in vitro*, we previously demonstrated that complex DSBs induced by heavy particle-irradiation (high-LET) are refractory to repair and are more potently tumorigenic compared to simple breaks induced by gamma-rays (low-LET) that can be rapidly repaired, correctly or incorrectly, by mammalian cells. Importantly, we found Ink4b loss to be a critical event in tumorigenesis triggered by complex DSBs (Camacho et al., 2010). Here, we have used the Nestin-Cre (Isaka et al., 1999) transgenic mouse line to study the tumor suppressor functions of Ink4a/Ink4b/Arf and/or PTEN in logical combinations representing progressive steps towards gliomagenesis. We have elucidated how

the different tumor suppressor backgrounds cooperate with complex and persistent versus simple and transient DSBs in the development of GBM.

MATERIALS AND METHODS

Mice, tissue collection and tumor analyses. Mice were obtained from the Mouse Cancer Models Consortium and maintained in a FVB/NJ and C57BL6 mixed background. Nestin-Cre, Ink4a/Arf$^{f/f}$, Ink4ab$^{-/-}$;Arf$^{f/f}$ and PTEN$^{f/f}$ lines have all been previously described (Isaka et al., 1999; Krimpenfort et al., 2001, Krimpenfort et al., 2007; Podsypanina et al., 1999). All procedures for mouse experiments were performed under protocols approved by the Institutional Animal Care and Use Committee of University of Texas Southwestern Medical Center. Irradiated mice were monitored daily and euthanized upon presentation of neurological symptoms. Symptomatic mice were perfused with 1X phosphate buffered saline (PBS). Brain tissue was sectioned coronally, tumor tissue isolated and immediately flash frozen for subsequent DNA/RNA preparations. When possible, tissue was also processed to generate *ex vivo* cultures. Tissue was also fixed by immersion in 4% paraformaldehyde (PFA), and either embedded in paraffin, or frozen for cryosectioning. Tumor classifications were assigned by a resident neuropathologist.

Irradiations. Fe ions with a kinetic energy of 600 MeV/nucleon were provided by the National Aeronautics and Space Administration Space

Radiation Laboratory at Brookhaven National Laboratory as previously described (Mukherjee et al., 2008). X-ray irradiations were carried out using an X-RAD 320 irradiator (Precision X-Ray). Animals were anesthetized for immobilization using 240mg/kg Avertin and placed in beamline or irradiation chamber with collimators in place for head only irradiations.

Immunofluorescence staining and western blotting.

Immunofluorescence staining of cells or tissue sections and western blotting of whole-cell extracts was performed as described (Mukherjee et al., 2009). Antibodies used were anti-actin (Sigma, St Louis, MO), anti-γH2AX, anti-Olig2, anti-NeuN (Millipore, Billerica, MA), anti-Ki67 (Novocastra, Wetzlar, Germany), anti-Nestin (BD Pharmingen, San Diego, CA), anti-GFAP (Biocare Medical, Concord, CA), anti-phospho- Akt (Ser473), anti- phospho-Erk1/Erk2(Thr202/Tyr204), anti-phospho-MET (Tyr1234/1235), anti-MET, anti-phospho-S6-ribosomal protein (Ser235/235) (Cell Signaling, Beverly, MA), and anti-Sox2 (Abcam, Cambridge, MA).

TUNEL staining. Peroxidase-based terminal deoxyribonucleotidyl transferase-mediated dUTP-digoxigenin nick and labeling (TUNEL) assay was performed according to the manufacturer's instructions using FragEL DNA Fragmentation Kit with colorimetric TdT-Enzyme (Calbiochem, Darmstadt, Germany) to detect fragmentation of DNA associated with apoptosis on formalin-fixed paraffin embedded tissue sections.

Nucleic acid preparation, quantitative PCR and quantitative reverse transcription-PCR. DNA or RNA were isolated from frozen tissues using the DNeasy Blood and Tissue Kit or RNeasy Mini Kit (Qiagen, Germantown, MD) following manufacturer's protocol. For qRT-PCR, complementary DNA was synthesized using SuperScriptIII First Strand Synthesis System (Invitrogen, Carlsbad, CA). qPCR and qRT-PCR were carried out as described (Camacho et al., 2010).

Array comparative genomic hybridization (aCGH). aCGH was carried out as previously described (Camacho et al., 2010) and data analyzed using Nexus Copy Number Analysis software (Biodiscovery, El Segundo, CA). To identify meaningful copy number variation (CNV) events, a systematic method called Genomic Identification of Significant Targets in Cancer (GISTIC) was used (Beroukhim et al., 2007). This method calculates a statistic (G score) that takes into account frequency of the occurrence and amplitude of the aberration, and also calculates statistical significance of each aberration.

Fluorescence in situ hybridization (FISH). FISH was performed on formalin-fixed paraffin-embedded sections using standard slide preparation, protease treatment, permeabilization and hybridization methods at the Institute of Cancer Genetics, Irving Cancer Research Center, Columbia University Medical Center (Zijlmans et al., 1997). Bacterial artificial chromosome clone RP23-73G15, which covers the mouse MET gene was used.

Cell culture. Primary murine astrocytes were isolated from Nestin-Cre; Ink4ab$^{-/-}$/Arf$^{f/f}$ 5-day old pups as described (Bachoo et al., 2002). Primary mouse astrocytes and *ex vivo* tumor cultures were all maintained in Dulbecco's Modified Eagle Medium (DMEM) containing 10% of a fetal bovine/newborn calf serum mixture or DMEM/F12 (with L-Glutamine, Invitrogen) medium containing glucose (0.3%), penicillin/streptomycin (50 mg/ml), Apo-Transferrin (0.1mg/ml), Progesterone (20 nM), sodium selenite (30 nM), putrescine (60mM), insulin (25 mg/ml),and 20 ng/ml EGF (all reagents from Sigma). Recombinant human HGF (R&D Systems, Minneapolis, MN) was used for activation of MET in *ex vivo* cultures. Cells were incubated at normal oxygen levels in a humidified 37°C incubator in the presence of 5% CO_2.

shRNA lentivirus production and infection. pLKO.1- scramble was a gift from David Sabatini (Addgene, Cambridge, MA; plasmid #1864), and pLKO.1-shMET was obtained from Open Biosystems (Hunstville, AL). Virus production was carried out using ViraPower Lentiviral Packaging Mix (Invitrogen, Carlsbad, CA), as specified by manufacturer. Cells were transduced with viral particles at a multiplicity of infection (MOI) of 2 with 4μg/ml polybrene. Cells were kept under selection using 2μg/ml puromycin.

RESULTS

Generation and irradiation of transgenic mice. We generated 3 transgenic mouse lines for this study. We crossed Nestin-Cre (Isaka et al., 1999) mice with previously described transgenic mouse lines, Ink4a/Arf$^{f/f}$ (Krimpenfort et al., 2001) or Ink4ab$^{-/-}$;Arf$^{f/f}$, which harbors germline inactivation of Ink4a and Ink4b, and conditional Arf alleles (Krimpenfort et al., 2007). Additional heterozygosity of PTEN (f/+) (Podsypanina et al., 1999) was bred into the Ink4ab$^{-/-}$;Arf$^{f/f}$ background. These three models, in a minimalistic way, represent progressive steps in gliomagenesis and based on our previously published work, we hypothesize that they may have heightened sensitivity to transformation by DNA double-strand breaks **(Fig 4.1).** Mice were irradiated with a single acute dose of 1 Gy Fe ions or 4 Gy X-rays. These doses were chosen based on our previously published *in vitro* data showing equal survival at these doses (Chapter III). Given the presence of germline mutations in our model systems, we irradiated the head only using special collimators to avoid possible transformation and tumorigenesis in more sensitive tissues.

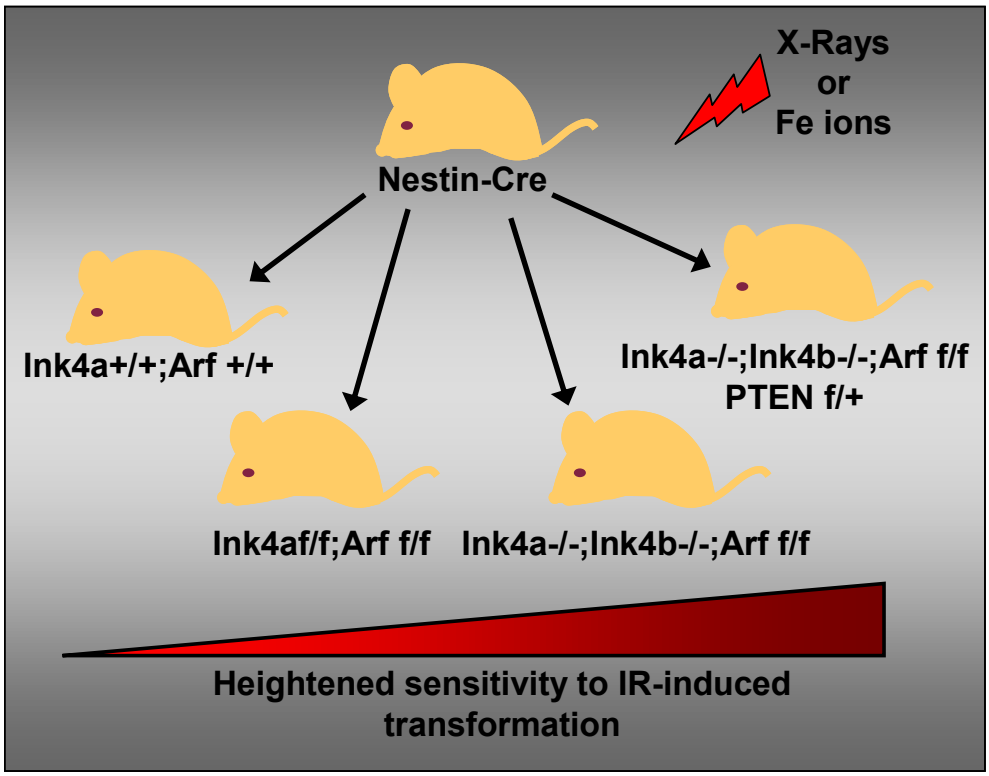

Figure 4.1. Schematic of mouse models. Transgenic mouse lines were generated that harbor combinations of Ink4a/Ink4b/Arf and/or PTEN in logical combinations representing progressive steps towards gliomagenesis, with hypothesized heightened sensitivity to IR-induced transformation.

Persistent DNA damage abolishes proliferating cells in the SVZ. Nestin-Cre; Ink4ab$^{-/-}$; Arf$^{f/f}$ mice, were irradiated with a single dose of 1 Gy Fe ions or 4 Gy X-rays, equitoxic doses based on in vitro colony formation assay (Chapter III). Short-term responses to these two qualities of radiation were examined. DNA damage was quantified in the two neurogenic niches, the subgranular zone (SGZ) and subventricular zone (SVZ), in the cortex and in astrocytes by looking at GFAP-positive cells. We find that DNA double-strand breaks induced by Fe particles are persistent in all regions of the mouse brain, with approximately 13% of cells harboring at least one γH2AX focus up to 1 month post-IR. In contrast, breaks induced after X-ray irradiation are efficiently repaired by 24 hrs, with only 3% of cells harboring DSBs at 1 month **(Fig 4.2A** and **B)**. Although the cell-of-origin for GBM remains a matter of debate, many studies imply neural stem cells as the cell-of-origin. For that reason, we next examined the effect of radiation on proliferating cells of the SVZ. High levels of apoptosis, as measured by TUNEL staining, were evident in both Fe- and X-ray irradiated brains 12 hrs post-irradiation. After 24 hrs, apoptotic cells were still detectable with both qualities of radiation, although higher levels after X-ray irradiation were noted **(Fig 4.3A)**. Irradiation with Fe ions results in a significant decrease in the number of proliferating cells, as examined by immunostaining for Ki67, a proliferative marker. This decrease is permanent, evident by significant

loss of proliferation observed at 1 month post-IR and is in stark contrast to X-rays, where proliferation resumes by day 7 **(Fig 4.3B)**.

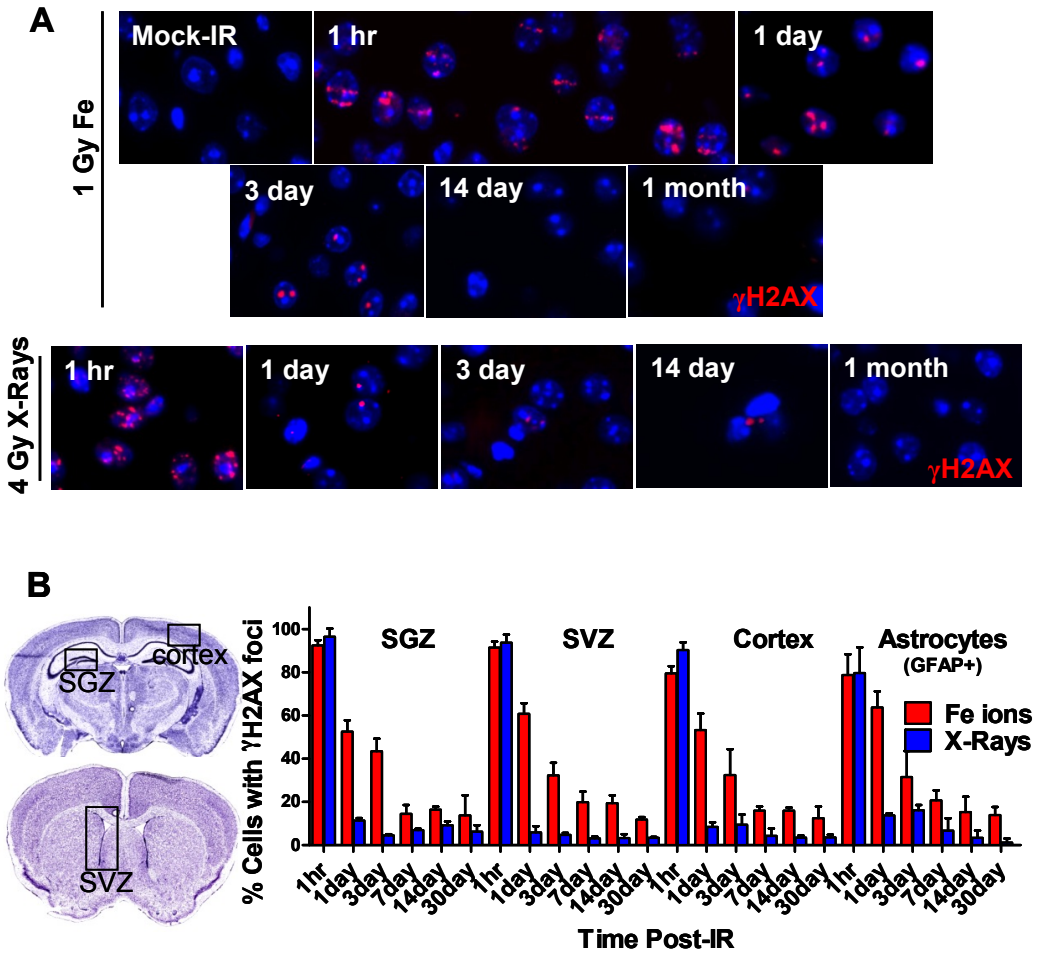

Figure 4.2. DNA damage in the adult mouse brain in response to Fe ions or X-rays. (A) Nestin-Cre; Ink4ab$^{-/-}$; Arf$^{f/f}$ mice were irradiated with 1 Gy Fe ions or 4 Gy X-rays and DNA damage examined at indicated timepoints. DNA damage was visualized by staining for γH2AX (red); nuclei stained with DAPI (blue). **(B)** DNA damage was quantified in the cortex, SGZ, SVZ, and astrocytes (GFAP+) by counting the percentage of nuclei with at least 1 γH2AX focus (y-axis) up to 1 month post-IR (x-axis). Note persistent lesions and higher percentage of γH2AX foci in Fe-irradiated brains.

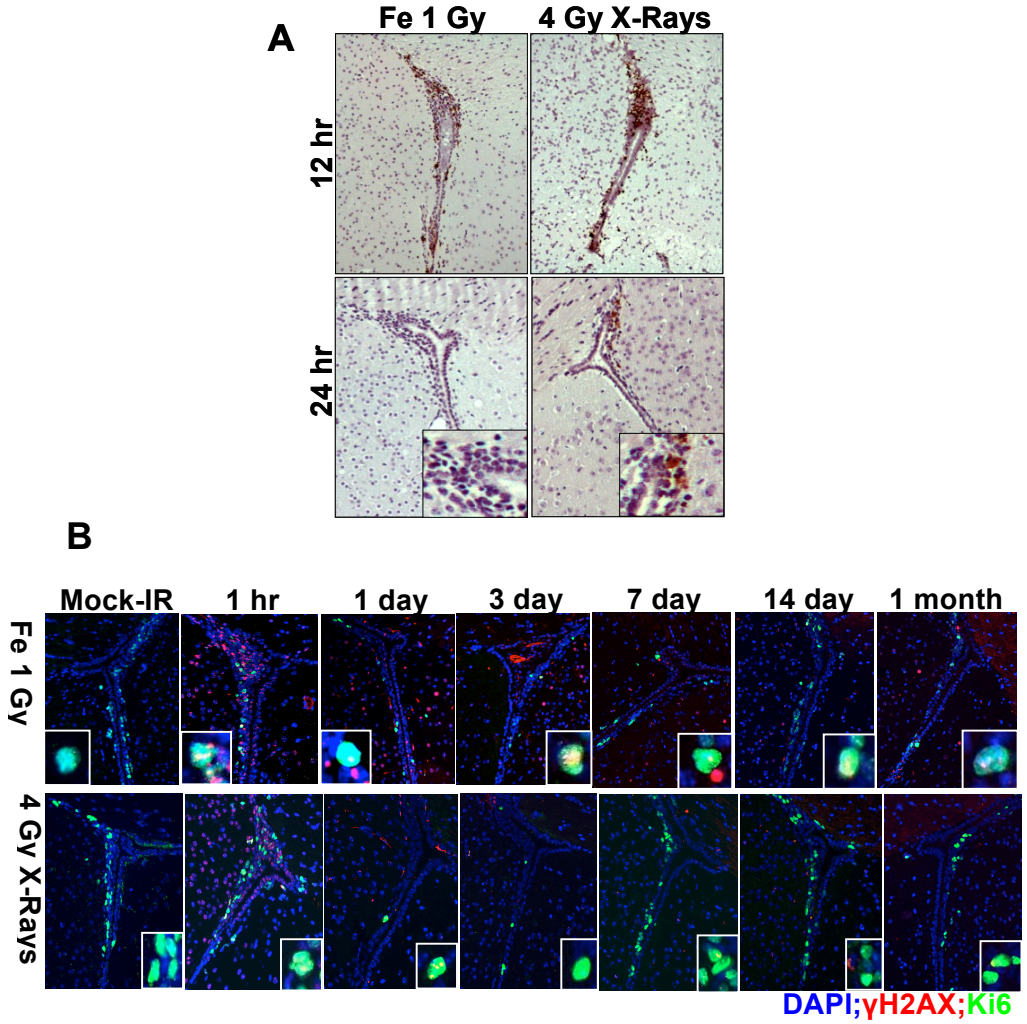

Figure 4.3. Apoptosis and proliferation in the SVZ in response to Fe ions or X-rays. (A) Peroxidase-based TUNEL staining performed on brains at 12- and 24 hr post-IR. High levels of apoptosis observed in the SVZ at 12hr in response to both Fe- and X-ray irradiation. At 24 hr, higher levels of apoptosis are observed after X-ray irradiation. **(B)** 1 Gy Fe or 4 Gy X-ray irradiated mice were sacrificed at indicated timepoints. Proliferation of cells in the SVZ was visualized by staining for Ki67 (green) and DNA damage visualized by γH2AX (red). Note the permanent loss of Ki67-positive cells after irradiation with Fe ions.

Combined inactivation of Ink4a/Ink4ab/Arf cooperates with DSBs inducing high-grade gliomas. Mice from all 3 tumor suppressor backgrounds, at 6-10 weeks of age, were irradiated with a single dose of 1 Gy Fe ions or 4 Gy X-rays. Mice were monitored post-irradiation for brain tumor development by examining clasp reflex, weight loss, and neurological symptoms such as seizure, ataxia, and/or paralysis. Brain tumor incidence observed at 8 months with loss of Ink4a and Arf alone was low after exposure to X-rays- 7.5% with an average latency of 180 days **(Fig 4.4)**. No brain tumors have been observed thus far at approximately 5 months post-exposure to Fe ions. Importantly, the incidence of brain tumors increased significantly with additional loss of Ink4b, when monitored up to 9 months post-IR. Surprisingly though, high-grade gliomas **(Fig 4.5A)** were induced in the Ink4a/Ink4b/Arf-null suppressor background with an incidence of 25% irrespective of the radiation quality **(Fig 4.4)**. The average latency to acute-onset of neurological symptoms was very similar for Fe- and X-ray irradiation, approximately 165 and 171 days. Animals with additional heterozygosity of PTEN have been observed up to 5 months post-irradiation. While loss of Ink4a/Ink4b/Arf alone was not enough to induce spontaneous brain tumors in mock-irradiated animals, additional PTEN heterozygosity results in a very low incidence of spontaneous tumors (2.5%). This incidence increases after X-ray irradiation, and more significantly upon exposure to Fe ions, although the final frequencies will be determined only after completion of the 9-month

observation period. Also, additional heterozygosity of PTEN appears to reduce the average tumor latency, especially after Fe ion irradiation. We conclude that the Ink4a/Ink4b/Arf tumor suppressor background is the most sensitive to radiation-induced gliomas, irrespective of the radiation quality.

All tumors were classified as high-grade gliomas (Grade III or IV), based on a range of histopathological features **(Figure 4.5B)**. Tumors were highly infiltrative, and exhibited high mitotic activity, pleomorphic nuclei, apoptotic cells with some cases showing necrosis and/or microvascular proliferation **(Fig 4.5C)**. Tumors also stained positive for Nestin, GFAP and Olig2 **(Fig 4.5D)**, classical human glioma markers, and showed elevated levels of phospho-Akt, p-Erk, and Ki67, all indicative of oncogenic and pro-proliferative signaling **(Fig 4.5E)**. To rule out occult lesions, all brains from asymptomatic mice were screened by serial sectioning and examination of H&Es. No early lesions or hyperproliferative clusters of cells were identified. We here on focus primarily on analysis of tumors from Ink4a/Ink4b/Arf background since it resulted in the most significant incidence of tumor development with minimal extent of tumor suppressor loss.

A

Nestin-Cre	WT		Ink4a/Arf $^{f/f}$		Ink4ab-/-/Arf $^{f/f}$	
	%	Latency	%	Latency	%	Latency
Mock-IR	0	n/a	0	n/a	0	n/a
Fe	0	n/a	N/D	N/D	25	165
X-Rays	0	n/a	7.5	180	25	171

B

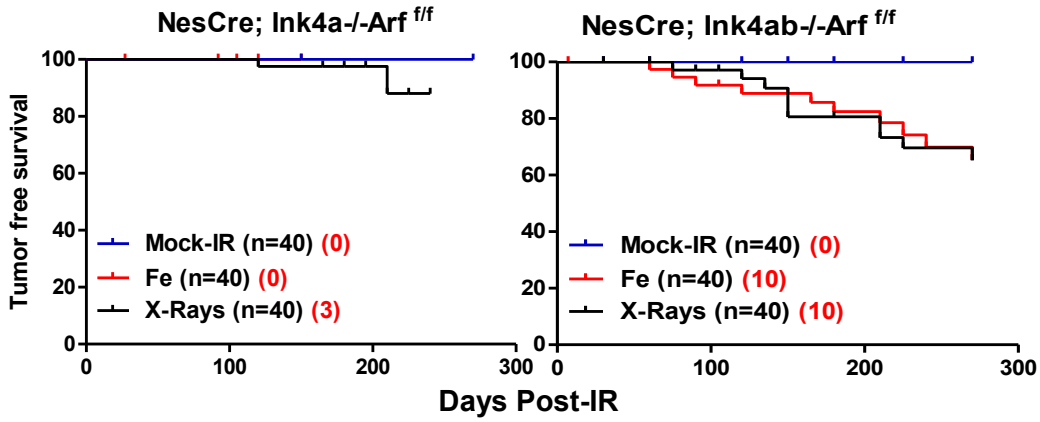

Figure 4.4. Incidence of high-grade gliomas. (A) Table summary of glioma incidence and latency in different mouse models used. No tumors were observed in WT background, or in mock-irradiated Ink4a/Arf and Ink4a/Ink4b/Arf mice (n/a= not applicable). Note low incidence of tumor formation in the absence Ink4a/Arf alone while additional loss of Ink4b significantly raises the incidence to 25%, irrespective of IR quality (ND: Not determined; cohort has not reached 9-month examination period) **(B)** Kaplan-Meier curves showing tumor free survival of mice from different genetic backgrounds; n= total number of mice irradiated; numbers in red indicate total number of gliomas observed.

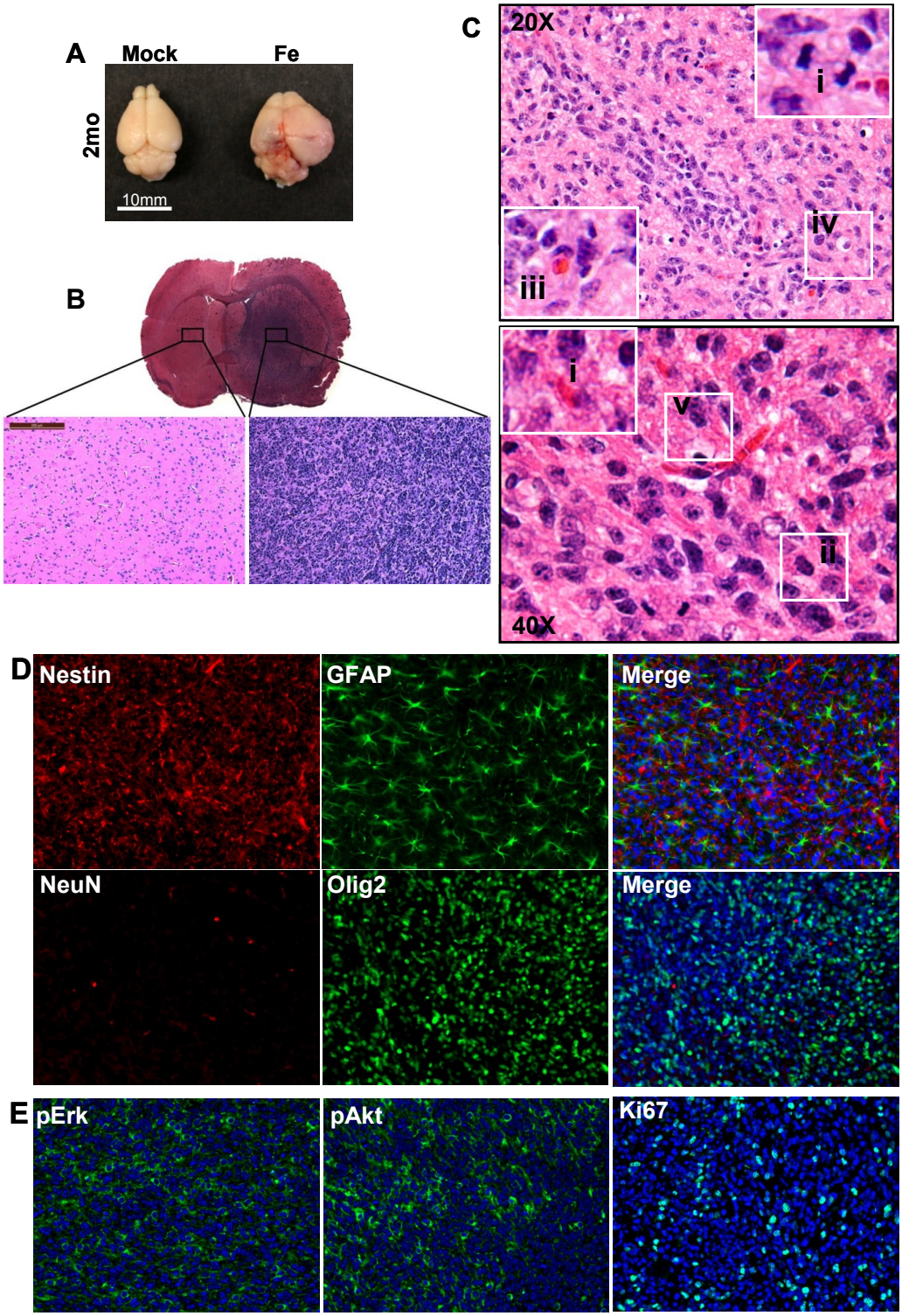
A
Mock
Fe
2mo
10mm
B
C
20X
i
iii
iv
i
v
ii
40X
D
Nestin
GFAP
Merge
NeuN
Olig2
Merge
E
pErk
pAkt
Ki67

Figure 4.5. Histopathological features of high-grade gliomas. (A) Representative Fe-irradiation induced brain tumor from mouse that became symptomatic 2 months post-IR compared to a normal mock-irradiated brain (also 2 months post-IR). **(B)** Hematoxylin and eosin (H&E) section of representative brain harboring a glioma showing infiltrative nature and hypercellularity. **(C)** Tumors were classified as high-grade gliomas based on histopathological features including (i) high mitotic index, (ii) pleomorphic nuclei, (iii) apoptotic cells, (iv) necrosis and/or (v) microvascular proliferation. **(D)** Immunofluorescence staining of tumors for classical human glioma markers, Nestin, GFAP, NeuN and Olig2. (E) Tumors were also highly positive for pErk, pAkt and Ki67.

High frequency of MET amplification in radiation-induced gliomas. Analysis was carried out on 16 Fe- and 2 X-ray induced tumors by array comparative genomic hybridization (aCGH), which revealed complex patterns of copy number variations (CNVs). To identify the regions of CNV that are most likely to drive cancer pathogenesis, we applied the GISTIC statistical method to our collection of 18 tumor samples (Beroukhim et al., 2007). We identified 121 genes with GISTIC scores >5 **(see Appendix B)**. The most significant and frequent amplification (G score= 38.04), found present in 72.2% (13/18) of tumors examined, including Fe- and X-ray derived tumors, localized to a small region on Chr6A2, where MET was the only gene spanned by the peak of the CNV **(Fig 4.6A)**. Of these, 61.5% (8/13) had amplifications spanning the entire MET locus, with log2 ratios typically above 3, implying more than 8 gene copies per cell **(Fig 4.6B)**. Amplification of MET was verified by qPCR in 5 representative tumors compared to tumors which showed no amplification **(Fig 4.6C)**. Other amplifications spanning RTKs implicated in glioma development were PDGFRβ and EGFR, found in 31.6% (6/18) and 16.6% (3/18) of tumors respectively. Log2 ratios for these two genes generally were between 0.5 and 1, indicating low copy amplification. Interestingly, we identified tumors with RTK co-amplification: 3/8 MET-amplified tumors harbored amplifications of PDGFRβ, including 1 tumor which also contained EGFR amplification **(Fig 4.7A)**. FISH was performed to evaluate extent of RTK amplification and tumor

heterogeneity. FISH analysis highly correlated with results obtained from aCGH, with exception of 1 case in which MET amplification could not be verified by FISH, and 1 in which amplification was not detected by aCGH. The pattern of amplification was predominantly of extrachromosomal double minute form **(Fig 4.7B)**. In most cases examined, the amplification of MET was uniform, with every tumor cell showing evidence of amplification. There were examples, however, of heterogeneous tumors, where only a subpopulation of tumor cells harbored the amplifications. Immunofluorescence staining of MET amplified tumors revealed focal regions of high MET expression, which did not always coincide with higher levels of phospho-ERK, phospho-AKT, or phospho-S6, again corroborating the existence of subclones with different RTK-dependencies **(Fig 4.7C)**.

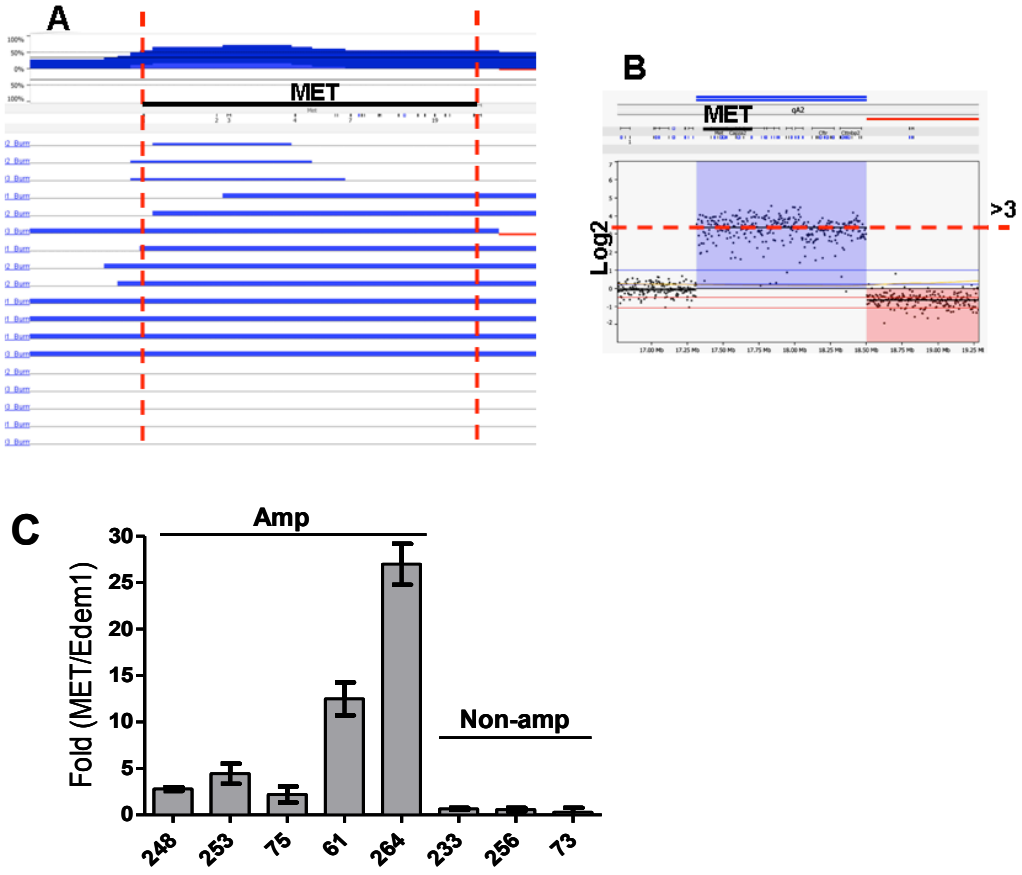

Figure 4.6. Frequent and significant amplification of MET in radiation-induced gliomas. (A) aCGH schematic of MET locus showing region of amplification (blue lines) across 18 tumor samples examined. **(B)** Representative probe view of region neighboring MET locus showing log2 ratios (y-axis) of individual probes along the chromosome (x-axis). **(C)** MET amplification was verified in 5 representative tumors by qPCR compared to 3 non-amplified samples.

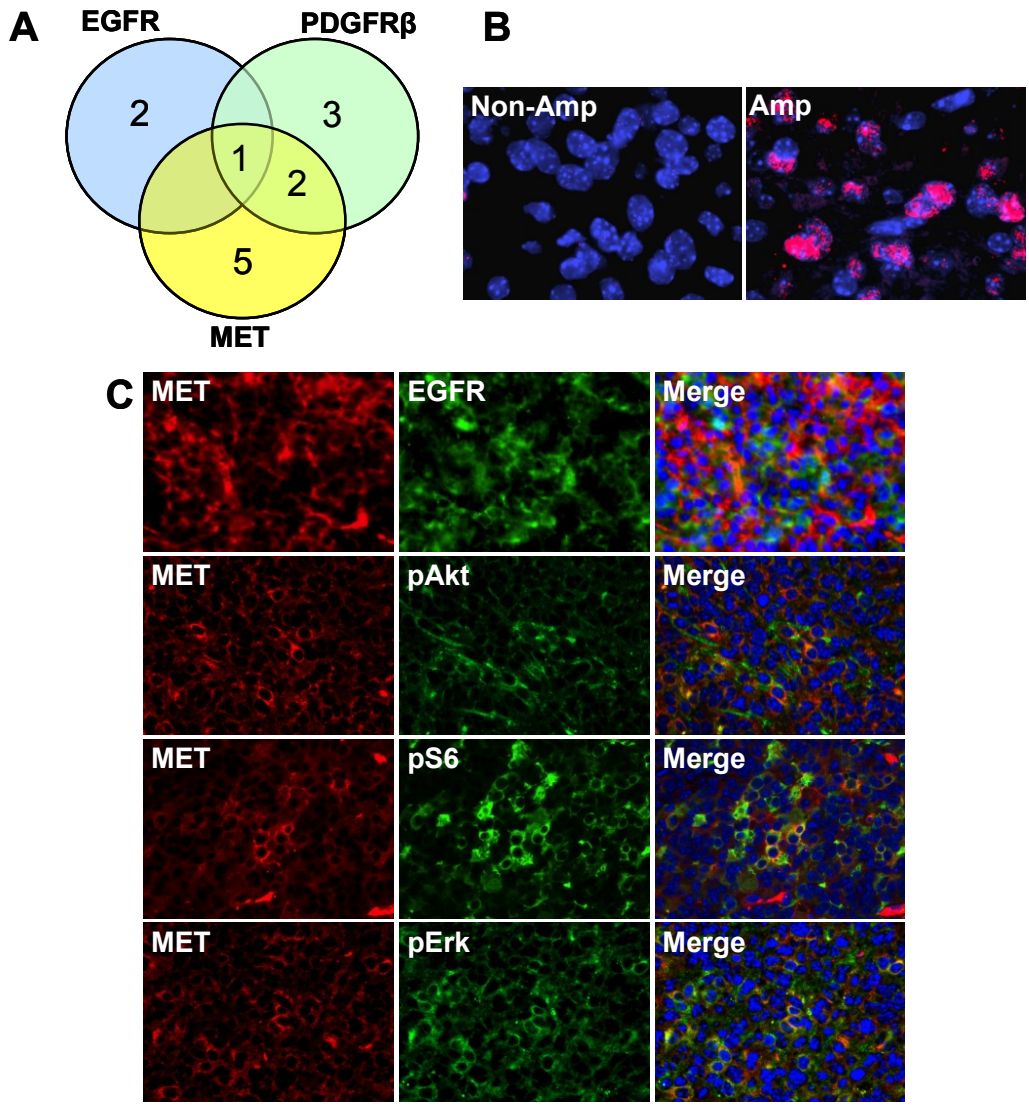

Figure 4.7. Co-amplification of RTKs. (A) Venn diagram showing the status of receptor co-amplification in 13 tumors. **(B)** FISH analysis showing amplification levels of MET (red). **(C)** Immunofluorescence staining of representative MET amplified tumor showing expression of MET and EGFR within the same tumor. Survey of downstream pathway activation by staining for pAkt, pS6, and pErk.

MET overexpression correlates with stem cell-like phenotype. We established *ex vivo* cultures of tumors from X-ray or Fe- irradiated Nestin-Cre; Ink4ab$^{-/-}$;Arf$^{f/f}$ mice. We screened the tumor cultures by examining protein levels of MET relative to primary Ink4ab/Arf-null astrocytes. We were unable to find a significant correlation between MET amplification and overexpression in culture. In fact, even though tissue sections were highly positive for MET **(Fig 4.7C)**, most cultures showed barely detectable levels, indicating absence of selection pressure under *in vitro* culture conditions, similar to what is seen with EGFR and EGFRvIII in human samples (Bigner et al., 1990). Early passage cells from one representative tumor (ID #256) were injected subcutaneously into the flank of a nude mouse. The subcutaneous tumor obtained (#256 subcu) was found to have elevated levels of MET. We proceeded to generate a culture with high MET expression, which we infected with lentivirus expressing a scramble shRNA or an shRNA against MET **(Fig 4.8A)**. Knockdown of MET correlated with significantly decreased levels of Sox2 **(Fig 4.8A and B)**. Based on the essential role of Sox2 in sustaining growth and self-renewal of embryonic stem cells, we examined the ability of these cultures to grow in neural stem cell media. We found that high expression of MET associated with growth as an adherent culture in NSC media (Pollard et al., 2009), which was lost upon MET knockdown, indicative of MET supporting a stem cell-like phenotype **(Fig 4.8C)**.

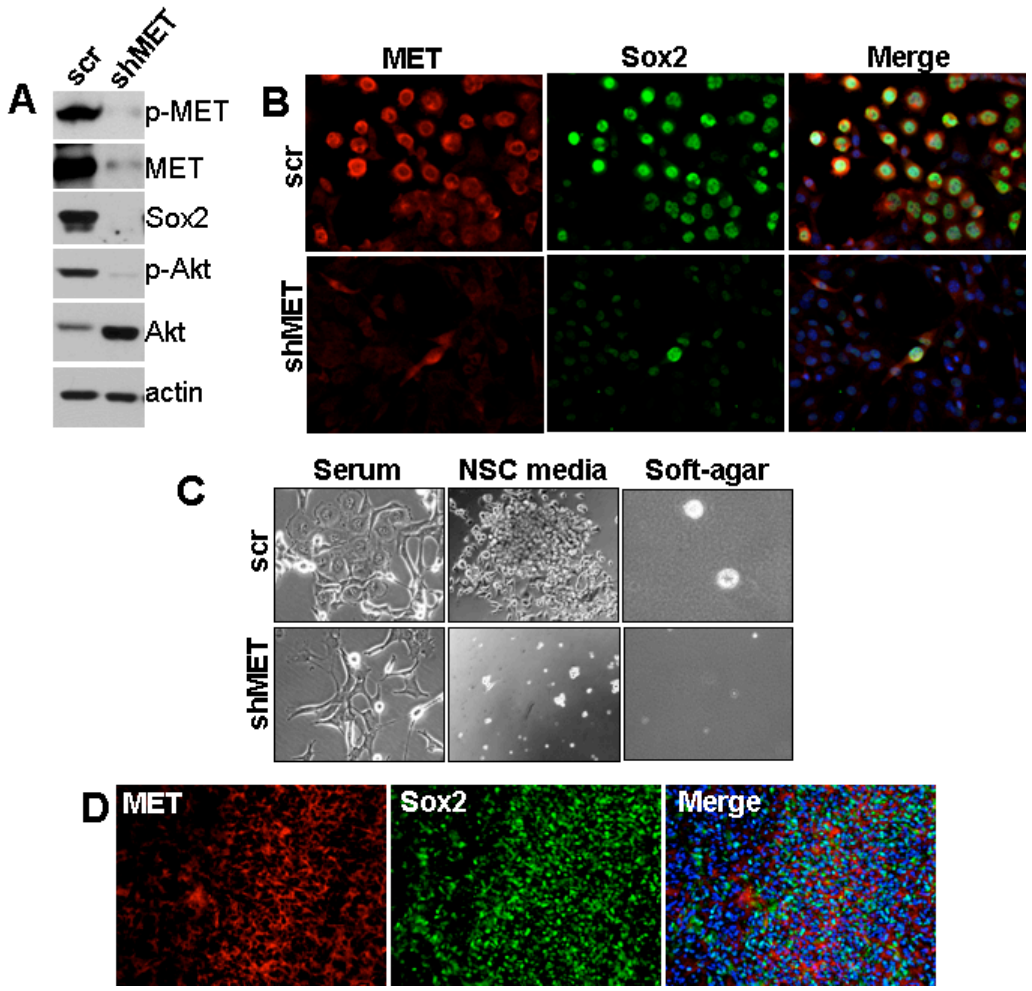

Figure 4.8. MET expression is associated with stem-like phenotype. (A) Western analysis of MET expression in cells infected with scramble shRNA (scr) or an shRNA against MET (shMET). **(B)** Immunofluorescent staining for MET (red) and Sox2 (green) in scramble versus MET knockdown cells. Note higher expression of MET in scramble cells and association with high levels of Sox2. **(C)** Brightfield images of scr or shMET cells growing under full serum, NSC media, or in soft-agar. Note rounded morphology of scr cells in full serum, their growth as adherent culture in NSC media, and formation of spheres in soft-agar. **(D)** Immunofluorescent staining of MET-amplified tumor showing Nestin and Sox2 expression.

This high-expressing MET cell line was also capable of anchorage- independent growth, indicating that MET is also responsible for enhancing tumorigenicity of cells **(Fig 4.8C).** Immunostaining of MET positive tumor sections also revealed positive staining for Nestin, a stem cell marker, and Sox2 **(Fig 4.8C)**. We conclude that MET expression in radiation-induced tumors may be responsible for maintaining a stem cell-like phenotype, which has important clinical implications.

DISCUSSION

Carcinogenesis is known to be a complex process, requiring multiple steps to initiate, promote, progress and maintain tumorigenesis. Ionizing radiation, through the induction of DNA DSBs, is extremely effective at promoting cell death, but breaks that are illegitimately repaired allowing cell survival, are responsible for chromosomal abnormalities and gene mutations, important events in the initiation of cancer (Wakeford, 2004; Little, 2000).

In this study, we have examined the role of simple versus complex DNA double-strand breaks in the induction of high-grade gliomas, using genetically accurate tumor suppressor mouse models. Observations from our lab and others have shown that densely ionizing radiation (Fe ions) is more cytotoxic than sparsely ionizing radiation (X-rays or gamma-rays), due to more severe and complex chromosomal damage. However, difficulty in repairing high-LET

induced damage also results in larger proportions of persistent/unrepaired DSBs, or misrepaired DSBs, which can presumably increase the tumorigenic potential of irradiated cells (Camacho et al., 2010; Sage and Harrison, 2010). *In vitro* studies have clearly shown that limiting the persistence of a DSB reduces the frequency of repair pathways that lead to significant genetic loss, diminishing its mutagenic potential (Bennardo et al., 2009).

Radiation-induced carcinogenesis in the context of GBM is extremely significant, given that IR is the only known risk factor for developing these lethal brain tumors. Loss of CDKN2A/B is speculated to be one of the earliest events in gliomagenesis (Attolini et al., 2010). Our results indicate that loss of these three tumor suppressors, Ink4a/Ink4b/Arf, is insufficient for gliomagenesis, but cooperate with DNA double-strand breaks to efficiently induce high-grade gliomas. Additional heterozygous loss of PTEN does not affect the incidence of brain tumors, but does shorten the latency to tumor formation, in agreement with other models suggesting a role for PTEN in tumor progression (Kwon et al., 2008; Wei et al., 2006; Xiao et al., 2002). Importantly, we observe a significantly lower incidence of gliomas with loss of Ink4a and Arf alone, corroborating our previous work showing that loss of p15/Ink4b is a critical event in radiation-induced transformation. Most surprising is the result that DSBs, whether simple or complex (resulting from X-ray or Fe- irradiation), are capable of generating high-grade gliomas after exposure to an acute, clinically-relevant dose in our

model systems. The results suggest the need to take greater caution when exposing an already susceptible population, such as cancer patients to radiation therapy. Indeed, the appearance of secondary malignancies in patients that have undergone radiation treatment is an emerging problem.

A great advantage to our model is the fact that radiation-induced aberrations are stochastic. Radiation creates genomic instability allowing us to identify the key genetic changes which are most advantageous for transformation to take place. Without bias towards a particular oncogene, we have identified genomic aberrations with strong selective pressure in Ink4a/Ink4b/Arf- knockout tumors. Most striking of all is the recurrent amplification of the receptor tyrosine kinase MET, which has been observed in other mouse models of gliomagenesis (Chow et al., 2011) and is a well-known target of amplification and/or mutation in human GBM. MET amplification and/or mutation, causing protein overexpression has been reported in a number of human primary tumors and has strong clinical implications. Studies have demonstrated that only cell lines with amplification of MET gene are responsive to MET inhibition and early clinical trials using MET inhibitors are currently underway (Comoglio et al., 2008; Smolen et al., 2006; McDermott et al., 2007). Interestingly, recent studies have also shown that MET gene amplification is a mechanism by which tumors acquire resistance EGFR inhibitors (Engelman et al., 2007). This is the case in non-small cell lung cancer, where MET expression plays a key role in mediating

acquired resistance to EGFR inhibitors, suggesting the need for combined therapies to provide therapeutic benefit (Jun et al., 2011; Turke et al., 2010). Combination therapy may be especially important in GBM, which has an innate ability to develop resistance to targeted drug therapies, very likely due to the presence of tumor subclones harboring different gene amplifications that allow for diverse RTK-dependencies, as observed in our model.

GBM resistance to drug therapies and recurrence has also been attributed to the presence of neoplastic stem-like cells, better known as glioblastoma stem cells. While the bulk of the tumor can be targeted with conventional therapies, a resistant stem-like population of tumor cells survive that are responsible for tumor repopulation (Wee et al., 2011, Dirks, 2006). Studies have shown that MET activation enhances both resistance to DNA damage and tumor-initiating capacity of human glioma lines, properties of stem cells (Li et al., 2005; Laterra et al., 1997; Koochekour et al., 1997). Notably, a recent study has implicated that MET signaling induces a reprogramming network that supports the glioblastoma stem-like phenotype (Li et al., 2011). Li et al., showed that MET signaling is activated in GBM-derived neurospheres, and is capable of regulating Sox2, c-Myc, Klf4, Oct4, and Nanog expression, expanding the population of stem-like cells. Our observations that MET expression correlates with high expression of Sox2 and the ability to grow in neural stem cell media and as anchorage-independent colonies (properties of stemmness) are in line with these studies.

The clinical implication is that inhibitors of MET signaling might be useful in targeting these so called glioblastoma stem cells.

In conclusion, the mouse models of radiation-induced gliomagenesis presented here are genetically accurate models, where stochastically acquired mutations lead to a spectrum of genomic aberrations and histopathological features commonly observed in human GBM, making them a useful tool for testing preclinical therapeutics.

CHAPTER V

Conclusions and Future Directions

CONCLUSIONS AND FUTURE DIRECTIONS

The work presented here is the first attempt to systematically evaluate the cooperativity between simple or complex DSBs and tumor suppressor loss that results in cellular transformation and ultimately, tumorigenesis. Carcinogenesis is known to be a complex process, requiring multiple steps to initiate, promote, progress and maintain tumorigenesis. Ionizing radiation, through the induction of DSBs, is extremely effective at promoting cell death, but breaks that are illegitimately repaired allowing cell survival, are responsible for chromosomal abnormalities, gene mutations and rearrangements, important events in the initiation of cancer (Wakeford, 2004; Little, 2000). In essence, this work demonstrates that radiation-induced DNA double-strand breaks can cooperate with pre-existing tumor suppressor loss to trigger high-grade gliomas in 'sensitized' mouse models that are not normally prone to gliomagenesis. The use of these 'sensitized' models allows for rapid evaluation of how loss of specific tumor suppressors contributes to tumor initiation in combination with DNA damage.

In response to DSBs, mammalian cells activate a network of signaling pathways that collectively execute the so called DNA damage response (DDR). Activation of this pathway results in transient cell cycle arrest, allowing time for the cell to repair the damage. However, if the damage is too severe, the cell can undergo programmed cell death (apoptosis) or enter permanent cell cycle arrest,

termed senescence. Activation of the DDR has therefore been postulated to be an anti-cancer barrier (Zhou and Elledge, 2000; Bartkova et al., 2005). Proper repair of DSBs is essential to ensure faithful transmission of the genetic material and maintenance of genomic stability. The presence of complex DSBs, such as those induced by heavy particles, increases the risk of mutagenic events. Even if the cell is able to process and repair complex lesions, misrepair can be more detrimental to the cell in terms of tumorigenesis than unrepaired lesions, which would result in cell death or senescence. The misrepair of complex DSBs might allow for cell cycle to resume and mitosis to take place, facilitating genome instability in the progeny of irradiated cells. This may account for the secondary phase of activation of the DDR observed in normal human skin fibroblasts at 3 days post heavy particle irradiation (Chapter II). Based on this study and published reports, the initial fast kinetics of repair observed within the first 30 minutes of irradiation rely on the NHEJ pathway for repair (Mladenov and Iliakis, 2011). More complex DSBs are repaired with slower kinetics and have been shown to rely heavily on ATM (Goodarzi et al, 2008; Magnander and Elmroth, 2012). Blocking ATM or DNA-PK however, does not abrogate repair completely, suggesting the involvement of the signaling kinase ATR, and other repair pathways, such as HRR or back-up NHEJ. The increased chromosomal instability and tumorigenic potential of cells irradiated with heavy particles favors NHEJ and or back-up NHEJ, the most error-prone repair processes.

A significant discrepancy was observed between our *in vitro* and *in vivo* models in terms of transformation rates observed after gamma (or X-ray) irradiation or Fe irradiation (Chapters III and IV). While the tumorigenic potential of Fe ions was greater compared to gamma-rays in an *in vitro* system (refer to **Fig 3.2**), no difference was observed in our Ink4a/Ink4b/Arf mouse model (refer to **Fig 4.4**). For transformation to take place in these "sensitized" model systems, there are two basic requirements: a mutagenic event and cell viability. In other words, there has to be a balance between a mutagenic event that enhances fitness/confers selective advantage and cell survival (cell must be able to propagate the genetic alterations). In the case of Fe ions, there is a possibility that with such a high burden of complex DNA damage, the repair machineries become saturated. With the inability to repair the damage the balance tips toward cell death or cell cycle arrest. Indeed, proliferation is more severely reduced in response to Fe ions in the SVZ when compared to X-ray irradiation (refer to **Fig 4.3**). Transformation then might be described by a normal distribution curve, with transformation rate on the y-axis and radiation dose on the x-axis. As the dose increases, so does transformation rate, leading to a peak at which point higher doses tip the balance towards cell death and/or cell cycle arrest and transformation rate decreases. I speculate therefore, that at 1 Gy of Fe ions, we may be past the peak of transformation rate. Examining the

transformation rates with lower doses of Fe ions would help to clarify these conflicting observations.

The Ink4-Arf locus encompasses a short stretch of only 35 kilobases in the mouse and human genome. It encodes three very important tumor suppressors: Ink4a, Ink4b and Arf. Given their significant roles in regulating RB and p53 (genes with important functions in carcinogenesis), it is not surprising that the entire locus is commonly deleted in many cancers. In fact, it is postulated that loss of this locus is an early event in multi-step process of cancer (Yasaei et al., 2012; Attolini et al., 2010). Loss of all three genes by a single deletion event has raised questions about the role of each in tumor suppression. Inactivating point mutations in Ink4a have been identified in human cancers, and germline deletion predisposes mice to spontaneous tumors, making Ink4a a bona fide tumor suppressor (Kim and Sharpless, 2006; Sharpless et al., 2001). Mutations targeting Ink4b though, are far less common and very few studies have examined the effect of Ink4b loss on tumorigenesis. Notably, a recent study carried out by Krimpenfort et al., clearly shows that Ink4b compensates for Ink4a loss, playing a very crucial ‘back-up’ role for Ink4a (2007).

Using our models with different combinations of these tumor suppressors, we reinforce the role of Ink4b in tumor suppression. *In vitro*, loss of Ink4b accompanies tumorigenesis triggered by complex DSBs in the context of Ink4a/Arf-null astrocytes. *In vivo*, we find that irrespective of the radiation

quality, the incidence of gliomas with loss of Ink4a and Arf alone is significantly lower when compared to the incidence in Ink4a, Ink4b and Arf-deficient mice. It is important to clarify, however, that loss of Ink4b alone is not a transforming event, given that our Ink4a/Ink4b/Arf mouse model does not spontaneously develop gliomas. Also supporting this point is the observation that re-expression of Ink4b in tumors is not sufficient to block tumorigenic potential of cells, rather it only serves to modulate tumor growth (refer to Fig 3.6). More accurately, loss of Ink4b facilitates initiation, creating an environment that is permissive to transformation by an oncogenic insult (refer to potential oncogenes in **Appendices A and B**). It remains to be seen if Ink4b loss occurs in Ink4a/Arf-null tumors *in vivo*.

An interesting observation regarding Ink4-Arf regulation is the fact that this locus is silenced in stem cells, but becomes more responsive in differentiated progenitors (He et al., 2009). The locus is also silenced in somatic cells through induced iPS (induced pluripotent stem) reprogramming (Li et al., 2009). The implication is that with loss of these tumor suppressors, cells gain a greater potential for 'stemmness.' In fact, one important question remains as to the cell-of-origin for gliomas in our model system. The specific cell-of-origin in human gliomas is unclear. There are three plausible candidates, a differentiated glial cell, a restricted progenitor cell, or an adult neural stem cell, either one acquiring genetic mutations that allow for transformation and tumor initiation and

progression (Rankin et al., 2011; Wee et al., 2011). Although many of the tumors obtained from the various genetic backgrounds were adjacent to proliferative niches **(Fig 4.5B)**, we cannot say with certainty that these tumors generated from a true stem cell. In order to identify the cell-of-origin, more sophisticated mouse models must be employed. By using Nestin-Cre (Isaka et al., 1999) for targeting gene deletion, we have induced widespread tumor suppressor loss, maximizing the number of targets for radiation-induced transformation. Ideally, spatial and temporal conditional targeting using inducible Cre expression would facilitate a more accurate identification of the cell-of-origin.

We can conclude that loss of Ink4a/Ink4b/Arf is an important initiating event (further confirmed by recently published work by Yasaei et al., 2012) and exposure to ionizing radiation promotes the acquisition of secondary mutations needed to drive tumorigenesis. This goal of this work was to identify those secondary events by using genomic and gene-expression analyses. These methods generate a substantial amount of data, but the biggest challenge is to carefully distinguish the 'driver' mutations, those that confer a biological advantage, from 'passenger' mutations, the random somatic events that confer no selective advantage (Beroukhim et al., 2007). A secondary driver mutation would be the activation of an oncogene, such as the receptor tyrosine kinase MET, which we observe in our mouse models. MET was found to have transforming potential when it was first identified in an osteosarcoma cell line as a fusion

protein with TRP (Translocated Promoter Region) (Cooper et al., 1984). Constitutive MET activation (by gene amplification, activating mutations, or transcriptional upregulation) has now been reported in variety of human primary tumors. In some cases, MET amplification is found to be required to maintain the transformed phenotype, in others MET appears to be a secondary event that influences later stages of neoplastic progression (Comoglio et al., 2008; Trusolino et al., 2010). In our model systems, amplification of MET was identified in tumors that were analyzed at the time of morbidity (late-stage), so we can only speculate on the sequence of events in the cancer's natural history. It's interesting that in some of our radiation-induced gliomas, the pattern of amplification is heterogeneous, with only a subset of tumor cells showing evidence of amplification, indicating that it was a late event. However, tumors with very uniform patterns of amplification, indicating an early event were also obtained.

High-level amplification of MET has been observed in a Brca1/Trp53 mouse model of mammary tumorigenesis (Smolen et al., 2006), and in a GFAP-CreER™; $PTEN^{f/f}$; $p53^{f/f}$; $RB^{f/f}$ model of gliomagenesis (Chow et al., 2011). In the case of breast cancer, upon examination of 100 sporadic human breast cancer samples, no high-level MET amplification was found (Smolen et al., 2006). Amplification of MET is a very relevant genetic event occurring in approximately 4% of human glioblastomas, granted a much lower frequency

when compared to other RTKs such as EGFR and PDGFRα.(TCGA, 2008). Again, there is a discrepancy between the human data and mouse models of gliomagenesis in regards to the amplitude of MET amplification. Apart from the lower frequency observed in human GBM samples, these amplifications do not occur at such high amplitudes as that observed in our mouse models. These differences may be due to the exposure to ionizing radiation, although this would not explain why such high levels of amplification are also observed in the GFAP-CreER™; PTEN$^{f/f}$; p53$^{f/f}$; RB$^{f/f}$ model (Chow et al., 2011). Most likely, this is attributed to species-specific susceptibilities of MET locus to rearrangements. This is a limitation with using mouse models, and the results suggest that caution be used in extrapolating genetic pathways from mouse to human. Regardless, the amplitude and frequency of MET amplification in our model argues for a prominent role of MET in radiation-induced gliomagenesis. It is plausible that the number of human glioblastomas with MET amplification is underrepresented given the genetic heterogeneity that is characteristic of this tumor type. A tumor may harbor a small subpopulation of cells with MET amplification that would fail to be detected by SNP (single nucleotide polymorphism) arrays due to dilution of the sample. Careful functional studies should be carried out in the future to examine the role MET in tumorigenesis. For example, *in vitro* experiments should be carried out to test the transforming potential of MET in Ink4a/Ink4b/Arf- null astrocytes. Our preliminary results **(Fig 4.8)** indicate that

MET signaling is playing an important role in maintaining a stem-cell like state, and enhancing tumorigenesis which has clinical implications. On the other hand, with many early phase clinical trials currently underway, the effects of MET loss of function, either by knockdown or chemical inhibition, on tumor growth should also be carefully studied. The models presented here accurately recapitulate the pathogenesis of GBM, making them a useful tool for testing these preclinical therapeutics.

With the available genomic and gene-expression data that has been gathered from these radiation-induced tumors, a next step would be to compare to what extent these tumors recapitulate gene expression subclasses of human glioblastoma. Two groups, using whole transcriptome analysis, identified four subclasses of GBM, classical, neural, proneural, and mesenchymal (Phillips et al., 2006; Verhaak et al., 2010). Comparing gene-expression signatures from our models to these subclasses, will allow us to understand whether radiation-induced gliomagenesis is fundamentally similar to that occurring spontaneously, both in mouse models and in human patients.

APPENDIX

APPENDIX A

Candidate oncogenes in common regions of CNV

Chrom 2 Gain: (qH1-qH3) Length of amplification: 13866346bp		
Gene Symbol	**Name**	**Reference**
Src	Rous sarcoma oncogene	Activation promotes tumor progression and invasion (Lu et al, Kim et al)
Nnat	neuronatin	Overexpression increases proliferation and soft agar colony formation and size (Siu et al)
Mafb	v-maf musculoaponeurotic fibrosarcoma oncogene family, protein B (avian)	Overexpressed in human cancers (Eychene et al)
Serinc3	serine incorporator 3	TDE1: accelerates tumor formation (Bossolasco et al)
Ada	adenosine deaminase	Increased activity in gastric cancer tissue (Gocmen et al)
Tomm34	translocase of outer mitochondrial membrane 34	Upregulated in colorectal tumors (Shimokawa et al)
Slpi	secretory leukocyte peptidase inhibitor	Overexpression associated with aggressive, hish-risk, or metastatic cancer (Bouchard et al)
Wfdc2	WAP four-disulfide core domain 2	Gene amplified in ovarian carcinomas (Hellstrom et al)
Ube2c	ubiquitin-conjugating enzyme E2C	Overexpressed in astrocytic tumors (Jiang et al)
Mmp9	matrix metallopeptidase 9	Expression correlates with glioma progression (Levicar et al)
Cdh22	cadherin 22	Overexpression is associated with tumor progression (Zhou et al)
Eya2	eyes absent 2 homolog (Drosophila)	Increased expression in lung adenocarcinoma (Guo et al)
Ncoa3	nuclear receptor coactivator 3	Frequently overexpressed in human cancers;Involved in cell cycle deregulation (Louie et al)
Prex1	phosphatidylinositol-3,4,5-trisphosphate-dependent Rac exchange factor 1	Promotes prostate cancer metastasis (Qin et al)
Ptpn1	protein tyrosine phosphatase, non-receptor type 1	Promotes transformation (Stuible et al)
Sall4	sal-like 4 (Drosophila)	Constitutively expression in acute lymphoblastic leukemia (Cui et al)

Cyp24a 1	cytochrome P450, family 24, subfamily a, polypeptide 1	Overexpressed in colorectal cancer (Horvath et al)

Chrom 4 Gain: (qD3-qE2)	**Length of Amplification: 17296787bp**	
Gene Symbol	**Name**	**Reference**
Epha2	Eph receptor A2	RTK: overexpression in high grade glioma (Liu et al, Wykosky et al)
Spen/Sharp	SPEN homolog, transcriptional regulator (Drosophila)	Positive regulator of Wnt-dependent signaling; elevated in cancer (Feng et al)
Ptchd2	patched domain containing 2	DISP3: Expressed in brain tumor (Katoh et al)
Angptl7	angiopoietin-like 7	Target of Wnt signaling; upregulate angiogenesis (Katoh et al)
Mtor	mechanistic target of rapamycin (serine/threonine kinase)	Involved in regulation of cell growth and proliferation (Liu et al, Engelman)
Pik3cd	phosphatidylinositol 3-kinase catalytic delta polypeptide	Induces transformation in cultured cells;constitutively activates Akt signaling pathway (Kang et al, Wee et al)
Ski	ski sarcoma viral oncogene homolog (avian)	Induces transformation upon over-expression (Deheuninck and Lou)
Dvl1	dishevelled, dsh homolog 1 (Drosophila)	Component of Wnt signaling pathway (Wharton, Wei et al)

Chrom 9 Gain: (qA5.1)	**Length of Amplification: 1811504bp**	
Gene Symbol	**Name**	**Reference**
Trim29	tripartite motif-containing 29	Elevated expression in invasive pancreatic cancers and precursor lesions (Wang et al)

References

Bossolasco M, Veillette F, Bertrand R, & Mes-Masson AM (2006) Human TDE1, a TDE1/TMS family member, inhibits apoptosis in vitro and stimulates in vivo tumorigenesis. (Translated from eng) *Oncogene* 25(33):4549-4558 (in eng).

Bouchard D, Morisset D, Bourbonnais Y, & Tremblay GM (2006) Proteins with whey-acidic-protein motifs and cancer. (Translated from eng) *Lancet Oncol* 7(2):167-174 (in eng).

Cui W, *et al.* (2006) Differential expression of the novel oncogene, SALL4, in lymphoma, plasma cell myeloma, and acute lymphoblastic leukemia. (Translated from eng) *Mod Pathol* 19(12):1585-1592 (in eng).

Deheuninck J & Luo K (2009) Ski and SnoN, potent negative regulators of TGF-beta signaling. (Translated from eng) *Cell Res* 19(1):47-57 (in eng).

Engelman JA (2009) Targeting PI3K signalling in cancer: opportunities, challenges and limitations. (Translated from eng) *Nat Rev Cancer* 9(8):550-562 (in eng).

Eychene A, Rocques N, & Pouponnot C (2008) A new MAFia in cancer. (Translated from eng) *Nat Rev Cancer* 8(9):683-693 (in eng).

Feng Y, *et al.* (2007) Drosophila split ends homologue SHARP functions as a positive regulator of Wnt/beta-catenin/T-cell factor signaling in neoplastic transformation. (Translated from eng) *Cancer Res* 67(2):482-491 (in eng).

Gocmen E, Tez M, Ozturk S, Koc M, & Demirci S (2009) Activities of adenosine deaminase and 5'-nucleotidase in cancereous and non-cancereous human gastric tissues. (Translated from eng) *Bratisl Lek Listy* 110(7):416-418 (in eng).

Guo JT, Ding LH, Liang CY, Zhou NK, & Ye QN (2009) [Expression of EYA2 in non-small cell lang cancer]. (Translated from chi) *Zhonghua Zhong Liu Za Zhi* 31(7):528-531 (in chi).

Hellstrom I, *et al.* (2003) The HE4 (WFDC2) protein is a biomarker for ovarian carcinoma. (Translated from eng) *Cancer Res* 63(13):3695-3700 (in eng).

Horvath HC, *et al.* (2009) The Candidate Oncogene CYP24A1: A Potential Biomarker for Colorectal Tumorigenesis. (Translated from Eng) *J Histochem Cytochem* (in Eng).

Jiang L, *et al.* (2008) Expression of ubiquitin-conjugating enzyme E2C/UbcH10 in astrocytic tumors. (Translated from eng) *Brain Res* 1201:161-166 (in eng).

Kang S, Denley A, Vanhaesebroeck B, & Vogt PK (2006) Oncogenic transformation induced by the p110beta, -gamma, and -delta isoforms of class I phosphoinositide 3-kinase. (Translated from eng) *Proc Natl Acad*

Sci U S A 103(5):1289-1294 (in eng).
Katoh Y & Katoh M (2005) Identification and characterization of DISP3 gene in silico. (Translated from eng) *Int J Oncol* 26(2):551-556 (in eng).
Katoh Y & Katoh M (2006) Comparative integromics on Angiopoietin family members. (Translated from eng) *Int J Mol Med* 17(6):1145-1149 (in eng).
Kim LC, Song L, & Haura EB (2009) Src kinases as therapeutic targets for cancer. (Translated from eng) *Nat Rev Clin Oncol* 6(10):587-595 (in eng).
Levicar N, Nuttall RK, & Lah TT (2003) Proteases in brain tumour progression. (Translated from eng) *Acta Neurochir (Wien)* 145(9):825-838 (in eng).
Liu F, *et al.* (2006) A genome-wide screen reveals functional gene clusters in the cancer genome and identifies EphA2 as a mitogen in glioblastoma. (Translated from eng) *Cancer Res* 66(22):10815-10823 (in eng).
Liu P, Cheng H, Roberts TM, & Zhao JJ (2009) Targeting the phosphoinositide 3-kinase pathway in cancer. (Translated from eng) *Nat Rev Drug Discov* 8(8):627-644 (in eng).
Louie MC, Revenko AS, Zou JX, Yao J, & Chen HW (2006) Direct control of cell cycle gene expression by proto-oncogene product ACTR, and its autoregulation underlies its transforming activity. (Translated from eng) *Mol Cell Biol* 26(10):3810-3823 (in eng).
Lu KV, *et al.* (2009) Fyn and SRC are effectors of oncogenic epidermal growth factor receptor signaling in glioblastoma patients. (Translated from eng) *Cancer Res* 69(17):6889-6898 (in eng).
Qin J, *et al.* (2009) Upregulation of PIP3-dependent Rac exchanger 1 (P-Rex1) promotes prostate cancer metastasis. (Translated from eng) *Oncogene* 28(16):1853-1863 (in eng).
Shimokawa T, *et al.* (2006) Identification of TOMM34, which shows elevated expression in the majority of human colon cancers, as a novel drug target. (Translated from eng) *Int J Oncol* 29(2):381-386 (in eng).
Siu IM, *et al.* (2008) Coexpression of neuronatin splice forms promotes medulloblastoma growth. (Translated from eng) *Neuro Oncol* 10(5):716-724 (in eng).
Stuible M, Doody KM, & Tremblay ML (2008) PTP1B and TC-PTP: regulators of transformation and tumorigenesis. (Translated from eng) *Cancer Metastasis Rev* 27(2):215-230 (in eng).
Wang L, *et al.* (2009) Oncogenic function of ATDC in pancreatic cancer through Wnt pathway activation and beta-catenin stabilization. (Translated from eng) *Cancer Cell* 15(3):207-219 (in eng).
Wee S, Lengauer C, & Wiederschain D (2008) Class IA phosphoinositide 3-kinase isoforms and human tumorigenesis: implications for cancer drug discovery and development. (Translated from eng) *Curr Opin Oncol* 20(1):77-82 (in eng).

Wei Q, *et al.* (2008) Dishevelled family proteins are expressed in non-small cell lung cancer and function differentially on tumor progression. (Translated from eng) *Lung Cancer* 62(2):181-192 (in eng).

Wharton KA, Jr. (2003) Runnin' with the Dvl: proteins that associate with Dsh/Dvl and their significance to Wnt signal transduction. (Translated from eng) *Dev Biol* 253(1):1-17 (in eng).

Wykosky J & Debinski W (2008) The EphA2 receptor and ephrinA1 ligand in solid tumors: function and therapeutic targeting. (Translated from eng) *Mol Cancer Res* 6(12):1795-1806 (in eng).

Zhou J, *et al.* (2009) Over-expression of CDH22 is associated with tumor progression in colorectal cancer. (Translated from eng) *Tumour Biol* 30(3):130-140 (in eng).

APPENDIX B

GISTIC Genes With G-Score >5

Gene Symbol	Chromosome	Name
BC145376	chr1	
Itln1	chr1	intelectin 1 (galactofuranose binding)
Cd244	chr1	CD244 natural killer cell receptor 2B4
Ttn	chr2	titin
AK086312	chr2	
Ttn	chr2	titin
Olfr1036	chr2	olfactory receptor 1036
Gm14403	chr2	predicted gene 14403
Sprr2a1	chr3	small proline-rich protein 2A1
Sprr2a2	chr3	small proline-rich protein 2A2
DQ697944	chr4	
DQ568775	chr4	
DQ550824	chr4	
Skint4	chr4	selection and upkeep of intraepithelial T cells 4
Skint3	chr4	selection and upkeep of intraepithelial T cells 3
Skint9	chr4	selection and upkeep of intraepithelial T cells 9
Skint5	chr4	selection and upkeep of intraepithelial T cells 5
2610528J11Rik	chr4	RIKEN cDNA 2610528J11 gene
Tmem125	chr4	transmembrane protein 125
Wdr65	chr4	WD repeat domain 65
Gm17019	chr5	predicted gene 17019
Gm9758	chr5	predicted gene 9758
Speer8-ps1	chr5	spermatogenesis associated glutamate (E)-rich protein 8, pseudogene 1
Speer7-ps1	chr5	spermatogenesis associated glutamate (E)-rich protein 7, pseudogene 1
Speer4d	chr5	spermatogenesis associated glutamate (E)-rich protein 4d
BC061212	chr5	cDNA sequence BC061212
AU018829	chr5	expressed sequence AU018829
Met	chr6	met proto-oncogene
TCRB13-1-1	chr6	
Tcrb	chr6	T-cell receptor beta chain
TCRB	chr6	T-cell receptor beta chain
TCR-beta chain	chr6	
Z12226	chr6	
Cntnap2	chr6	contactin associated protein-like 2
AK018905	chr6	

AK019592	chr6	
Klra5	chr6	killer cell lectin-like receptor, subfamily A, member 5
Klra21	chr6	killer cell lectin-like receptor subfamily A, member 21
Klra8	chr6	killer cell lectin-like receptor, subfamily A, member 8
CH29-493D4.3	chr6	
Klra14	chr6	killer cell lectin-like receptor subfamily A, member 14
Klra9	chr6	killer cell lectin-like receptor subfamily A, member 9
Ly-49W	chr6	
Klra12	chr6	killer cell lectin-like receptor subfamily A, member 12
Klra18	chr6	killer cell lectin-like receptor, subfamily A, member 18
Ly49A	chr6	
Klra22	chr6	killer cell lectin-like receptor subfamily A, member 22
Klra15	chr6	killer cell lectin-like receptor, subfamily A, member 15
Lilrb3	chr7	leukocyte immunoglobulin-like receptor, subfamily B (with TM and ITIM domains), member 3
Pirb	chr7	
Pira2	chr7	paired-Ig-like receptor A2
AK137448	chr7	
Pira7	chr7	paired-Ig-like receptor A7
Gm14548	chr7	predicted gene 14548
Pira4	chr7	paired-Ig-like receptor A4
Pira11	chr7	paired-Ig-like receptor A11
Pira1	chr7	paired-Ig-like receptor A1
Cyp2b13	chr7	cytochrome P450, family 2, subfamily b, polypeptide 13
Ipw	chr7	imprinted gene in the Prader-Willi syndrome region
Snord116	chr7	small nucleolar RNA, C/D box 116 cluster
Snord116l1	chr7	small nucleolar RNA, C/D box 116-like 1
Snord116l2	chr7	small nucleolar RNA, C/D box 116-like 2
Snord116	chr7	small nucleolar RNA, C/D box 116 cluster
Trim34	chr7	tripartite motif-containing 34A
Trim34a	chr7	tripartite motif-containing 34A
Trim5	chr7	tripartite motif-containing 5
Trim12a	chr7	tripartite motif-containing 12A
Trim12	chr7	tripartite motif-containing 12A

AK085986	chr7	
Trim30d	chr7	tripartite motif-containing 30D
Trim30e-ps1	chr7	tripartite motif-containing 30E, pseudogene 1
EG625321	chr7	tripartite motif-containing 30E, pseudogene 1
Mrgprf	chr7	MAS-related GPR, member F
Mrgprd	chr7	MAS-related GPR, member D
Gm15308	chr8	predicted gene 15308
AK006380	chr8	
Wwox	chr8	WW domain-containing oxidoreductase
H60b	chr10	histocompatibility 60b
Raet1a	chr10	retinoic acid early transcript 1, alpha
Raet1b	chr10	retinoic acid early transcript beta
Raet1c	chr10	retinoic acid early transcript gamma
AK080063	chr10	
AK153639	chr10	
C920009B18Rik	chr10	RIKEN cDNA C920009B18 gene
Raet1d	chr10	retinoic acid early transcript delta
Nlrp1b	chr11	NLR family, pyrin domain containing 1B
Tmem92	chr11	transmembrane protein 92, pseudogene
Tmem92-ps	chr11	transmembrane protein 92, pseudogene
abParts	chr12	
X73024	chr12	
Gm10324	chr13	predicted gene 10324
AK041589	chr14	
AK086039	chr14	
AK202488	chr14	
Gm10394	chr14	predicted gene 10394
Ang3	chr14	angiogenin, ribonuclease A family, member 3
Ang5	chr14	angiogenin, ribonuclease A family, member 5
Ang6	chr14	angiogenin, ribonuclease A family, member 6
Gm5622	chr14	predicted gene 5622
BC117090	chr16	cDNA sequence BC1179090
Tmem181a	chr17	transmembrane protein 181A
Dynlt1e	chr17	dynein light chain Tctex-type 1E
Tulp4	chr17	tubby like protein 4
H2-T22	chr17	histocompatibility 2, T region locus 22
H2-T10	chr17	histocompatibility 2, T region locus 10
H2-t9	chr17	histocompatibility 2, T region locus 9
Gm6034	chr17	predicted gene 6034
Gm7030	chr17	predicted gene 7030
AK161769	chr17	
2410017I17Rik	chr17	RIKEN cDNA 2410017I17 gene
Gm8909	chr17	predicted gene 8909

Gm6623	chr17	akirin 1 pseudogene
Olfr137	chr17	olfactory receptor 137
Olfr136	chr17	olfactory receptor 136
Mir717	chrX	microRNA 717
Gpc3	chrX	glypican 3
Gm15127	chrX	predicted gene 15127
Cnksr2	chrX	connector enhancer of kinase suppressor of Ras 2
Ube1y1	chrY	ubiquitin-activating enzyme E1, Chr Y 1
Zfy1	chrY	zinc finger protein 1, Y linked
Rbmy1a1	chrY	RNA binding motif protein, Y chromosome, family 1, member A1

BIBLIOGRAPHY

BIBLIOGRAPHY

Abel TW, Clark C, Bierie B, Chytil A, Aakre M, Gorska A *et al* (2009). GFAP-Cre-mediated activation of oncogenic K-ras results in expansion of the subventricular zone and infiltrating glioma. *Mol Cancer Res* **7:** 645-53.

Alcantara Llaguno S, Chen J, Kwon CH, Jackson EL, Li Y, Burns DK *et al* (2009). Malignant astrocytomas originate from neural stem/progenitor cells in a somatic tumor suppressor mouse model. *Cancer Cell* **15:** 45-56.

Alpen EL, Powers-Risius P, Curtis SB, DeGuzman R (1993). Tumorigenic potential of high-Z, high-LET charged-particle radiations. *Radiat Res* **136:** 382-91.

Altomare DA, Testa JR (2005). Perturbations of the AKT signaling pathway in human cancer. *Oncogene* **24:** 7455-64.

Antonelli F, Belli M, Campa A, Chatterjee A, Dini V, Esposito G *et al* (2004). DNA fragmentation induced by Fe ions in human cells: shielding influence on spatially correlated damage. *Adv Space Res* **34:** 1353-7.

Asaithamby A, Uematsu N, Chatterjee A, Story MD, Burm S, Chen DJ (2008). Repair of HZE-particle-induced DNA double-strand breaks in normal human fibroblasts. *Radiat Res*. Apr;169(4):437-46.

Attolini CS, Cheng YK, Beroukhim R, Getz G, Abdel-Wahab O, Levine RL *et al* (2010) A mathematical framework to determine the temporal sequence of somatic genetic events in cancer. *Proc Natl Acad Sci U S A* **107:** 17604-9.

Bachoo RM, Maher EA, Ligon KL, Sharpless NE, Chan SS, You MJ *et al* (2002). Epidermal growth factor receptor and Ink4a/Arf: convergent mechanisms governing terminal differentiation and transformation along the neural stem cell to astrocyte axis. *Cancer Cell* **1:** 269-77.

Bakkenist CJ, Kastan MB (2003). DNA damage activates ATM through intermolecular autophosphorylation and dimer dissociation. *Nature* **421:** 499-506.

Banin S, Moyal L, Shieh S, Taya Y, Anderson CW, Chessa L *et al* (1998). Enhanced phosphorylation of p53 by ATM in response to DNA damage. *Science* **281:** 1674-7.

Bargonetti J, Manfredi JJ (2002). Multiple roles of the tumor suppressor p53. *Curr Opin Oncol* **14:** 86-91.

Bartkova J, Horejsi Z, Koed K, Kramer A, Tort F, Zieger K *et al* (2005). DNA damage response as a candidate anti-cancer barrier in early human tumorigenesis. *Nature* **434:** 864-70.

Bartkova J, Rezaei N, Liontos M, Karakaidos P, Kletsas D, Issaeva N *et al* (2006). Oncogene-induced senescence is part of the tumorigenesis barrier imposed by DNA damage checkpoints. *Nature* **444:** 633-7.

Bayani J, Squire J (2004). Multi-color FISH techniques. *Curr Protoc Cell Biol* **Chapter 22:** Unit 22 5.

Behin A, Hoang-Xuan K, Carpentier AF, Delattre JY (2003). Primary brain tumours in adults. *Lancet* **361:** 323-31.

Bennardo N, Gunn A, Cheng A, Hasty P, Stark JM (2009). Limiting the persistence of a chromosome break diminishes its mutagenic potential. *PLoS Genet* Oct;5(10):e1000683.

Beroukhim R, Getz G, Nghiemphu L, Barretina J, Hsueh T, Linhart D *et al* (2007). Assessing the significance of chromosomal aberrations in cancer: methodology and application to glioma. *Proc Natl Acad Sci U S A* **104:** 20007-12.

Bigner SH, Humphrey PA, Wong AJ, Vogelstein B, Mark J, Friedman HS *et al* (1990). Characterization of the epidermal growth factor receptor in human glioma cell lines and xenografts. *Cancer Res* **50:** 8017-22.

Bode AM, Dong Z (2004). Post-translational modification of p53 in tumorigenesis. *Nat Rev Cancer* **4:** 793-805.

Boei JJ, Natarajan AT (1996). Classification of X-ray-induced Robertsonian fusion-like configurations in mouse splenocytes. *Int J Radiat Biol* **69:** 421-7.

Borek C, Hall EJ, Rossi HH (1978). Malignant transformation in cultured hamster embryo cells produced by X-rays, 460-keV monoenergetic neutrons, and heavy ions. *Cancer Res* **38:** 2997-3005.

Brandes AA, Franceschi E, Tosoni A, Hegi ME, Stupp R (2008). Epidermal growth factor receptor inhibitors in neuro-oncology: hopes and disappointments. *Clin Cancer Res* **14:** 957-60.

Brennan C (2011) Genomic profiles of glioma. *Curr Neurol Neurosci Rep* **11:** 291-7.

Brooks A, Bao S, Rithidech K, Couch LA, Braby LA (2001). Relative effectiveness of HZE iron-56 particles for the induction of cytogenetic damage in vivo. *Radiat Res* **155:** 353-9.

Brustle O, Ohgaki H, Schmitt HP, Walter GF, Ostertag H, Kleihues P (1992). Primitive neuroectodermal tumors after prophylactic central nervous system irradiation in children. Association with an activated K-ras gene. *Cancer* **69:** 2385-92.

Bublil EM, Yarden Y (2007). The EGF receptor family: spearheading a merger of signaling and therapeutics. *Curr Opin Cell Biol* **19:** 124-34.

Burma S, Chen BP, Chen DJ (2006). Role of non-homologous end joining (NHEJ) in maintaining genomic integrity. *DNA Repair (Amst)* **5:** 1042-8.

Burma S, Chen BP, Murphy M, Kurimasa A, Chen DJ (2001). ATM phosphorylates histone H2AX in response to DNA double-strand breaks. *J Biol Chem* **276:** 42462-7.

Burma S, Chen DJ (2004). Role of DNA-PK in the cellular response to DNA double-strand breaks. *DNA Repair (Amst)* **3:** 909-18.

Camacho CV, Mukherjee B, McEllin B, Ding LH, Hu B, Habib AA *et al* (2010) Loss of p15/Ink4b accompanies tumorigenesis triggered by complex DNA double-strand breaks. *Carcinogenesis* **31:** 1889-96.

Campisi J (2007). Aging and cancer cell biology, 2007. *Aging Cell* **6:** 261-3.

Canman CE, Lim DS, Cimprich KA, Taya Y, Tamai K, Sakaguchi K *et al* (1998). Activation of the ATM kinase by ionizing radiation and phosphorylation of p53. *Science* **281:** 1677-9.

Cannon-Albright LA, Goldgar DE, Meyer LJ, Lewis CM, Anderson DE, Fountain JW *et al* (1992). Assignment of a locus for familial melanoma, MLM, to chromosome 9p13-p22. *Science* **258:** 1148-52.

Cavin LW, Dalrymple GV, McGuire EL, Maners AW, Broadwater JR (1990). CNS tumor induction by radiotherapy: a report of four new cases and estimate of dose required. *Int J Radiat Oncol Biol Phys* **18:** 399-406.

Cerami E, Demir E, Schultz N, Taylor BS, Sander C (2010) Automated network analysis identifies core pathways in glioblastoma. *PLoS One* Feb 12;5(2):e8918.

Cheon DJ, Orsulic S (2011) Mouse models of cancer. *Annu Rev Pathol* **6:** 95-119.

Chow LM, Baker SJ (2012) Capturing the molecular and biological diversity of high-grade astrocytoma in genetically engineered mouse models. *Oncotarget* **3:** 67-77.

Chow LM, Endersby R, Zhu X, Rankin S, Qu C, Zhang J *et al* (2011) Cooperativity within and among Pten, p53, and Rb pathways induces high-grade astrocytoma in adult brain. *Cancer Cell* **19:** 305-16.

Comoglio PM, Giordano S, Trusolino L (2008). Drug development of MET inhibitors: targeting oncogene addiction and expedience. *Nat Rev Drug Discov* **7:** 504-16.

Cooper CS, Park M, Blair DG, Tainsky MA, Huebner K, Croce CM *et al* (1984). Molecular cloning of a new transforming gene from a chemically transformed human cell line. *Nature* **311:** 29-33.

Cuadrado M, Martinez-Pastor B, Fernandez-Capetillo O (2006). "ATR activation in response to ionizing radiation: still ATM territory". *Cell Div* **1:** 7.

Cucinotta FA, Durante M (2006). Cancer risk from exposure to galactic cosmic rays: implications for space exploration by human beings. *Lancet Oncol* **7:** 431-5.

Cucinotta FA, Schimmerling W, Wilson JW, Peterson LE, Badhwar GD, Saganti PB *et al* (2001). Space radiation cancer risks and uncertainties for Mars missions. *Radiat Res* **156:** 682-8.

Cully M, You H, Levine AJ, Mak TW (2006). Beyond PTEN mutations: the PI3K pathway as an integrator of multiple inputs during tumorigenesis. *Nat Rev Cancer* **6:** 184-92.

de Vries NA, Bruggeman SW, Hulsman D, de Vries HI, Zevenhoven J, Buckle T *et al* (2010) Rapid and robust transgenic high-grade glioma mouse models for therapy intervention studies. *Clin Cancer Res* **16:** 3431-41.

Desai N, Davis E, O'Neill P, Durante M, Cucinotta FA, Wu H (2005). Immunofluorescence detection of clustered gamma-H2AX foci induced by HZE-particle radiation. *Radiat Res* **164:** 518-22.

Di Micco R, Fumagalli M, Cicalese A, Piccinin S, Gasparini P, Luise C *et al* (2006). Oncogene-induced senescence is a DNA damage response triggered by DNA hyper-replication. *Nature* **444:** 638-42.

Dimri GP, Lee X, Basile G, Acosta M, Scott G, Roskelley C *et al* (1995). A biomarker that identifies senescent human cells in culture and in aging skin in vivo. *Proc Natl Acad Sci U S A* **92:** 9363-7.

Ding LH, Shingyoji M, Chen F, Hwang JJ, Burma S, Lee C *et al* (2005). Gene expression profiles of normal human fibroblasts after exposure to ionizing radiation: a comparative study of low and high doses. *Radiat Res* **164:** 17-26.

Dirks PB (2006). Cancer: stem cells and brain tumours. *Nature* **444:** 687-8.

Dittmann K, Mayer C, Fehrenbacher B, Schaller M, Raju U, Milas L *et al* (2005). Radiation-induced epidermal growth factor receptor nuclear import is linked to activation of DNA-dependent protein kinase. *J Biol Chem* **280:** 31182-9.

Durante M, Cucinotta FA (2008). Heavy ion carcinogenesis and human space exploration. *Nat Rev Cancer* **8:** 465-72.

Durante M, George K, Gialanella G, Grossi G, La Tessa C, Manti L *et al* (2005). Cytogenetic effects of high-energy iron ions: dependence on shielding thickness and material. *Radiat Res* **164:** 571-6.

Ekstrand AJ, Longo N, Hamid ML, Olson JJ, Liu L, Collins VP *et al* (1994). Functional characterization of an EGF receptor with a truncated extracellular domain expressed in glioblastomas with EGFR gene amplification. *Oncogene* **9:** 2313-20.

Endersby R, Baker SJ (2008). PTEN signaling in brain: neuropathology and tumorigenesis. *Oncogene* **27:** 5416-30.

Engelman JA, Zejnullahu K, Mitsudomi T, Song Y, Hyland C, Park JO *et al* (2007). MET amplification leads to gefitinib resistance in lung cancer by activating ERBB3 signaling. *Science* **316:** 1039-43.

Esposito G, Antonelli F, Belli M, Campa A, Dini V, Furusawa Y *et al* (2005). DNA DSB induced by iron ions in human fibroblasts: LET dependence and shielding efficiency. *Adv Space Res* **35:** 243-8.

Fei P, El-Deiry WS (2003). P53 and radiation responses. *Oncogene* **22:** 5774-83.

Fernandez-Capetillo O, Lee A, Nussenzweig M, Nussenzweig A (2004). H2AX: the histone guardian of the genome. *DNA Repair (Amst)* **3:** 959-67.

Fry RJ, Powers-Risius P, Alpen EL, Ainsworth EJ (1985). High-LET radiation carcinogenesis. *Radiat Res Suppl* **8:** S188-95.

Fuster JJ, Sanz-Gonzalez SM, Moll UM, Andres V (2007). Classic and novel roles of p53: prospects for anticancer therapy. *Trends Mol Med* **13:** 192-9.

Gaveriaux-Ruff C, Kieffer BL (2007). Conditional gene targeting in the mouse nervous system: Insights into brain function and diseases. *Pharmacol Ther* **113:** 619-34.

George K, Wu H, Willingham V, Furusawa Y, Kawata T, Cucinotta FA (2001). High- and low-LET induced chromosome damage in human lymphocytes: a time-course of aberrations in metaphase and interphase. *Int J Radiat Biol* **77:** 175-83.

Gilbert MR (2011) Recurrent glioblastoma: a fresh look at current therapies and emerging novel approaches. *Semin Oncol* **38 Suppl 4:** S21-33.

Golding SE, Morgan RN, Adams BR, Hawkins AJ, Povirk LF, Valerie K (2009). Pro-survival AKT and ERK signaling from EGFR and mutant EGFRvIII enhances DNA double-strand break repair in human glioma cells. *Cancer Biol Ther* **8:** 730-8.

Goodarzi AA, Noon AT, Deckbar D, Ziv Y, Shiloh Y, Lobrich M *et al* (2008). ATM signaling facilitates repair of DNA double-strand breaks associated with heterochromatin. *Mol Cell* **31:** 167-77.

Gorgoulis VG, Vassiliou LV, Karakaidos P, Zacharatos P, Kotsinas A, Liloglou T *et al* (2005). Activation of the DNA damage checkpoint and genomic instability in human precancerous lesions. *Nature* **434:** 907-13.

Hada M, Georgakilas AG (2008). Formation of clustered DNA damage after high-LET irradiation: a review. *J Radiat Res* **49:** 203-10.

Hada M, Sutherland BM (2006). Spectrum of complex DNA damages depends on the incident radiation. *Radiat Res* **165:** 223-30.

Halatsch ME, Schmidt U, Behnke-Mursch J, Unterberg A, Wirtz CR (2006). Epidermal growth factor receptor inhibition for the treatment of glioblastoma multiforme and other malignant brain tumours. *Cancer Treat Rev* **32:** 74-89.

Halazonetis TD (2004). Constitutively active DNA damage checkpoint pathways as the driving force for the high frequency of p53 mutations in human cancer. *DNA Repair (Amst)* **3:** 1057-62.

Hall, Eric J, and Amato J Giaccia. *Radiobiology for the Radiologist*. 6th Edition, Boston: Lippincott Williams and Wilkins Publishing, 2006. Print.

Halperin EC (2006). Particle therapy and treatment of cancer. *Lancet Oncol* **7:** 676-85.

Hamatani K, Eguchi H, Ito R, Mukai M, Takahashi K, Taga M *et al* (2008). RET/PTC rearrangements preferentially occurred in papillary thyroid cancer among atomic bomb survivors exposed to high radiation dose. *Cancer Res* **68:** 7176-82.

Hambardzumyan D, Amankulor NM, Helmy KY, Becher OJ, Holland EC (2009). Modeling Adult Gliomas Using RCAS/t-va Technology. *Transl Oncol* **2:** 89-95.

Hambardzumyan D, Parada LF, Holland EC, Charest A (2011) Genetic modeling of gliomas in mice: new tools to tackle old problems. *Glia* **59:** 1155-68.

Hanahan D, Weinberg RA (2011) Hallmarks of cancer: the next generation. *Cell* **144:** 646-74.

Haymaker W, Rubinstein LJ, Miquel J (1972). Brain tumors in irradiated monkeys. *Acta Neuropathol* **20:** 267-77.

He S, Nakada D, Morrison SJ (2009). Mechanisms of stem cell self-renewal. *Annu Rev Cell Dev Biol* **25:** 377-406.

Hei TK, Zhao YL, Roy D, Piao CQ, Calaf G, Hall EJ (2001). Molecular alterations in tumorigenic human bronchial and breast epithelial cells induced by high LET radiation. *Adv Space Res* **27:** 411-9.

Hickson I, Zhao Y, Richardson CJ, Green SJ, Martin NM, Orr AI *et al* (2004). Identification and characterization of a novel and specific inhibitor of the ataxia-telangiectasia mutated kinase ATM. *Cancer Res* **64:** 9152-9.

Holland EC (2000). Glioblastoma multiforme: the terminator. *Proc Natl Acad Sci U S A* **97:** 6242-4.

Holland EC (2001). Gliomagenesis: genetic alterations and mouse models. *Nat Rev Genet* **2:** 120-9.

Holland EC, Hively WP, DePinho RA, Varmus HE (1998). A constitutively active epidermal growth factor receptor cooperates with disruption of G1 cell-cycle arrest pathways to induce glioma-like lesions in mice. *Genes Dev* **12:** 3675-85.

Horn HF, Vousden KH (2007). Coping with stress: multiple ways to activate p53. *Oncogene* **26:** 1306-16.

ICRP Recommendations of the International Commission on Radiological Protection, Ann. ICRP 1, No.3, 1991.

Isaka F, Ishibashi M, Taki W, Hashimoto N, Nakanishi S, Kageyama R (1999). Ectopic expression of the bHLH gene Math1 disturbs neural development. *Eur J Neurosci* **11:** 2582-8.

Jakob B, Scholz M, Taucher-Scholz G (2003). Biological imaging of heavy charged-particle tracks. *Radiat Res* **159:** 676-84.

Jazayeri A, Falck J, Lukas C, Bartek J, Smith GC, Lukas J *et al* (2006). ATM- and cell cycle-dependent regulation of ATR in response to DNA double-strand breaks. *Nat Cell Biol* **8:** 37-45.

Jeggo PA, Lobrich M (2005). Artemis links ATM to double strand break rejoining. *Cell Cycle* **4:** 359-62.

Jen J, Harper JW, Bigner SH, Bigner DD, Papadopoulos N, Markowitz S *et al* (1994). Deletion of p16 and p15 genes in brain tumors. *Cancer Res* **54:** 6353-8.

Jun HJ, Acquaviva J, Chi D, Lessard J, Zhu H, Woolfenden S *et al* (2011) Acquired MET expression confers resistance to EGFR inhibition in a mouse model of glioblastoma multiforme. *Oncogene*.

Karlsson KH, Stenerlow B (2004). Focus formation of DNA repair proteins in normal and repair-deficient cells irradiated with high-LET ions. *Radiat Res* **161:** 517-27.

Khanna KK, Jackson SP (2001). DNA double-strand breaks: signaling, repair and the cancer connection. *Nat Genet* **27:** 247-54.

Kim ST, Xu B, Kastan MB (2002). Involvement of the cohesin protein, Smc1, in Atm-dependent and independent responses to DNA damage. *Genes Dev* **16:** 560-70.

Kim WY, Sharpless NE (2006). The regulation of INK4/ARF in cancer and aging. *Cell* **127:** 265-75.

Koochekpour S, Jeffers M, Rulong S, Taylor G, Klineberg E, Hudson EA *et al* (1997). Met and hepatocyte growth factor/scatter factor expression in human gliomas. *Cancer Res* **57:** 5391-8.

Krex D, Klink B, Hartmann C, von Deimling A, Pietsch T, Simon M *et al* (2007). Long-term survival with glioblastoma multiforme. *Brain* **130:** 2596-606.

Krimpenfort P, Ijpenberg A, Song JY, van der Valk M, Nawijn M, Zevenhoven J *et al* (2007). p15Ink4b is a critical tumour suppressor in the absence of p16Ink4a. *Nature* **448:** 943-6.

Krimpenfort P, Quon KC, Mooi WJ, Loonstra A, Berns A (2001). Loss of p16Ink4a confers susceptibility to metastatic melanoma in mice. *Nature* **413:** 83-6.

Kuhne M, Riballo E, Rief N, Rothkamm K, Jeggo PA, Lobrich M (2004). A double-strand break repair defect in ATM-deficient cells contributes to radiosensitivity. *Cancer Res* **64:** 500-8.

Kurimasa A, Ouyang H, Dong LJ, Wang S, Li X, Cordon-Cardo C *et al* (1999). Catalytic subunit of DNA-dependent protein kinase: impact on lymphocyte development and tumorigenesis. *Proc Natl Acad Sci U S A* **96:** 1403-8.

Kwon CH, Zhao D, Chen J, Alcantara S, Li Y, Burns DK *et al* (2008). Pten haploinsufficiency accelerates formation of high-grade astrocytomas. *Cancer Res* **68:** 3286-94.

Laterra J, Rosen E, Nam M, Ranganathan S, Fielding K, Johnston P (1997). Scatter factor/hepatocyte growth factor expression enhances human glioblastoma tumorigenicity and growth. *Biochem Biophys Res Commun* **235:** 743-7.

Lavin MF (2007). ATM and the Mre11 complex combine to recognize and signal DNA double-strand breaks. *Oncogene* **26:** 7749-58.

Lee M, Wrensch M, Miike R (1997). Dietary and tobacco risk factors for adult onset glioma in the San Francisco Bay Area (California, USA). *Cancer Causes Control* **8:** 13-24.

Lehmann AR (2005). The role of SMC proteins in the responses to DNA damage. *DNA Repair (Amst)* **4:** 309-14.

Li A, Walling J, Kotliarov Y, Center A, Steed ME, Ahn SJ *et al* (2008). Genomic changes and gene expression profiles reveal that established glioma cell lines are poorly representative of primary human gliomas. *Mol Cancer Res* **6:** 21-30.

Li H, Collado M, Villasante A, Strati K, Ortega S, Canamero M *et al* (2009). The Ink4/Arf locus is a barrier for iPS cell reprogramming. *Nature* **460:** 1136-9.

Li H, Gu Y, Miki J, Hukku B, McLeod DG, Hei TK *et al* (2007). Malignant transformation of human benign prostate epithelial cells by high linear energy transfer alpha-particles. *Int J Oncol* **31:** 537-44.

Li Y, Lal B, Kwon S, Fan X, Saldanha U, Reznik TE *et al* (2005). The scatter factor/hepatocyte growth factor: c-met pathway in human embryonal central nervous system tumor malignancy. *Cancer Res* **65:** 9355-62.

Li Y, Li A, Glas M, Lal B, Ying M, Sang Y *et al* c-Met signaling induces a reprogramming network and supports the glioblastoma stem-like phenotype. *Proc Natl Acad Sci U S A* **108:** 9951-6.

Little JB (2000). Radiation carcinogenesis. *Carcinogenesis* **21:** 397-404.

Lobrich M, Jeggo PA (2005). Harmonising the response to DSBs: a new string in the ATM bow. *DNA Repair (Amst)* **4:** 749-59.

Lorimer IA (2002). Mutant epidermal growth factor receptors as targets for cancer therapy. *Curr Cancer Drug Targets* **2:** 91-102.

Louis DN, Ohgaki H, Wiestler OD, Cavenee WK, Burger PC, Jouvet A *et al* (2007). The 2007 WHO classification of tumours of the central nervous system. *Acta Neuropathol* **114:** 97-109.

Lozano G (2007). The oncogenic roles of p53 mutants in mouse models. *Curr Opin Genet Dev* **17:** 66-70.

Lukas J, Parry D, Aagaard L, Mann DJ, Bartkova J, Strauss M *et al* (1995). Retinoblastoma-protein-dependent cell-cycle inhibition by the tumour suppressor p16. *Nature* **375:** 503-6.

Maalouf M, Durante M, Foray N (2011) Biological effects of space radiation on human cells: history, advances and outcomes. *J Radiat Res* **52:** 126-46.

Magee JL, Chatterjee A (1980). Radiation chemistry of heavy particle tracks. 1. General considerations. *J Phys Chem* **84:** 3529-36.

Magnander K, Elmroth K (2012) Biological consequences of formation and repair of complex DNA damage. *Cancer Lett*. [In press].

Maher EA, Furnari FB, Bachoo RM, Rowitch DH, Louis DN, Cavenee WK *et al* (2001). Malignant glioma: genetics and biology of a grave matter. *Genes Dev* **15:** 1311-33.

Marumoto T, Tashiro A, Friedmann-Morvinski D, Scadeng M, Soda Y, Gage FH *et al* (2009). Development of a novel mouse glioma model using lentiviral vectors. *Nat Med* **15:** 110-6.

McDermott U, Sharma SV, Dowell L, Greninger P, Montagut C, Lamb J *et al* (2007). Identification of genotype-correlated sensitivity to selective kinase inhibitors by using high-throughput tumor cell line profiling. *Proc Natl Acad Sci U S A* **104:** 19936-41.

Milas L, Fan Z, Andratschke NH, Ang KK (2004). Epidermal growth factor receptor and tumor response to radiation: in vivo preclinical studies. *Int J Radiat Oncol Biol Phys* **58:** 966-71.

Miller J, Hei TK, Eds. (2005). Space Life Sciences: Ground-Based Iron-Ion Biology and Physics, Including Shielding. *Adv Space Res* **35**

Mladenov E, Iliakis G (2011) Induction and repair of DNA double strand breaks: the increasing spectrum of non-homologous end joining pathways. *Mutat Res* **711:** 61-72.

Mochan TA, Venere M, DiTullio RA, Jr., Halazonetis TD (2004). 53BP1, an activator of ATM in response to DNA damage. *DNA Repair (Amst)* **3:** 945-52.

Morton LM, Chanock SJ (2011) A step toward slaying the hydra of second cancers. *Nat Med* **17:** 924-5.

Mukherjee B, Camacho CV, Tomimatsu N, Miller J, Burma S (2008). Modulation of the DNA-damage response to HZE particles by shielding. *DNA Repair (Amst)* **7:** 1717-30.

Mukherjee B, Choy H, Nirodi C, Burma S (2010) Targeting nonhomologous end-joining through epidermal growth factor receptor inhibition: rationale and strategies for radiosensitization. *Semin Radiat Oncol* **20:** 250-7.

Mukherjee B, Kessinger C, Kobayashi J, Chen BP, Chen DJ, Chatterjee A *et al* (2006). DNA-PK phosphorylates histone H2AX during apoptotic DNA fragmentation in mammalian cells. *DNA Repair (Amst)* **5:** 575-90.

Mukherjee B, McEllin B, Camacho CV, Tomimatsu N, Sirasanagandala S, Nannepaga S *et al* (2009). EGFRvIII and DNA Double-Strand Break Repair: A Molecular Mechanism for Radioresistance in Glioblastoma. *Cancer Res*.

Murnane JP (2006). Telomeres and chromosome instability. *DNA Repair (Amst)* **5:** 1082-92.

Nagane M, Coufal F, Lin H, Bogler O, Cavenee WK, Huang HJ (1996). A common mutant epidermal growth factor receptor confers enhanced tumorigenicity on human glioblastoma cells by increasing proliferation and reducing apoptosis. *Cancer Res* **56:** 5079-86.

National Academy of Sciences, Space Radiation Hazards and the Vision for Space Exploration: Report of a Workshop, 2006, http://www.nap.edu/catalog/11760.html.

Neglia JP, Meadows AT, Robison LL, Kim TH, Newton WA, Ruymann FB *et al* (1991). Second neoplasms after acute lymphoblastic leukemia in childhood. *N Engl J Med* **325:** 1330-6.

Newhauser WD, Durante M (2011) Assessing the risk of second malignancies after modern radiotherapy. *Nat Rev Cancer* **11:** 438-48.

Nobori T, Miura K, Wu DJ, Lois A, Takabayashi K, Carson DA (1994). Deletions of the cyclin-dependent kinase-4 inhibitor gene in multiple human cancers. *Nature* **368:** 753-6.

Nussenzweig A, Nussenzweig MC (2007). A backup DNA repair pathway moves to the forefront. *Cell* **131:** 223-5.

O'Driscoll M, Jeggo PA (2006). The role of double-strand break repair - insights from human genetics. *Nat Rev Genet* **7:** 45-54.

Ohgaki H, Kleihues P (2007). Genetic pathways to primary and secondary glioblastoma. *Am J Pathol* **170:** 1445-53.

Paulsen RD, Cimprich KA (2007). The ATR pathway: fine-tuning the fork. *DNA Repair (Amst)* **6:** 953-66.

Pazzaglia S, Tanori M, Mancuso M, Rebessi S, Leonardi S, Di Majo V *et al* (2006). Linking DNA damage to medulloblastoma tumorigenesis in patched heterozygous knockout mice. *Oncogene* **25:** 1165-73.

Phillips HS, Kharbanda S, Chen R, Forrest WF, Soriano RH, Wu TD *et al* (2006). Molecular subclasses of high-grade glioma predict prognosis, delineate a pattern of disease progression, and resemble stages in neurogenesis. *Cancer Cell* **9:** 157-73.

Podsypanina K, Ellenson LH, Nemes A, Gu J, Tamura M, Yamada KM *et al* (1999). Mutation of Pten/Mmac1 in mice causes neoplasia in multiple organ systems. *Proc Natl Acad Sci U S A* **96:** 1563-8.

Pollard SM, Yoshikawa K, Clarke ID, Danovi D, Stricker S, Russell R *et al* (2009). Glioma stem cell lines expanded in adherent culture have tumor-specific phenotypes and are suitable for chemical and genetic screens. *Cell Stem Cell* **4:** 568-80.

Price RE, Tinkey PT, Leeds NE, Hazle JD, Langford LA, Stephens LC *et al* (1996). Glioblastoma multiforme arising in the irradiated spinal cord of a rhesus monkey (Macaca mulatta). *J Med Primatol* **25:** 140-5.

Raizer JJ (2005). HER1/EGFR tyrosine kinase inhibitors for the treatment of glioblastoma multiforme. *J Neurooncol* **74:** 77-86.

Rankin SL, Zhu G, Baker SJ (2011) Insights Gained from Modeling High-Grade Glioma in the Mouse. *Neuropathol Appl Neurobiol*.

Riballo E, Kuhne M, Rief N, Doherty A, Smith GC, Recio MJ *et al* (2004). A pathway of double-strand break rejoining dependent upon ATM, Artemis, and proteins locating to gamma-H2AX foci. *Mol Cell* **16:** 715-24.

Roberts PJ, Der CJ (2007). Targeting the Raf-MEK-ERK mitogen-activated protein kinase cascade for the treatment of cancer. *Oncogene* **26:** 3291-310.

Robinson JP, VanBrocklin MW, Guilbeault AR, Signorelli DL, Brandner S, Holmen SL (2010) Activated BRAF induces gliomas in mice when combined with Ink4a/Arf loss or Akt activation. *Oncogene* **29:** 335-44.

Robinson JP, Vanbrocklin MW, Lastwika KJ, McKinney AJ, Brandner S, Holmen SL (2010) Activated MEK cooperates with Ink4a/Arf loss or Akt activation to induce gliomas in vivo. *Oncogene* **30:** 1341-50.

Ron E, Modan B, Boice JD, Jr., Alfandary E, Stovall M, Chetrit A *et al* (1988). Tumors of the brain and nervous system after radiotherapy in childhood. *N Engl J Med* **319:** 1033-9.

Rosidi B, Wang M, Wu W, Sharma A, Wang H, Iliakis G (2008). Histone H1 functions as a stimulatory factor in backup pathways of NHEJ. *Nucleic Acids Res*.

Sadetzki S, Chetrit A, Freedman L, Stovall M, Modan B, Novikov I (2005). Long-term follow-up for brain tumor development after childhood exposure to ionizing radiation for tinea capitis. *Radiat Res* **163:** 424-32.

Sage E, Harrison L (2011) Clustered DNA lesion repair in eukaryotes: relevance to mutagenesis and cell survival. *Mutat Res* **711:** 123-33.

Salmena L, Carracedo A, Pandolfi PP (2008). Tenets of PTEN tumor suppression. *Cell* **133:** 403-14.

Salvati M, Frati A, Russo N, Caroli E, Polli FM, Minniti G *et al* (2003). Radiation-induced gliomas: report of 10 cases and review of the literature. *Surg Neurol* **60:** 60-7; discussion 67.

Samet JM (2011) Radiation and cancer risk: a continuing challenge for epidemiologists. *Environ Health* **10 Suppl 1:** S4.

Sasai K, Evans JW, Kovacs MS, Brown JM (1994). Prediction of human cell radiosensitivity: comparison of clonogenic assay with chromosome aberrations scored using premature chromosome condensation with fluorescence in situ hybridization. *Int J Radiat Oncol Biol Phys* **30:** 1127-32.

Scherthan H (2002). Detection of chromosome ends by telomere FISH. *Methods Mol Biol* **191:** 13-31.

Schulz-Ertner D, Jakel O, Schlegel W (2006). Radiation therapy with charged particles. *Semin Radiat Oncol* **16:** 249-59.

Schulz-Ertner D, Tsujii H (2007). Particle radiation therapy using proton and heavier ion beams. *J Clin Oncol* **25:** 953-64.

Serrano M, Lee H, Chin L, Cordon-Cardo C, Beach D, DePinho RA (1996). Role of the INK4a locus in tumor suppression and cell mortality. *Cell* **85:** 27-37.

Setlow RB (2003). The hazards of space travel. *EMBO Rep* **4:** 1013-6.

Shapiro S, Mealey J, Jr., Sartorius C (1989). Radiation-induced intracranial malignant gliomas. *J Neurosurg* **71:** 77-82.

Sharpless NE (2004). Ink4a/Arf links senescence and aging. *Exp Gerontol* **39:** 1751-9.

Sharpless NE, Bardeesy N, Lee KH, Carrasco D, Castrillon DH, Aguirre AJ *et al* (2001). Loss of p16Ink4a with retention of p19Arf predisposes mice to tumorigenesis. *Nature* **413:** 86-91.

Shete S, Hosking FJ, Robertson LB, Dobbins SE, Sanson M, Malmer B *et al* (2009). Genome-wide association study identifies five susceptibility loci for glioma. *Nat Genet* **41:** 899-904.

Shiloh Y (2003). ATM and related protein kinases: safeguarding genome integrity. *Nat Rev Cancer* **3:** 155-68.

Shiloh Y (2006). The ATM-mediated DNA-damage response: taking shape. *Trends Biochem Sci* **31:** 402-10.

Shinojima N, Tada K, Shiraishi S, Kamiryo T, Kochi M, Nakamura H *et al* (2003). Prognostic value of epidermal growth factor receptor in patients with glioblastoma multiforme. *Cancer Res* **63:** 6962-70.

Simpson JA (1983). in Composition and Origin of Galactic Cosmic Rays (M.M. Shapiro, Ed.), Reidel, Dordrecht. *Adv Space Res*

Smolen GA, Muir B, Mohapatra G, Barmettler A, Kim WJ, Rivera MN *et al* (2006). Frequent met oncogene amplification in a Brca1/Trp53 mouse model of mammary tumorigenesis. *Cancer Res* **66:** 3452-5.

Strom L, Lindroos HB, Shirahige K, Sjogren C (2004). Postreplicative recruitment of cohesin to double-strand breaks is required for DNA repair. *Mol Cell* **16:** 1003-15.

Sutter R, Yadirgi G, Marino S (2007). Neural stem cells, tumour stem cells and brain tumours: dangerous relationships? *Biochim Biophys Acta* **1776:** 125-37.

The Cancer Genome Atlas Network (2008). Comprehensive genomic characterization defines human glioblastoma genes and core pathways. *Nature* **455:** 1061-8.

Theriault G, Goldberg M, Miller AB, Armstrong B, Guenel P, Deadman J *et al* (1994). Cancer risks associated with occupational exposure to magnetic fields among electric utility workers in Ontario and Quebec, Canada, and France: 1970-1989. *Am J Epidemiol* **139:** 550-72.

Toledo F, Wahl GM (2006). Regulating the p53 pathway: in vitro hypotheses, in vivo veritas. *Nat Rev Cancer* **6:** 909-23.

Toledo LI, Murga M, Gutierrez-Martinez P, Soria R, Fernandez-Capetillo O (2008). ATR signaling can drive cells into senescence in the absence of DNA breaks. *Genes Dev* **22:** 297-302.

Trusolino L, Bertotti A, Comoglio PM (2010) MET signalling: principles and functions in development, organ regeneration and cancer. *Nat Rev Mol Cell Biol* **11:** 834-48.

Turke AB, Zejnullahu K, Wu YL, Song Y, Dias-Santagata D, Lifshits E *et al* (2010) Preexistence and clonal selection of MET amplification in EGFR mutant NSCLC. *Cancer Cell* **17:** 77-88.

Uhrbom L, Dai C, Celestino JC, Rosenblum MK, Fuller GN, Holland EC (2002). Ink4a-Arf loss cooperates with KRas activation in astrocytes and neural progenitors to generate glioblastomas of various morphologies depending on activated Akt. *Cancer Res* **62:** 5551-8.

Uhrbom L, Kastemar M, Johansson FK, Westermark B, Holland EC (2005). Cell type-specific tumor suppression by Ink4a and Arf in Kras-induced mouse gliomagenesis. *Cancer Res* **65:** 2065-9.

Urushibara A, Shikazono N, O'Neill P, Fujii K, Wada S, Yokoya A (2008). LET dependence of the yield of single-, double-strand breaks and base lesions in fully hydrated plasmid DNA films by 4He(2+) ion irradiation. *Int J Radiat Biol* **84:** 23-33.

Verhaak RG, Hoadley KA, Purdom E, Wang V, Qi Y, Wilkerson MD *et al* (2010) Integrated genomic analysis identifies clinically relevant subtypes of

glioblastoma characterized by abnormalities in PDGFRA, IDH1, EGFR, and NF1. *Cancer Cell* **17:** 98-110.

Veuger SJ, Curtin NJ, Richardson CJ, Smith GC, Durkacz BW (2003). Radiosensitization and DNA repair inhibition by the combined use of novel inhibitors of DNA-dependent protein kinase and poly(ADP-ribose) polymerase-1. *Cancer Res* **63:** 6008-15.

Vilchez RA, Kozinetz CA, Arrington AS, Madden CR, Butel JS (2003). Simian virus 40 in human cancers. *Am J Med* **114:** 675-84.

Volpato CB, Martinez-Alfaro M, Corvi R, Gabus C, Sauvaigo S, Ferrari P *et al* (2008). Enhanced sensitivity of the RET proto-oncogene to ionizing radiation in vitro. *Cancer Res* **68:** 8986-92.

Wakeford R (2004). The cancer epidemiology of radiation. *Oncogene* **23:** 6404-28.

Wang H, Wang X, Zhang P, Wang Y (2008). The Ku-dependent non-homologous end-joining but not other repair pathway is inhibited by high linear energy transfer ionizing radiation. *DNA Repair (Amst)* May 3;7(5):725-33

Wawrzynow B, Zylicz A, Wallace M, Hupp T, Zylicz M (2007). MDM2 chaperones the p53 tumor suppressor. *J Biol Chem* **282:** 32603-12.

Wechsler-Reya R, Scott MP (2001). The developmental biology of brain tumors. *Annu Rev Neurosci* **24:** 385-428.

Wee B, Charles N, Holland EC (2011) Animal models to study cancer-initiating cells from glioblastoma. *Front Biosci* **17:** 2243-58.

Wei Q, Clarke L, Scheidenhelm DK, Qian B, Tong A, Sabha N *et al* (2006). High-grade glioma formation results from postnatal pten loss or mutant epidermal growth factor receptor expression in a transgenic mouse glioma model. *Cancer Res* **66:** 7429-37.

Weinstock DM, Richardson CA, Elliott B, Jasin M (2006). Modeling oncogenic translocations: distinct roles for double-strand break repair pathways in translocation formation in mammalian cells. *DNA Repair (Amst)* **5:** 1065-74.

Weppler SA, Li Y, Dubois L, Lieuwes N, Jutten B, Lambin P *et al* (2007). Expression of EGFR variant vIII promotes both radiation resistance and hypoxia tolerance. *Radiother Oncol* **83:** 333-9.

Westphal M, Lamszus K (2011) The neurobiology of gliomas: from cell biology to the development of therapeutic approaches. *Nat Rev Neurosci* **12:** 495-508.

Wiemels JL, Wiencke JK, Sison JD, Miike R, McMillan A, Wrensch M (2002). History of allergies among adults with glioma and controls. *Int J Cancer* **98:** 609-15.

Williams D (2008). Radiation carcinogenesis: lessons from Chernobyl. *Oncogene* **27 Suppl 2:** S9-18.

Won J, Kim M, Kim N, Ahn JH, Lee WG, Kim SS *et al* (2006). Small molecule-based reversible reprogramming of cellular lifespan. *Nat Chem Biol* **2:** 369-74.

Xiao A, Wu H, Pandolfi PP, Louis DN, Van Dyke T (2002). Astrocyte inactivation of the pRb pathway predisposes mice to malignant astrocytoma development that is accelerated by PTEN mutation. *Cancer Cell* **1:** 157-68.

Yang TC, Craise LM, Mei MT, Tobias CA (1985). Neoplastic cell transformation by heavy charged particles. *Radiat Res Suppl* **8:** S177-87.

Yang TC, Georgy KA, Craise LM, Durante M (1997). Initiation of oncogenic transformation in human mammary epithelial cells by charged particles. *Radiat Oncol Investig* **5:** 134-8.

Yasaei H, Gilham E, Pickles JC, Roberts TP, O'Donovan M, Newbold RF (2012) Carcinogen-specific mutational and epigenetic alterations in INK4A, INK4B and p53 tumour-suppressor genes drive induced senescence bypass in normal diploid mammalian cells. *Oncogene*. [In press].

Yazdi PT, Wang Y, Zhao S, Patel N, Lee EY, Qin J (2002). SMC1 is a downstream effector in the ATM/NBS1 branch of the human S-phase checkpoint. *Genes Dev* **16:** 571-82.

Zeitlin C, Heilbronn L, Miller J (1998). Detailed characterization of the 1087 MeV/nucleon iron-56 beam used for radiobiology at the alternating gradient synchrotron. *Radiat Res* **149:** 560-9.

Zhang H, Berezov A, Wang Q, Zhang G, Drebin J, Murali R *et al* (2007). ErbB receptors: from oncogenes to targeted cancer therapies. *J Clin Invest* **117:** 2051-8.

Zhao Y, Shao G, Piao CQ, Berenguer J, Hei TK (2004). Down-regulation of Betaig-h3 gene is involved in the tumorigenesis in human bronchial epithelial cells induced by heavy-ion radiation. *Radiat Res* **162:** 655-9.

Zheng H, Ying H, Yan H, Kimmelman AC, Hiller DJ, Chen AJ *et al* (2008). p53 and Pten control neural and glioma stem/progenitor cell renewal and differentiation. *Nature* **455:** 1129-33.

Zheng T, Cantor KP, Zhang Y, Chiu BC, Lynch CF (2001). Risk of brain glioma not associated with cigarette smoking or use of other tobacco products in Iowa. *Cancer Epidemiol Biomarkers Prev* **10:** 413-4.

Zhu Y, Guignard F, Zhao D, Liu L, Burns DK, Mason RP *et al* (2005). Early inactivation of p53 tumor suppressor gene cooperating with NF1 loss induces malignant astrocytoma. *Cancer Cell* **8:** 119-30.